FZD-522

The Mobilization of Actinides by Microbial Ligands Taking into Consideration the Final Storage of Nuclear Waste

Interactions of Selected Actinides U(VI), Cm(III), and Np(V) with Pyoverdins Secreted by *Pseudomonas fluorescens* and Related Model Compounds

Henry Moll, Maja Glorius, Astrid Barkleit,
André Roßberg, Gert Bernhard

August 2009

Wissenschaftlich-Technische Berichte
FZD-522 2009 · ISSN 1437-322X

WISSENSCHAFTLICH-TECHNISCHE BERICHTE

Forschungszentrum
Dresden Rossendorf

Abstract

The groundwater bacterium *Pseudomonas fluorescens* (CCUG 32456) isolated at a depth of 70 m in the Äspö Hard Rock Laboratory secretes a pyoverdin–mixture with four main components (two pyoverdins and two ferribactins). The dominant influence of the pyoverdins of this mixture could be demonstrated by an absorption spectroscopy study.

The comparison of the stability constants of U(VI), Cm(III), and Np(V) species with ligands simulating the functional groups of the pyoverdins results in the following order of complex strength: pyoverdins (PYO) ≥ trihydroxamate (DFO) > catecholates (NAP, 6-HQ) > simple hydroxamates (SHA, BHA). The pyoverdin chromophore functionality shows a large affinity to bind actinides.

As a result, pyoverdins are also able to complex and to mobilize elements other than Fe(III) at a considerably high efficiency. It is known that EDTA may form the strongest actinide complexes among the various organic components in nuclear wastes. The stability constants of 1:1 species formed between Cm^{3+} and UO_2^{2+} and pyoverdins are by a factor of 1.05 and 1.3, respectively, larger compared to the corresponding EDTA stability constants. The Np(V)–PYO stability constant is even by a factor of 1.83 greater than the EDTA stability constant. The identified NpO_2^+–PYO species belong to the strongest NpO_2^+ species with organic material reported so far. All identified species influence the actinide speciation within the biologically relevant pH range.

The metal binding properties of microbes are mainly determined by functional groups of their cell wall (LPS: Gram-negative bacteria and PG: Gram-positive bacteria). On the basis of the determined stability constants raw estimates are possible, if actinides prefer to interact with the microbial cell wall components or with the secreted pyoverdin bioligands. By taking pH 5 as an example, U(VI)–PYO interactions are slightly stronger than those observed with LPS and PG. For Cm(III) we found a much stronger affinity to aqueous pyoverdin species than to functional groups of the cell wall compartments. A similar behavior was observed for Np(V). This shows the importance of indirect interaction processes between actinides and bioligands secreted by resident microbes.

Zusammenfassung

Das Grundwasserbakterium *Pseudomonas fluorescens* (CCUG 32456), isoliert in einer Tiefe von 70 m im Äspö Hard Rock Laboratory, setzt eine Pyoverdin–Mischung frei, die 4 Hauptkomponenten enthält (2 Pyoverdine und 2 Ferribactine). Der dominierende Einfluss der Pyoverdine konnte mittels Absorptionsspektroskopie bestätigt werden.

Der Vergleich der Stabilitätskonstanten von U(VI), Cm(III) und Np(V) Spezies mit Liganden, die die metallbindenden funktionellen Gruppen der Pyoverdine simulieren, ergab folgende Reihenfolge der Komplexstabilitäten: Pyoverdine (PYO) ≥ Trihydroxamat (DFO) > Catecholate (NAP, 6-HQ) > einfache Hydroxamate (SHA, BHA). Die Chromophorfunktionalität der Pyoverdine zeigt die höchste Affinität in der Actinidenkoordination.

Man kann schlussfolgern, dass Pyoverdine neben Fe(III) auch Actinide mit hoher Effektivität binden und somit mobilisieren können. Es ist bekannt, dass EDTA als organische Komponente im nuklearen Abfall die stärksten Actinidenkomplexe bildet. Die Stabilitätskonstanten der 1:1 Spezies zwischen Cm^{3+} und UO_2^{2+} und den Pyoverdinen sind um Faktoren von 1.05 und 1.3 größer als die entsprechenden EDTA-Konstanten. Die Np(V)–PYO Stabilitätskonstante ist sogar um einen Faktor von 1.83 größer. Die NpO_2^+–PYO Komplexe gehören zu den stärksten NpO_2^+ Spezies mit Organika, die bisher beschrieben wurden. Alle bestimmten Spezies beeinflussen die Actinidenspeziation im biologisch relevanten pH-Bereich.

Die Metallbindungseigenschaften der Mikroben werden hauptsächlich durch die funktionellen Gruppen der Zellwand bestimmt (LPS: Gram-negative Bakterien und PG: Gram-positive Bakterien). Auf der Basis der bestimmten Stabilitätskonstanten ist es möglich, einzuschätzen, ob die Actinide bevorzugt mit den Zellwandkomponenten wechselwirken oder mit von den Zellen freigesetzten Bioliganden. Bei einem pH-Wert von 5, zum Beispiel, sind die U(VI)–PYO Wechselwirkungen leicht stärker als die mit LPS und PG. Bei Cm(III) und Np(V) hingegen wurden wesentlich stärkere Wechselwirkungen mit den wässrigen Pyoverdin–Spezies ermittelt. Dies zeigt die große Bedeutung der Untersuchung und Einbeziehung von indirekten Wechselwirkungsprozessen zwischen Actiniden und Bioliganden, die durch anwesende Mikroben in den Grundwasserleiter abgegeben werden können.

Content

1 Introduction

The direct (e.g., biosorption, bioaccumulation, biotransformation) and indirect (e.g., actinide mobilization by microbially produced bioligands) influence of microorganisms on migration processes of actinides has to be taken into account for the risk assessment of potential high level nuclear waste disposal sites. Within our last project (02E9491) we investigated direct interaction paths of bacteria with actinides [1] whereas this new study is concentrated on the indirect interaction path of the actinide mobilization by microbially produced bioligands. The stability constants to be determined will be used directly in modeling calculations of the long term performance assessment of nuclear waste repositories in hard rock formations as well as in other rock formations (salt, clay). The mobilizations of actinides by microbially produced and released bioligands, e.g., siderophores, have not yet been intensively studied in the Äspö aquifer. The Äspö HRL was established in Sweden in a granite rock formation for in-situ experiments with radionuclides. The aims of this facility are to examine which methods are most suitable for research in the bedrock, to develop and to demonstrate methods for deciding in what way a deep repository can be planned and constructed in accordance with the local characteristics of the bedrock, to increase scientific understanding of a deep repository's safety margins and to develop and demonstrate the technique that will be used during the disposal of spent nuclear fuel.

Investigations of the microbial diversity at the Äspö site were published by Pedersen et al. [2-4]. The total number of microorganisms measured at Äspö range from 1×10^3 to 5×10^6 cells mL^{-1}. Among other microbes, bacteria from the genus *Pseudomonas* could be isolated. Pseudomonads are ubiquitous soil and ground water bacteria. They were isolated or identified also under harsh environmental conditions for instance uranium waste piles [5] or sewage from uranium mill tailings [6]. Fluorescent Pseudomonads secrete pyoverdin-type siderophores with a high potential to complex and transport metals. This is known especially for Fe^{3+} [7-10] but their interactions with actinides in different oxidation states are unknown. Powell et al. (1980) demonstrated the occurrence of hydroxamate siderophores produced by microorganisms in concentrations ranging from 10^{-7} to 10^{-8} M in a variety of soils [11].

Our project is focused on the pyoverdins secreted by the Äspö bacterium *Pseudomonas fluorescens* (CCUG 32456) isolated at a depth of 70 m in the Äspö HRL, Sweden [12]. The aim of the presented work is to explore interaction reactions of the *P. fluorescens* (CCUG 32456) pyoverdins with the actinides uranium, curium, and neptunium. This includes also the

investigation of model systems simulating a) the functionalities of the pyoverdins and b) the surface of microbes. To summarize, the main goals of the project are:

i) Isolation and characterization of microbial ligands produced from the Äspö bacterium *Pseudomonas fluorescens* (CCUG 32456).

ii) Interaction of uranium, neptunium, and curium with these microbial ligands including compounds simulating the functionality of the microbial ligands (simple hydroxamate and catecholate ligands) and the surface of the bacteria (Gram-negative: lipopolysaccharide and Gram-positive: peptidoglycan).

iii) Spectroscopic characterization of the formed actinide complexes/compounds.

The obtained results should help to improve the scientific basis for the performance assessment and safety of nuclear waste repositories concerning the influence of microbial ligands produced by microorganisms on actinide migration.

The scientific results of this project are described in detail in the following sections.

2 Pyoverdins secreted by the Äspö-bacterium *Pseudomonas fluorescens* and related model compounds

2.1 The pyoverdins

Several ubiquitous *Pseudomonas* species synthesize bacterial pyoverdin-type siderophores under iron-deficient conditions [10]. In general microbes produce and secrete siderophores in concentration ranges between 0.1 and 1 μM. Pyoverdins produced by different species display many similarities: they are yellow-green, water-soluble, and, due to the presence of a chromophore, fluorescent pigments that are very effective in complexing and transport Fe^{3+} [7-10]. Structurally, they can be divided into three different parts: a) a peptide chain composed of 6 to 12 mainly hydrophilic amino acids bound via their N-termini to the carboxyl group of the chromophore, b) the chromophore (1S)-5-amino-2,3-dihydro-8,9-dihydroxy-1H-pyrimido[1,2-a]quinoline-1-carboxylic acid, and c) an acyl chain attached to the NH_2 group of the chromophore consisting of dicarboxylic acid residues, for example, succinate or its amide form depending on the growth conditions [9, 13]. The composition of the peptide chain displays great diversity depending on the producing strain. To date, more than 50 different pyoverdins have been reported in the literature [10]. So far only one pyoverdin produced by a *Pseudomonas fluorescens* strain has been structurally determined using X-ray analysis [14]. This study explores the unknown characteristics of pyoverdins secreted by the Äspö-bacterium *Pseudomonas fluorescens* (CCUG 32456). The aim is to quantify their potential to bind and thus to mobilize actinides in different oxidation states in the environment.

2.1.1 Pyoverdin isolation

Fig. 2.1 illustrates in a schematic way the pyoverdin recovery. *P. fluorescens* (CCUG 32456 A), isolated at a depth of 70 m in the Äspö Hard Rock Laboratory (Äspö HRL), Sweden [12], was grown in batch cultures under aerobic conditions. The medium used was the standard succinate medium (SSM) as described in [15]. Cultures were inoculated by adding 200 μL of the active bacterial culture, pre-grown in SSM, into 200 mL amounts of fresh growth medium. Cultures were incubated at room temperature and agitated on an SO1 orbital shaker (Stuart Scientific, GTF, Göteborg, Sweden). The yellow-green color of the SSM shows the production of pyoverdin siderophores (see Fig. 2.1). After one week, the cultures were pooled

and centrifuged at 8000 g for 10 min in a Sörvall RC-5B superspeed centrifuge (Thermo Fisher Scientific, Waltham, MA, USA).

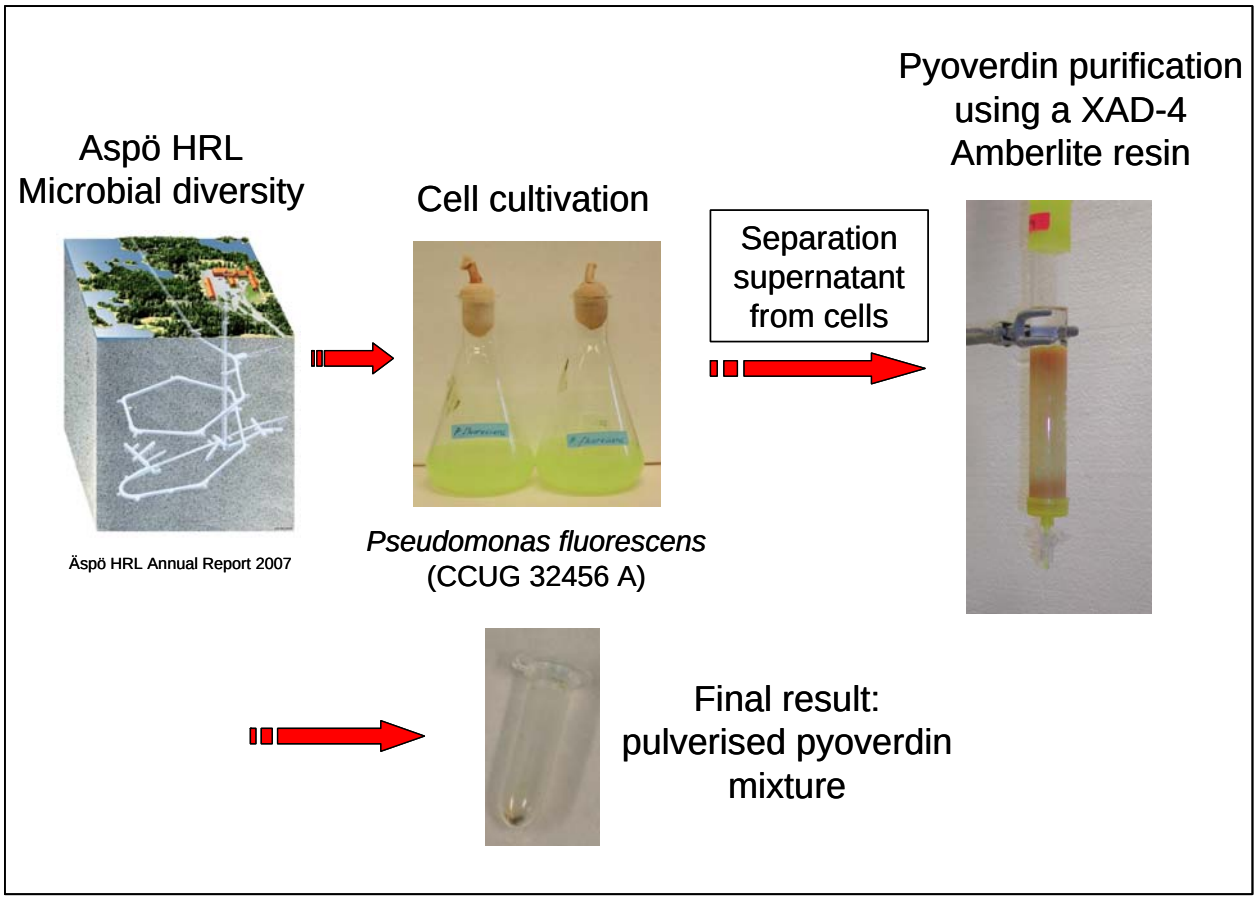

Fig. 2.1 Simplified scheme illustrating the isolation of *Pseudomonas fluorescens* (CCUG 32456) pyoverdins.

To remove cells remaining in the supernatant after centrifugation, approximately 500 mL of the supernatant was then suction-filtered through a 0.2-µm pore size BT 50 bottle top filter (Filtropur, Landskrona, Sweden) into a sterile glass bottle. The pH of the filtered supernatant was adjusted to 6.0 with 1 M NaOH, and then frozen at -18°C pending purification. The uncomplexed pyoverdin was purified from the filtered supernatant as outlined in [15]. Briefly, the filtered supernatant was loaded onto XAD-4 Amberlite resin (Rohm and Haas, Philadelphia, PA, USA), which was then rinsed with milli-Q water. The pyoverdin was eluted using 50% methanol in water, the methanol was evaporated, and the resulting pulverized pyoverdin mixtures were used for the characterization and complexation studies [16-18].

2.1.2 Pyoverdin characterization

The pulverized pyoverdin mixtures were analyzed using mass spectrometry, absorption spectroscopy (UV-vis) and time-resolved laser-induced fluorescence spectroscopy with ultrafast pulses (fs-TRLFS).

2.1.2.1 Experimental

Mass spectrometry measurements

The dry pyoverdin mixtures were dissolved in a 50:50:0.1 (v/v) water, methanol, and trifluoroacetic acid mixture. Mass spectra were obtained using a MAT 900 ST mass spectrometer equipped with an electrostatic and magnetic analyzer (EB part) using quadrupole ion trap (QIT) geometry and an electrospray ionization (ESI II) ion source (Finnigan MAT, Bremen, Germany); the spray voltage was 3.4–3.6 kV and the capillary temperature 230 °C. The monoisotopic signal of doubly charged precursor ions $[M + 2H]^{2+}$ was selected and isolated in the double focusing (EB) sector part of the mass spectrometer. Collision activation (CA) in the octapole unit in front of the QIT, He diffusing from the QIT being used as the collision gas, was followed by product ion analysis in the QIT. In CA MS^n–experiments in the QIT, precursor ion isolation and detection and product ion detection were all performed in the QIT.

Preparation of aqueous pyoverdin solutions

The pH was adjusted with $HClO_4$ or NaOH (carbonate free) and measured using a Blue Line 16 pH combined glass electrode (Schott Instruments, Mainz, Germany) and a pH540GLP pH meter (WTW, Weinheim, Germany). The electrode was calibrated using standard buffers. The pH measurements had a precision of 0.07 units. The absorption at 379 nm and the molar absorption coefficient of 20000 L mol^{-1} cm^{-1} reported in Albrecht-Gary et al. [7, 8] and in Meyer and Abdallah [15] were used in calculating the pyoverdin concentrations in this study. All experiments were made in an ionic medium in which the sodium concentration was kept constant at 0.1 M by adding analytical grade $NaClO_4$ (Merck, Darmstadt, Germany). In the UV-vis experiments the pyoverdin concentration $[LH_4]$ was fixed at 5.8×10^{-5} M while varying the pH between 3 and 10. The fs-TRLFS measurements were carried out at $[LH_4]$ 8.1×10^{-6} M between pH 2 and 9.

Absorption spectroscopy: UV-vis experimental setup

The absorption spectroscopy experiments were performed using a CARY5G UV-vis-NIR spectrometer (Varian, Palo Alto, CA, USA) at a temperature of 22 ± 1 ºC. The absorption spectra were recorded from 220 to 500 nm with a data interval of 0.1 nm. The speciation calculations were made using SOLGASWATER software [19]. Three scans were measured for each sample; the results were then averaged and baseline corrected using ORIGIN 6.1G software (OriginLab, Northhampton, MA, USA).

The complexation constants were calculated using the SPECFIT factor analysis program [20]. The approach of SPECFIT to analyze, e.g. absorption spectra, is a quantitative decomposition of the spectra of mixtures into different spectral components/constituents. This program determines the protonation/complexation constants from the variation in the absorption spectra arising from the parameter varied (e.g., pH, ligand, and/or metal concentration), the single components, their spectra, and the underlying complexation reactions.

Fluorescence spectroscopy: fs-TRLFS experimental setup

The fluorescence experiments were performed using a spectrometer consisting of a laser system as the excitation source for ultrafast laser pulses (the manufacturer of all parts of the laser system was Spectra Physics Laser Inc., Mountain View, CA, USA), a Spex 270M spectrograph (Jobin Yvon, Edison, NJ, USA) with a cuvette holder at the entrance slit, and an intensified charge-coupled device (CCD) PicoStar camera (LaVision, Göttingen, Germany) at the output. The generation of the femtosecond laser pulses starts with a Ti:sapphire oscillator (Tsunami), which is pumped by an continuous-wave Nd:YVO_4 laser (Millennia). The laser pulses are amplified (Super Spitfire), and due to the generation of third harmonics, the excitation wavelength for the pyoverdin fluorescence was set to 266 nm. The luminescence measurements were performed with a laser pulse energy of 80 μJ. A detailed description of the experimental setup can be found in [21].

2.1.2.2 Results and discussion

Characterization of the P. fluorescens (CCUG 32456) pyoverdin mixture using mass spectrometry

Fig. 2.2A shows the molecular ion region ($[M + 2H]^{2+}$) of the pyoverdin mixture secreted by *P. fluorescens* (CCUG 32456). Comparison of the fragmentation patterns of the various species obtained by collision activation with spectra obtained in collaboration with Baysse et

al. [22] indicated the presence of siderophores corresponding to those produced by the strain *P. fluorescens* ATCC 17400 [23]. Specifically, the following species were observed: *m/z* 650.24 pyoverdin with a succinamide side chain (Fig. 2.2); *m/z* 650.74 pyoverdin with a succinic acid side chain; *m/z* 644.25 ferribactin with a succinamide side chain (cf. [24]); *m/z* 659.27 ferribactin with a glutamic acid side chain; and *m/z* 653.27 and 668.27 ferribactin, which are probably the open chain analogues of *m/z* 644.25 and 659.27 ferribactin with glutamine (Gln) and 2,4-diaminobutanoic acid (Dab) instead of their tetrahydropyrimidine condensation product (cf. [25]).

A

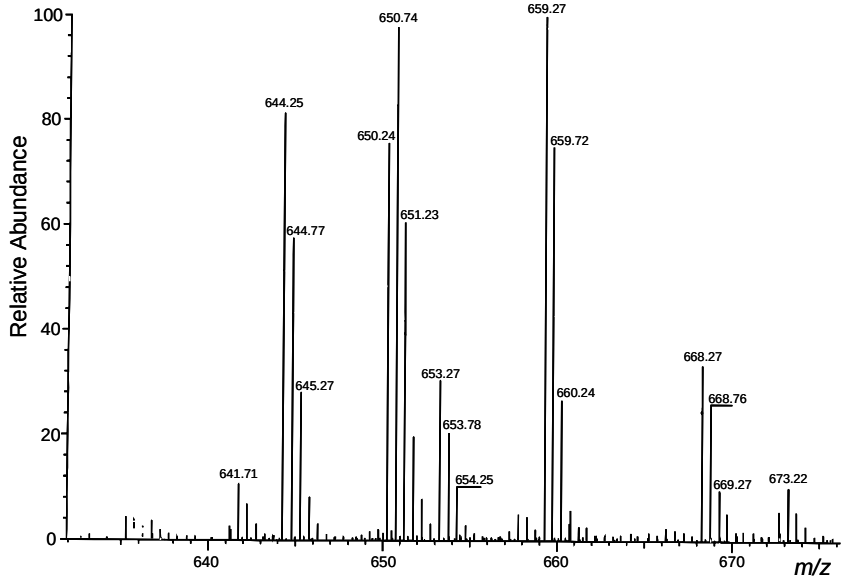

B

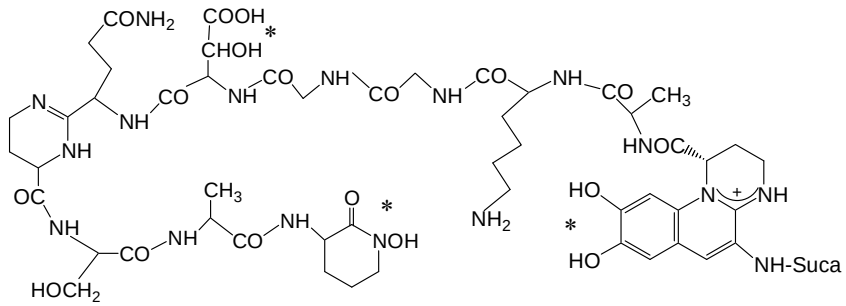

Fig. 2.2 A) Molecular ion region ($[M + 2H]^{2+}$) of the pyoverdin mixture produced from *P. fluorescens* (CCUG 32456). B) Structure of the pyoverdin from *P. fluorescens* (CCUG 32456) with a succinamide (Suca) side chain (Suca-Chr-Ala-Lys-Gly-Gly-OHAsp-(Gln-Dab)-Ser-Ala-cOHOrn). Asterisks indicate the complexation sites. The amino acids Ala, Lys, and Gln (underlined) are d-configured.

This was evident because the B_7^{++} ions (cleavage after Dab) at *m/z* 509 (side chain succinic acid amide, Suca) and *m/z* 524 (side chain glutamic acid, Glu) are very abundant, especially in the QIT product ion mass spectra, while analogous ions are missing from the spectra of the analogues with the tetrahydropyrimidine condensation product. The free Dab stabilizes the second ionizing proton. These open forms are probably not artifacts, since the tetrahydropyrimidine ring can be hydrolyzed only under extreme conditions, for example, using 6 N HCl at 90-110 °C and reaction times between 5 min and 10 h, as described in Gipp et al. [26]. As frequently observed in succinate cultures, the production of ferribactin, i.e., biogenetic precursors of pyoverdin [10], prevailed over that of pyoverdin [27], here, in a ratio of 2:1.

Protonation equilibria of the P. fluorescens (CCUG 32456) pyoverdins investigated using absorption spectroscopy (UV-vis)

The pH sensitivity of the absorption spectra of the pyoverdin mixture is depicted in Fig. 2.3A. At pH values below 5, the absorption spectra are characterized by two peaks, at 365 and 379 nm. Whereas the maximum at 365 nm decreases with increasing pH, the maximum at 379 nm remains nearly unchanged up to pH 6. In the pH region above 7, a single absorption band at 403 nm dominates the informative wavelength region.

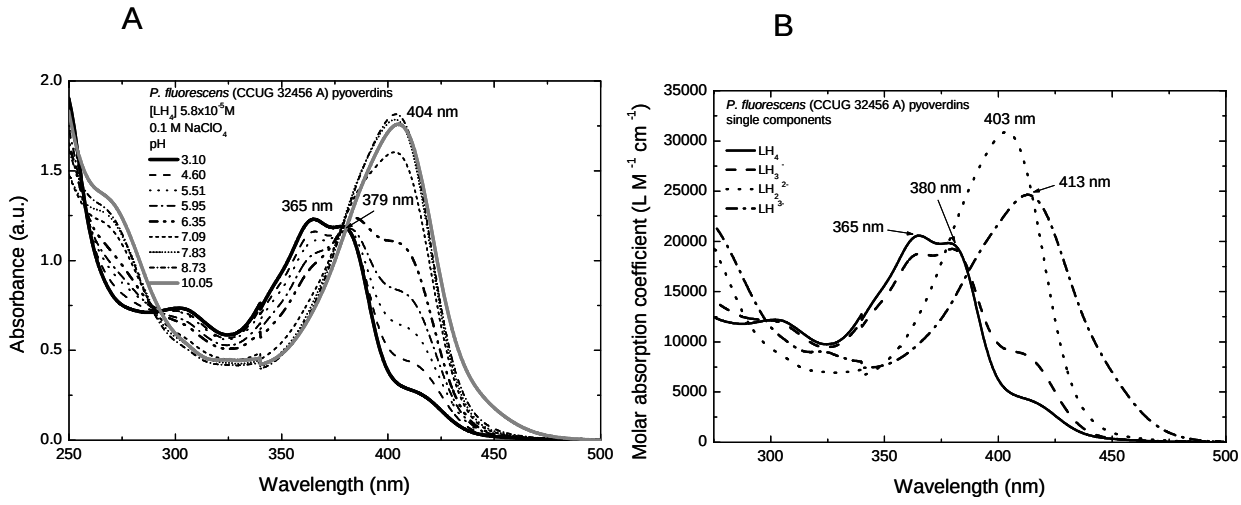

Fig. 2.3 A) Absorption spectra of the *P. fluorescens* (CCUG 32456) pyoverdin mixture as a function of pH at an ionic strength of 0.1 M ($NaClO_4$). B) Absorption spectra of the individual components of the aqueous *P. fluorescens* (CCUG 32456) pyoverdin system, as derived by peak deconvolution using SPECFIT.

In our model used in evaluating the absorption spectra, the pyoverdin molecule is denoted LH_4, according to the general assumption that pyoverdin molecules can liberate four labile protons from the complexing sites most likely responsible for metal binding [14, 28] (see also

Fig. 2.2B). Three pK values were calculated from the measured UV-vis spectra. The absorption spectrum of the deprotonated catechol-type moiety, L^{4-}, could not be characterized with sufficient accuracy, likely due to indications of the decomposition of the pyoverdin molecule at pH > 10. The value of $\log \beta_{011} = 12.20$, i.e., deprotonation of an amino acid substituent (e.g., arginine) on the peptide moiety, was taken from the literature [8]. The determined protonation reactions can be expressed as follows:

$$L^{4-} + 2H^{+} \rightleftharpoons LH_2^{2-} \quad (1)$$

$$L^{4-} + 3H^{+} \rightleftharpoons LH_3^{-} \quad (2)$$

$$L^{4-} + 4H^{+} \rightleftharpoons LH_4 \quad (3)$$

Formation constants for reactions (1)-(3) were calculated to be $\log \beta_{012} = 22.67 \pm 0.15$ ($pK_1 = 4.40$), $\log \beta_{013} = 29.15 \pm 0.05$ ($pK_2 = 6.48$), and $\log \beta_{014} = 33.55 \pm 0.05$ ($pK_3 = 10.47$), respectively. The formation constants, molar absorption coefficients, and main absorption bands of the individual species are summarized in Tab. 5.2. The calculated spectra of the different aqueous pyoverdin species are shown in Fig. 2.3B.

Aqueous species of the P. fluorescens (CCUG 32456) pyoverdins investigated using fluorescence spectroscopy with ultrafast pulses (fs-TRLFS)

In Fig. 2.4 the luminescence spectra of the *P. fluorescens* (CCUG 32456) pyoverdins are presented as a function of pH.

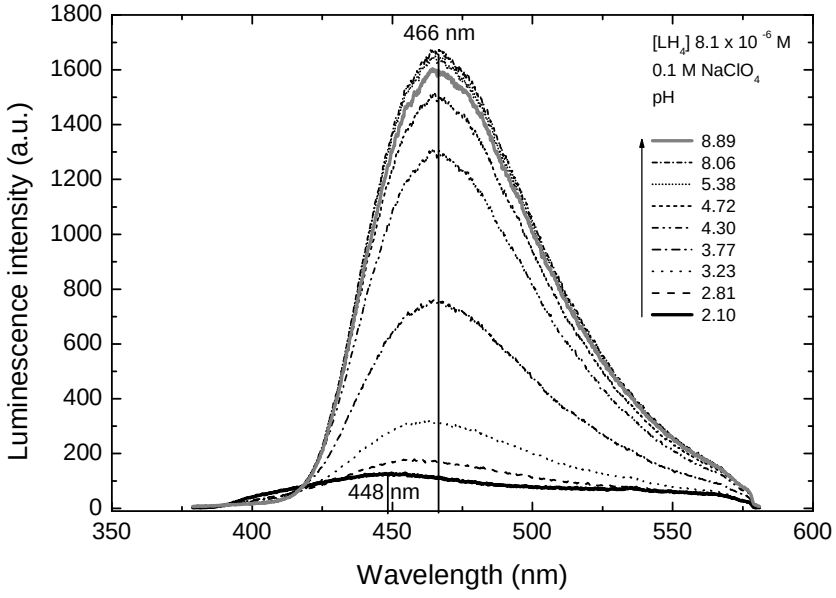

Fig. 2.4 fs-TRLFS spectra of *P. fluorescens* (CCUG 32456) pyoverdins at an ionic strength of 0.1 M ($NaClO_4$) at $[LH_4]$ 8.1×10^{-6} M as a function of pH (not all data shown).

The luminescence maximum and luminescence intensity are pH dependent: at pH 2.1 the luminescence maximum lies at 448 nm whereas between pH 3.8 and 8.9 the luminescence maximum is at 466 nm independent of pH. For comparison, a luminescence maximum of 465 nm after excitation at 405 nm was measured for a pyoverdin mixture secreted by *P. aeruginosa* ATCC 9027 [29]. A strong increase in luminescence intensity was observed between pH 2.1 and 4.7, while at pH values above 4.7 the luminescence intensity remained nearly unchanged. The SPECFIT factor analysis program was used to evaluate the measured fs-TRLFS spectra. As a result, one pK value of 3.83 could be determined, which corresponds fairly well to the pK_1 value obtained from the UV-vis measurements. The single-component spectra of the species 0:1:4 and 0:1:3 are then used as input values for evaluating the data from the UO_2^{2+} experiments. The other pyoverdin species could not be distinguished on the basis of the measured TRLFS data because of the consistency and near similarity of their individual luminescence spectra. Time-resolved measurements indicated that the luminescence decay of the *P. fluorescens* (CCUG 32456) pyoverdins in aqueous solution was dependent on the pH. At pH < 3.0, bi-exponential decay behavior involving a fast decay component with a decay time of 2135 ± 600 ps and a second luminescence component with a longer decay time of 5865 ± 638 ps were detected. The fast luminescence decay component decreased to 580 ± 195 ps between pH 3 and 4, whereas the lifetime of the second luminescence component remained unchanged. At pH > 4.0, mono-exponential luminescence behavior with a decay time of 5865 ± 638 ps is dominant.

Summary

The spectroscopic characteristics of the studied bioligand mixture are determined by the pyoverdin chromophore. The approach taken in this study was, thus to explore the UO_2^{2+} complexation behavior of the pyoverdin mixture of *P. fluorescens* (CCUG 32456) using UV-vis spectroscopy. The visible absorption bands shown in Fig. 2.3A are dominated by the pyoverdin chromophore even when the pyoverdin mixture contained 1/3 pyoverdins and 2/3 ferribactins. An indication in the UV-vis spectra of the presence of ferribactin might be the shoulder at 270 nm observed at pH values above 7 (Fig. 2.3A), possibly resulting from tyrosine (the ferribactin chromophore is a condensation product of D-tyrosine and L-2,4-diaminobutanoic acid; [10]). Ferribactins exhibit no characteristic absorption bands in the evaluated wavelength range between 275 and 500 nm under the given experimental conditions (Fig. 2.3A). Moreover, the complexation of ferribactin with Fe^{3+} is over nine orders of magnitude weaker than that of pyoverdins [30]. Therefore, we conclude that the

presence of ferribactins does not affect the evaluation of either the UV-vis spectra or the UO_2^{2+}–pyoverdin formation constants determined in this study. Comparing our spectrophotometric titration results with those reported in the literature revealed close agreement regarding the absorption band positions and spectrum shapes of the various pyoverdins observed, for example, pyoverdins isolated from different Pseudomonads [8, 10, 14, 28]. This indicates that different strains of *P. fluorescens* produce pyoverdins with similar absorption properties, due to identical chromophore structures, even when grown under different conditions. Moreover, this might suggest similar coordination environments for the metals provided by the individual pyoverdin molecules.

The determined pH-dependent variations in luminescence intensity shown in Fig. 2.4 reflect the well-known pH relationship of benzoic hydroxyl compounds as described in [31]. At low pH, the OH groups, for example, of the chromophore, are protonated and the luminescence is weak, while at pH > 3, deprotonation of the OH groups leads to an increase in luminescence intensity. Kumke et al. observed such changes in luminescence intensity with pH in their investigations of the artificial siderophore pyridinochelin in aqueous solutions [31].

2.2 Pyoverdin model compounds

The structure of one pyoverdin-molecule present in the secreted bioligand mixture from *P. fluorescens* (CCUG 32456) is depicted in Fig. 2.2B. The metal complexation sites are marked. Hence, the functional groups that participate in the metal binding are the catechol group of the chromophore and two ligand sites in the peptide chain, i.e. one or two hydroxamate groups, whereas the α-hydroxy acid moieties seem to be of less importance. As shown, the pyoverdin molecule provides different functional groups for metal ion coordination. For an estimate which functional group contributes more in actinide binding the following model systems were investigated: a) simple hydroxamates: salicylhydroxamic acid (SHA) and benzohydroxamic acid (BHA); b) a trihydroxamate: desferrioxamine B (DFO); and c) catecholates: 6-hydroxyquinoline (6-HQ) and 2,3-dihydroxynaphthalene (NAP).

2.2.1 Experimental

The aqueous speciation of the model ligands was investigated based on their spectroscopic properties. We used absorption spectroscopy and fs-TRLFS. The experimental details of both techniques are summarized in chapter 2.1.2.1. The dissociation constants were calculated based on the variations in the measured spectra using the factor analysis program SPECFIT

[20]. Three scans were measured for each sample; the results were then averaged and baseline corrected using ORIGIN 6.1G software (OriginLab, Northhampton, MA, USA).

As a background electrolyte, analytical grade 0.1 M $NaClO_4$ (Merck, Darmstadt, Germany) was used. The pH was measured using an InLab 427 combination pH puncture electrode (Mettler-Toledo, Giessen, Germany) calibrated with standard buffers. The pH was changed by adding analytical grade NaOH or $HClO_4$ with an accuracy of ± 0.02 units. SHA, BHA, and NAP were of analytical grade. The purity of 6-HQ and DFO were 95%. SHA, DFO and 6-HQ were provided by Sigma-Aldrich, Germany whereas BHA and NAP were ordered from Merck, Germany. The stock solutions of the ligands were freshly prepared for each experiment.

The concentration of the hydroxamate ligands was fixed at 1×10^{-4} M while the pH was changed between 2 and 13. The concentration of the catecholate ligands was held constant at 5×10^{-5} M. In general the pH-dependent ligand absorption bands between 190 and 420 nm were evaluated. The NAP concentration during the fs-TRLFS measurements was 1×10^{-4} M and the luminescence bands were detected between 300 and 470 nm.

2.2.2 Results and discussion

2.2.2.1 Hydroxamate models

SHA

Salicylhydroxamic acid (SHA) was a model ligand for the hydroxamate functionality of the pyoverdins. The structure of SHA is depicted in Fig. 2.5. SHA has two functional groups, the hydroxamic acid group and the phenolic hydroxyl group.

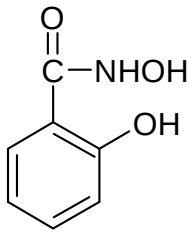

Fig. 2.5 Structure of salicylhydroxamic acid (SHA).

Fig. 2.6 shows the measured absorption spectra of salicylhydroxamic acid as a function of pH and the absorption spectra of the single components in the aqueous system of SHA calculated with the factor analysis program SPECFIT. SHA can liberate two protons, one from the OH-group of the hydroxamic acid function and one from the phenolic hydroxyl group.

Therefore, SHA forms three different species in aqueous solution: the protonated form $HOC_6H_4CONHOH$ in the acid pH-range, the single deprotonated form $HOC_6H_4CONHO^-$ in the pH region between 7 and 10 and the doubled deprotonated form $OC_6H_4CONHO^{2-}$ at pH values greater than 10. The protonation reactions can be written as follows:

$$OC_6H_4CONHO^{2-} + H^+ \rightleftharpoons HOC_6H_4CONHO^- \qquad \log \beta_{011} \qquad (4)$$

$$OC_6H_4CONHO^{2-} + 2H^+ \rightleftharpoons HOC_6H_4CONHOH \qquad \log \beta_{012} \qquad (5)$$

The formation constants for the reaction (4) and (5) were calculated to be $\log \beta_{011} = 10.05 \pm 0.03$ and $\log \beta_{012} = 17.72 \pm 0.09$ ($pK_1 = 7.67$, $pK_2 = 10.05$), respectively.

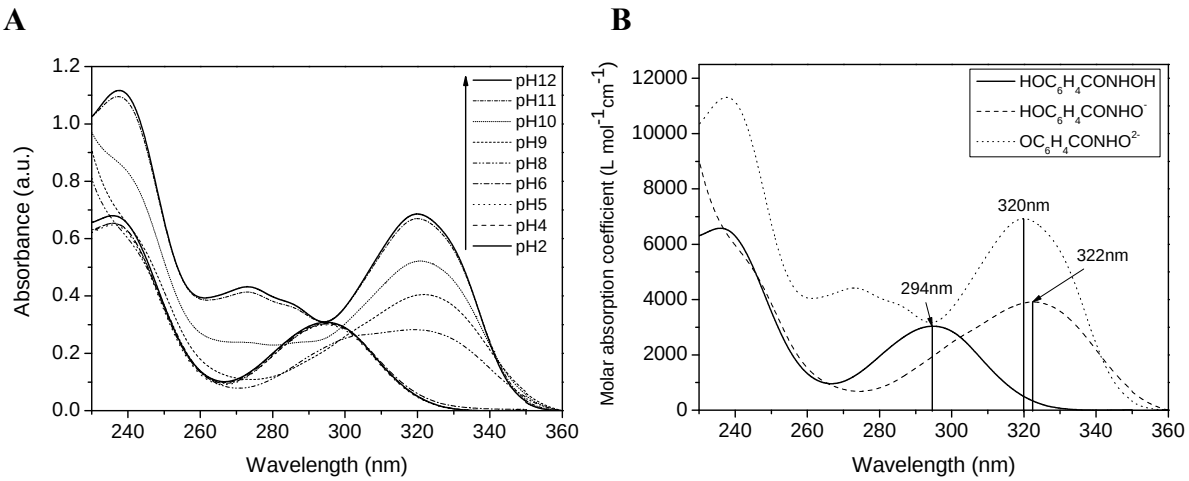

Fig. 2.6 A) Absorption spectra of [SHA] 1×10^{-4} M at an ionic strength of 0.1 M ($NaClO_4$) as a function of pH. B) Absorption spectra of the single components in the aqueous system of SHA.

Formation constants, molar absorption coefficients, and main absorption bands of the individual species are summarized in Tab. 2.1. The calculated spectra of the three different aqueous species are shown in Fig. 2.6B.

Tab. 2.1 Summary of formation constants, molar absorption coefficients and main absorption bands of the individual species of SHA.

Species	***p q r***	**log β**	**ε [$Lmol^{-1}cm^{-1}$]**	**λ_{max} [nm]**
$OC_6H_4CONHO^{2-}$	0 1 0		6924	320
$HOC_6H_4CONHO^-$	0 1 1	10.05 ± 0.03	3894	322
$HOC_6H_4CONHOH$	0 1 2	17.72 ± 0.09	3030	294

The protonation constants determined with absorption spectroscopy are in good agreement with the constants from the literature [32] determined by potentiometric titration ($\log \beta_{011} = 9.68 \pm 0.01$, $\log \beta_{012} = 17.18 \pm 0.01$).

BHA

Benzohydroxamic acid (BHA) was a further model ligand for the hydroxamate functionality of the pyoverdins. In contrast to SHA, BHA contains no phenolic OH-group. Fig. 2.7 shows the structure of BHA.

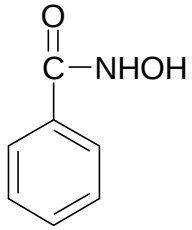

Fig. 2.7 Structure of benzohydroxamic acid (BHA).

Fig. 2.8 illustrates the measured absorption spectra of BHA as a function of pH and the calculated spectra of the two different aqueous species of BHA.

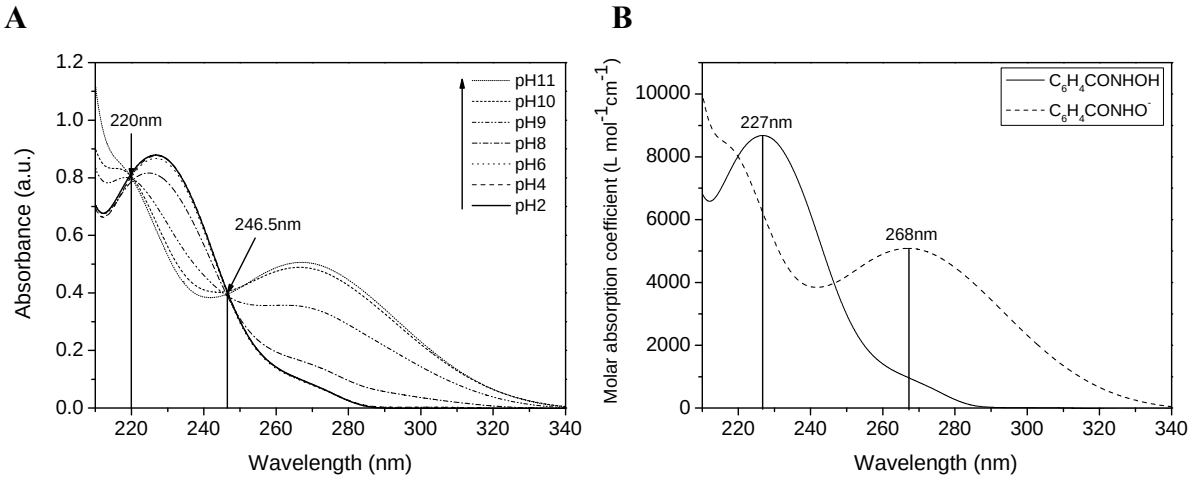

Fig. 2.8 A) Absorption spectra of [BHA] 1×10^{-4} M at an ionic strength of 0.1 M ($NaClO_4$) as a function of pH. B) Absorption spectra of the single components in the aqueous system of BHA.

Benzohydroxamic acid forms two species in aqueous solution, the protonated neutral form $C_6H_4CONHOH$ in the pH range less than 9 and the negative charged deprotonated form $C_6H_4CONHO^-$ at pH values above 9. Two isosbestic points at 220.0 nm and 246.5 nm were observed in the absorption spectra shown in Fig. 2.8A. At these wavelengths the different species have the same molar absorption coefficient. The protonation reaction can be described as follows:

$$C_6H_4CONHO^- + H^+ \rightleftharpoons C_6H_4CONHOH \qquad \log \beta_{011} \qquad (6)$$

The calculated protonation constant $\log \beta_{011} = 8.76 \pm 0.05$ is in good agreement with the constant from the literature $\log \beta_{011} = 8.78 \pm 0.01$ [33] determined with potentiometric titration. The molar absorption coefficients and the main absorption bands are summarized in Tab. 2.2. The determined spectra of the two aqueous species of BHA are shown in Fig. 2.8B.

Tab. 2.2 Summary of formation constant, molar absorption coefficients and main absorption bands of the individual species of BHA.

Species	***p q r***	**log β**	**ε [Lmol^{-1}cm^{-1}]**	**λ_{max} [nm]**
$C_6H_4CONHO^-$	0 1 0		5055	268
$C_6H_4CONHOH$	0 1 1	8.76 ± 0.05	8664	227

DFO

Desferrioxamine B (DFO) is a natural microbially produced linear trihydroxamate ligand. The structure (Fig. 2.9) is characterized by three hydroxamic acid groups and a terminal NH_2-group as functionality. DFO was chosen as model ligand for the pyoverdins to compare the stability constants and spectroscopic properties with those of the pyoverdins. Therefore, it is possible to estimate the influence of the hydroxamate groups to the complex formation of the pyoverdins with actinides.

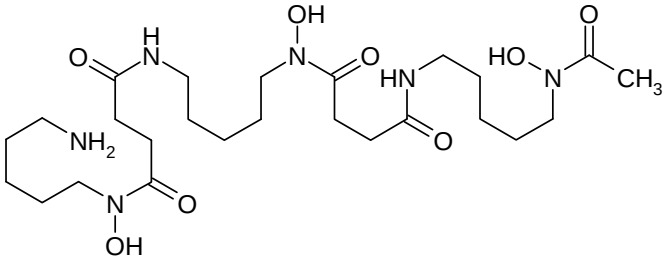

Fig. 2.9 Structure of desferrioxamine B (DFO).

Fig. 2.10 shows the measured absorption spectra of DFO as a function of pH and the absorption spectra of the single components in the aqueous system of DFO calculated with SPECFIT. DFO forms five different species in aqueous solution. The protonation reactions can be expressed as follows:

$$C_{25}H_{45}N_6O_3^{3-} + H^+ \rightleftharpoons C_{25}H_{45}N_6(OH)O_2^{2-} \qquad \log \beta_{011} \qquad (7)$$

$$C_{25}H_{45}N_6O_3^{3-} + 2H^+ \rightleftharpoons C_{25}H_{45}N_6(OH)_2O^- \qquad \log \beta_{012} \qquad (8)$$

$$C_{25}H_{45}N_6O_3^{3-} + 3H^+ \rightleftharpoons C_{25}H_{45}N_6(OH)_3 \qquad \log \beta_{013} \qquad (9)$$

$$C_{25}H_{45}N_6O_3^{3-} + 4H^+ \rightleftharpoons C_{25}H_{45}N_6(OH)_3H^+ \qquad \log \beta_{014} \qquad (10)$$

Formation constants for the reactions (7)-(10), molar absorption coefficients and main absorption bands for the different species are summarized in Tab. 2.3. The calculated spectra of the five different aqueous species of DFO are shown in Fig. 2.10B.

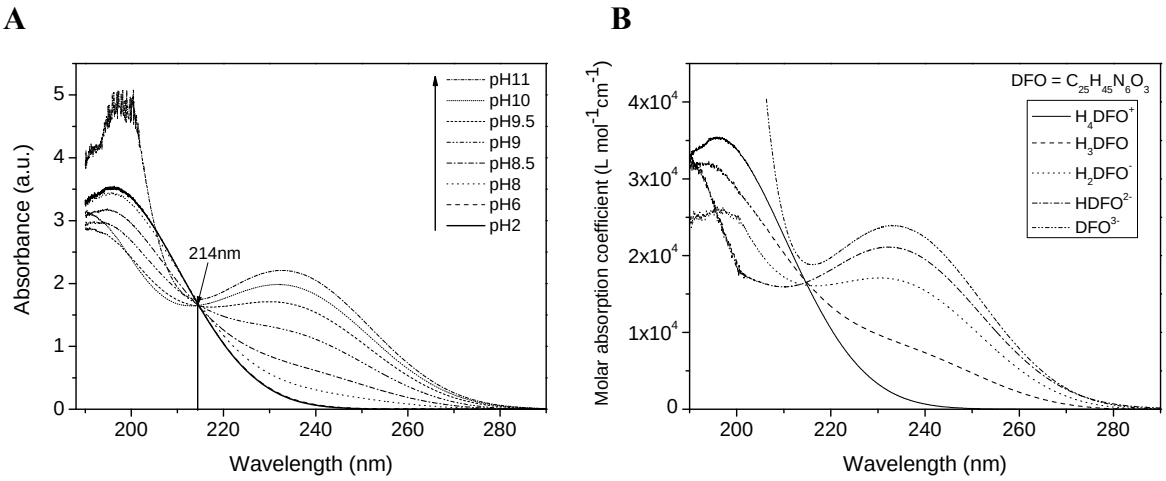

Fig. 2.10 A) Absorption spectra of [DFO] 1×10^{-4} M at an ionic strength of 0.1 M ($NaClO_4$) as a function of pH. B) Absorption spectra of the single components in the aqueous system of DFO.

Tab. 2.3 Summary of formation constants, molar absorption coefficients and main absorption bands of the individual species of DFO.

Species	***p q r***	**log β**	**ε [$Lmol^{-1}cm^{-1}$]**	**λ_{max} [nm]**
$C_{25}H_{45}N_6O_3^{3-}$	0 1 0		24160	233
$C_{25}H_{45}N_6(OH)O_2^{2-}$	0 1 1	*11.18 ± 0.39*	*21007*	*233*
$C_{25}H_{45}N_6(OH)_2O^{-}$	0 1 2	20.78 ± 0.53	23725 17229	194 231
$C_{25}H_{45}N_6(OH)_3$	0 1 3	29.72 ± 0.55	31739 7351	191 233
$C_{25}H_{45}N_6(OH)_3H^{+}$	0 1 4	38.08 ± 0.66	35070	195

The determined protonation constants of DFO are $pK_1 = 8.36$, $pK_2 = 8.94$, $pK_3 = 9.60$ and $pK_4 = 11.18$. For the last protonation constant of 11.18 only an estimated value can be given, because the measurement of the absorption as a function of pH could be done only to pH 11.
The protonation constants determined by spectroscopy are in very good agreement with the values from the literature [34] determined with potentiometric titration ($pK_1 = 8.30$, $pK_2 = 9.00$, $pK_3 = 9.46$, $pK_4 = 10.84$).

2.2.2.2 Chromophore models

6-HQ

6-hydroxyquinoline (6-HQ) was chosen as a model ligand for the chromophore functionality of the pyoverdins. 6-HQ forms four different species, the neutral molecule (N), the cation (C), the anion (A) and the zwitterion (Z). Two or more ions of these forms coexist in hydroxylic solutions. Fig. 2.11 shows the structures of the different species and the equilibration between them. At pH values lower than 3 the cationic form, at pH values above 11 the anionic form and at pH 7 the neutral form are predominant [35].

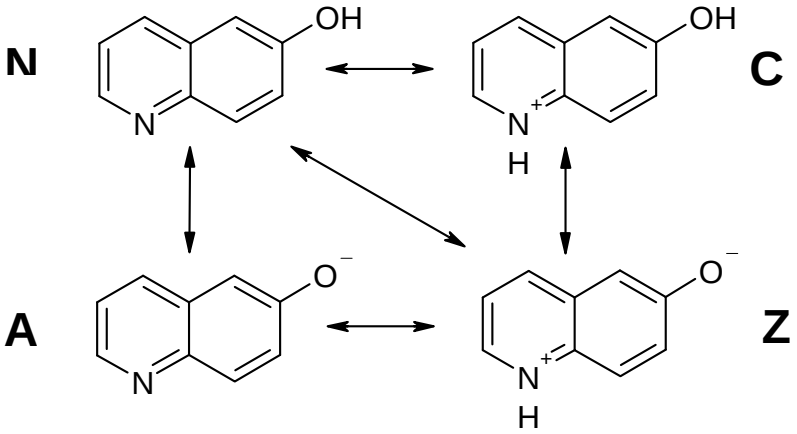

Fig. 2.11 Structure and different protonation species in aqueous solution of 6-hydroxyquinoline (6-HQ).

Fig. 2.12 depicts the measured absorption spectra of 6-HQ as a function of pH and the calculated spectra of the different aqueous species of 6-HQ.

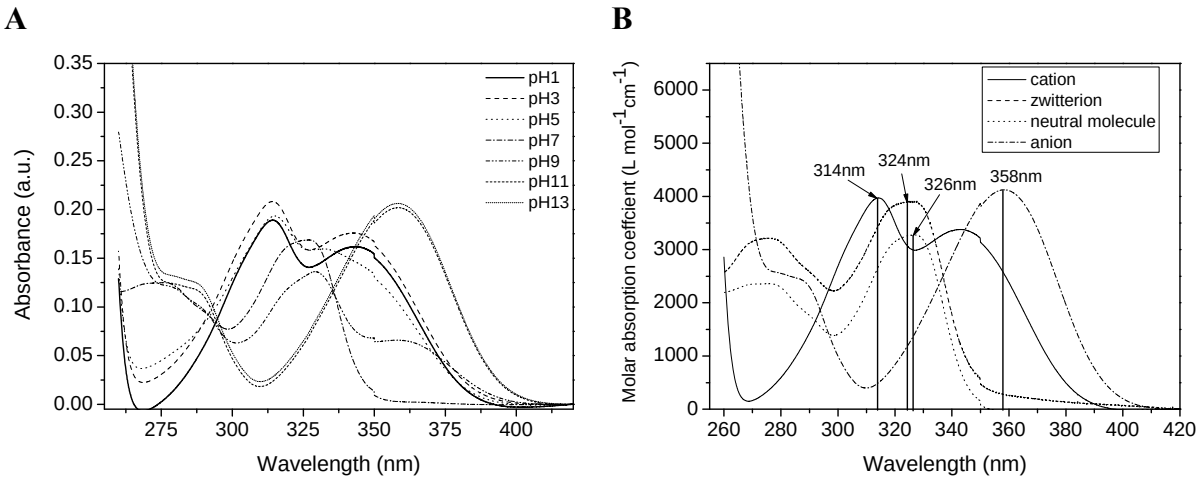

Fig. 2.12 A) Absorption spectra of [6-HQ] 5×10^{-5} M at an ionic strength of 0.1 M ($NaClO_4$) as a function of pH. B) Absorption spectra of the single components in the aqueous system of 6-HQ.

Four different species of 6-HQ in aqueous solution could be identified with the factor analysis program SPECFIT, the cation, the anion, the zwitterion and the neutral molecule. This is in agreement with the species described in the literature [35]. Because the neutral molecule and the zwitterion have very similar main absorption bands and molar absorption coefficients, it was not possible to discriminate these two species.

Tab. 2.4 summarizes the calculated protonation constants, main absorption bands and molar absorption coefficients of the individual species of 6-HQ. The determined spectra of the four aqueous species of 6-HQ are shown in Fig. 2.12B.

The protonation constant for the zwitterion could not be calculated. The protonation constants determined with SPECFIT are slightly different from the literature values ($pK_C = 5.18$, $pK_Z = 7.02$, $pK_N = 7.03$, $pK_A = 8.87$) [35]. A possible reason therefore could be the very similar absorption spectra of the neutral molecule and the zwitterion.

Tab. 2.4 Summary of protonation constants, molar absorption coefficients and main absorption bands of the individual species of 6-HQ.

Species	**pK_A**	**ε [$Lmol^{-1}cm^{-1}$]**	**λ_{max} [nm]**
Cation	5.62 ± 0.23	3960	314
Zwitterion		3880	324
neutral molecule	6.34 ± 0.58	3273	326
Anion	9.32 ± 0.07	4130	358

NAP

A further model ligand for the chromophore functionality of the pyoverdins was 2,3-dihydroxynaphthalene (NAP). The structure of NAP is shown in Fig. 2.13.

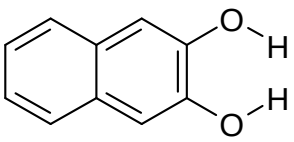

Fig. 2.13 Structure of 2,3-dihydroxynaphthalene (NAP).

Fig. 2.14 illustrates the measured absorption spectra of NAP as a function of pH and the calculated spectra of the different aqueous species of NAP. NAP forms three different species in aqueous solution, the protonated neutral form $C_{10}H_6(OH)_2$ at pH values lower than 8, the single deprotonated form $C_{10}H_6OHO^-$ in the pH region between 8 and 12 and the deprotonated form $C_{10}H_6O_2^{2-}$ at pH values above 12. The protonation reactions can be written as follows:

$$C_{10}H_6O_2^{2-} + H^+ \rightleftharpoons C_{10}H_6OHO^- \qquad \log \beta_{011} \qquad (11)$$

$$C_{10}H_6O_2^{2-} + 2H^+ \rightleftharpoons C_{10}H_6(OH)_2 \qquad \log \beta_{012} \qquad (12)$$

Formation constants for the reactions (11) and (12), molar absorption coefficients and main absorption bands for the different species are summarized in Tab. 2.5. The calculated spectra of the three different aqueous species of NAP are shown in Fig. 2.14B.

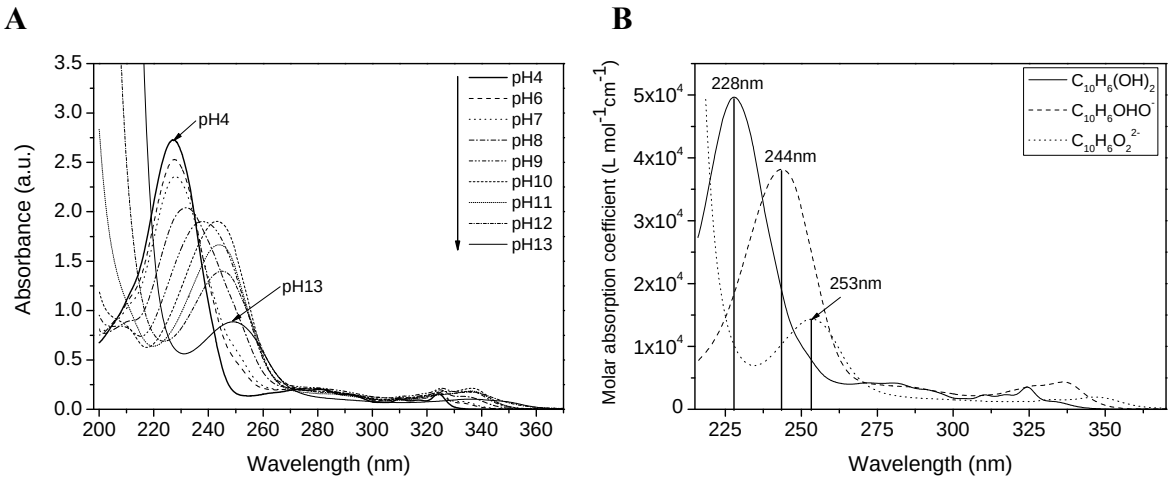

Fig. 2.14 A) Absorption spectra of [NAP] 5×10^{-5} M at an ionic strength of 0.1 M ($NaClO_4$) as a function of pH. B) Absorption spectra of the single components in the aqueous NAP system.

Tab. 2.5 Summary of formation constants, molar absorption coefficients and main absorption bands of the individual species of NAP.

Species	***p q r***	**log β**	**ε [Lmol^{-1}cm^{-1}]**	**λ_{max} [nm]**
$C_{10}H_6O_2^{2-}$	0 1 0		14225	253
$C_{10}H_6OHO^-$	0 1 1	12.37 ± 0.20	38056	244
$C_{10}H_6(OH)_2$	0 1 2	21.39 ± 0.33	49609	228

The determined protonation constants of NAP are $pK_1 = 8.02$ and $pK_2 = 12.37$. They are in agreement with the values from the literature [36] determined with potentiometric titration ($pK_1 = 8.68$, $pK_2 = 12.50$).

Furthermore, the pH dependence of the luminescence spectra of NAP was determined using fs-TRFLS. Fig. 2.15 shows the measured luminescence spectra as a function of pH and the luminescence spectra of the identified single components in the aqueous system of NAP. In the pH range lower than 8, the luminescence spectra are characterized by an emission maximum at 342 nm with two shoulders at 327 and 350 nm. At pH values greater than 8, a second species with an emission maximum at 417 nm dominates more and more the

luminescence spectra. A slightly increase of the luminescence intensity was observed up to pH 5.4. Then a decrease of the luminescence intensity was identified with increasing pH. At the pH range above 10 the luminescence intensity was independent of the pH. The two identified species are characterized by luminescence lifetimes of 12.5 and 1.63 ns, respectively.

The calculation of the protonation constants was made with the factor analysis program SPECFIT based on the observed changes in the luminescence spectra of NAP by varying the pH.

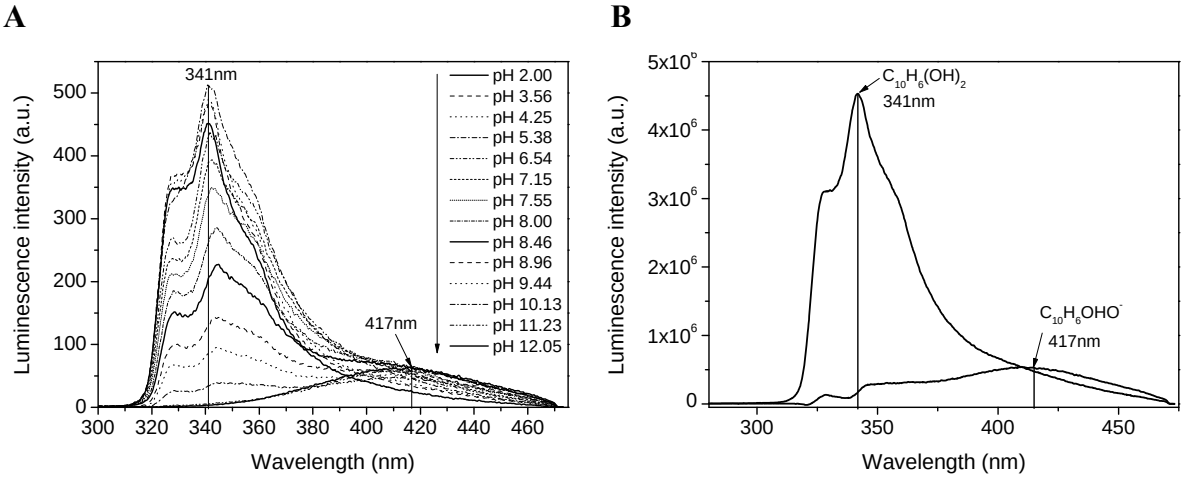

Fig. 2.15 A) fs-TRLFS spectra of [NAP] 1×10^{-4} M at an ionic strength of 0.1 M ($NaClO_4$) as a function of pH. B) Luminescence spectra of the single components in the aqueous NAP system.

The protonation constant was determined to be 8.37 ± 0.11, which correspond well to the pK_1 value obtained from the absorption spectroscopy measurements. It was not possible to determine the second protonation constant according to deprotonation of the second catechol group with fs-TRLFS because of the high protonation constant of 12.4.

2.3 Models simulating the functionality of the bacteria cell wall – Isolated bacterial cell wall components

Due to differences in the cell wall structure bacteria can be divided into two major groups: Gram-positive and Gram-negative (see Fig. 2.16). Lipopolysaccharide (LPS) is one important compartment of the cell envelope of Gram-negative bacteria (Fig. 2.16). It is embedded in the outer membrane and sticks out in the outer environment of the microbe. LPS plays a key role in protection of contaminants and selective assimilation of needful small molecules or metals. It constitutes about 30 % of the whole cell wall of Gram-negative bacteria, and contains

especially a high amount of phosphoryl groups, beneath other functionalities for metal binding like carboxyl, hydroxyl or amino groups.

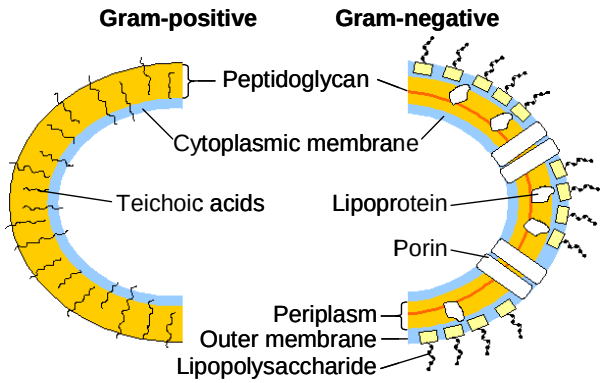

Fig. 2.16 Scheme of bacterial cell walls of Gram-positive and Gram-negative bacteria.

Peptidoglycan (PG) is the main part of Gram-positive cell walls, and also Gram-negative cell walls have a thin PG layer (Fig. 2.16). It consists of polysaccharide (glycan) chains which are crosslinked with oligopeptide units. Functionalities of interest for metal binding are carboxyl and amino groups from the peptide chains, and hydroxyl groups from the polysaccharide chains; phosphoryl groups are missing in PG, they are provided by the teichoic acids. We investigated the interaction processes of LPS from *Pseudomonas aeruginosa* S10 and PG from *Bacillus subtilis* with the selected actinides [37, 38]. The aims are a systematic study of actinide interactions with isolated cell wall compartments on a molecular level and a comparison of their stability constants with those measured with the pyoverdins. From the strength of the individual stability constants one can estimate if the actinides are primarily bound by the cells (isolated cell compartments) or by the secreted pyoverdins. In this chapter we describe the determination of the deprotonation constants and site densities of the individual functional groups of both biomacromolecules [37, 38].

2.3.1 Experimental

Solutions and reagents

Peptidoglycan (PG) from *B. subtilis* was purchased from Fluka and used without further purification. In water it is relatively poorly soluble, which restricted its experimental concentration to 0.2 g/L. Lipopolysaccharide (LPS) from *P. aeruginosa* S10, prepared by trichloroacetic acid extraction, was purchased from Sigma and used without further purification. The ionic strength was kept constant for all experiments at 0.1 M by adding stock

solutions from $NaClO_4 \times H_2O$ (Merck, p.A.). All solutions were prepared with carbonate free deionized water.

Potentiometric titrations

The potentiometric titration experiments were carried out in a glove box under inert gas atmosphere (nitrogen) excluding CO_2 from air to avoid unwanted carbonate complexation at 22 ± 1 °C. The ionic strength was kept constant at 0.1 M by adding $NaClO_4 \times H_2O$ (Merck, p.A.). For each LPS titration, 10 mg LPS was dissolved in 50 mL water, resulting in an LPS concentration of 0.2 g/L. Three samples were acidified with $HClO_4$ (carbonate free) to obtain a starting pH of about 4 and were titrated with 1 mM NaOH (carbonate free, Merck, Titrisol), and three samples were alkalized with NaOH to obtain a starting pH of about 10 and were titrated with 1 mM $HClO_4$ (carbonate free; exact molarity was determined with 0.01 M NaOH, Merck, Titrisol).

For each PG titration (5 measurements), 3 mg PG was dissolved in 30 mL water, resulting in a PG concentration of 0.1 g/L. The mixtures were acidified with 6 µmol $HClO_4$ (2×10^{-4} M) to obtain a starting pH of about 4 and titrated with 10^{-3} M NaOH (Merck, Titrisol).

The pH values were measured with a BlueLine 16 pH electrode (Schott). The electrode was calibrated for each experiment with NBS buffers (4.01 and 6.86, Schott). All samples were titrated with an automatic titrator (TitroLine alpha, Schott) and monitored by the accompanied software (Titrisoft 2.1, Schott). The titration procedure was a dynamic titration with a minimum drift of 5 mV/min. The titration curves were analyzed with the programs ProtoFit 2.3 [39] (LPS) and HYPERQUAD 2006 [40] (PG).

2.3.2 Results and discussion

The data of the biopolymer titrations were analyzed based on the deprotonation of discrete monoprotic acids according to the reaction

$$R\text{–}A_iH \rightleftharpoons R\text{–}A_i^- + H^+, \tag{13}$$

where R is the polymer with the attached functional groups A_i. The corresponding proton binding constant K_a can be written as

$$K_a = \frac{[R - A_i^-][H^+]}{[R - A_iH]}. \tag{14}$$

[R–A_i^-] and [R–A_iH] represent the concentrations of the deprotonated and protonated form of the functional group A_i, respectively, and [H^+] represents the proton concentration in the solution. The following deprotonation reactions are possible in the aqueous biomacromolecule solutions:

$$R\text{–}COOH \rightleftharpoons R\text{–}COO^- + H^+, \tag{15}$$

$$R\text{–}O\text{–}PO_3H^- \rightleftharpoons R\text{–}O\text{–}PO_3^{2-} + H^+ \tag{16}$$

$$R\text{–}NH_3^+ \rightleftharpoons R\text{–}NH_2 + H^+, \tag{17}$$

$$R\text{–}OH \rightleftharpoons R\text{–}O^- + H^+. \tag{18}$$

Lipopolysaccharide (LPS) [37]

Fig. 2.17 depicts the structure of the LPS molecule of *Pseudomonas aeruginosa* [41, 42]. The whole LPS molecule can be divided into three main parts: the lipid A, the core region and the repeating unit, the O-antigen. Mainly the core region contains a high density of phosphoryl and carboxyl groups.

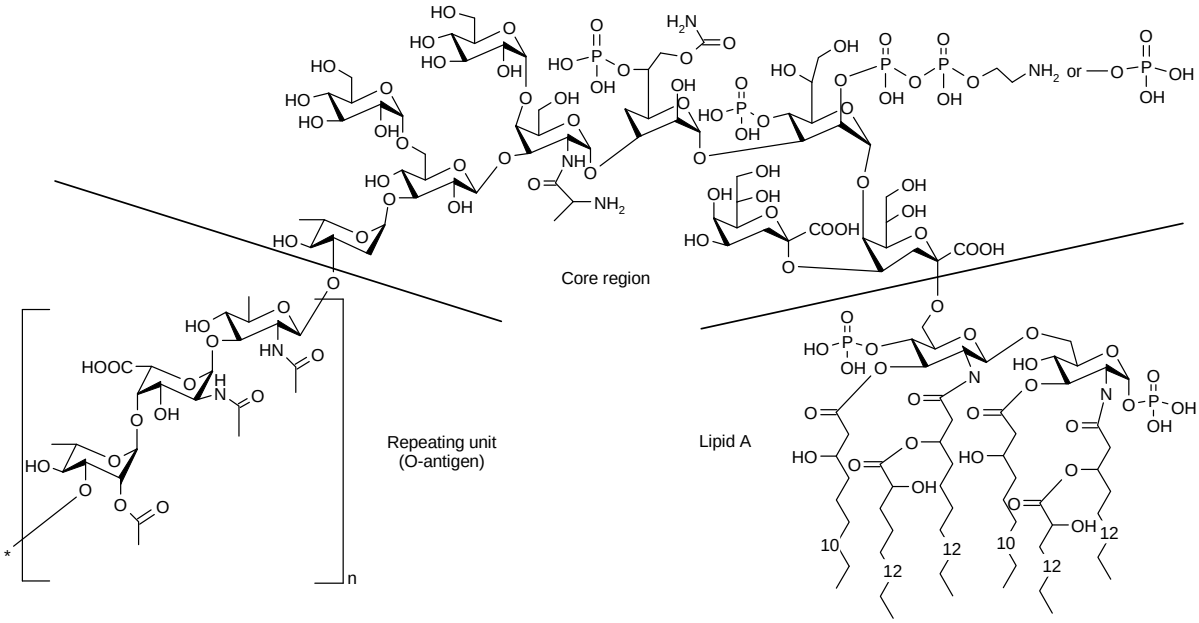

Fig. 2.17 Structure of LPS [41, 42].

The best fit of the titration data of LPS was obtained with a four-site model. The results are summarized in Tab. 2.6. The pK_a of 5.56 ± 0.28 can be assigned to carboxyl groups, the pK_a of 6.96 ± 0.24 to the second dissociation step of phosphoryl groups, and the pK_a of 8.90 ± 0.56 to amino or hydroxyl groups. With some test solutions titrated up to pH 11 an additional pK_a over 10 could be detected, due to the dissociation of amino or hydroxyl groups,

too. The site densities of carboxyl and phosphoryl groups are with about 0.3 mmol/g LPS nearly equal. This result is easy explainable with the structure model (Fig. 2.17). Altogether, we have four to five end standing phosphoryl groups in the core region and on the N-acetylglucosamine units of the Lipid A part. In the core region there are only two carboxyl groups to be found, but the repeating unit contains carboxyl groups, too. Depending on the repeating factor n of the O-antigen, the amount of carboxyl groups is variable. The site density of the third functional group of about 0.6 mmol/g LPS is afflicted with a relatively large error, but it is considerably less than those of the fourth functionality. If we compare these concentration values with the structure model (Fig. 2.17), we can dedicate the third dissociation constant of about 8.9 to amino groups and the fourth one, which is higher than 10, to hydroxyl groups. There are at least three NH_2-units to be found in the core region, and in the repeating unit it is possible, that some amino groups are not acetylated. Hence the amount of amino groups is variable, too. Nevertheless, the density of hydroxyl groups is much higher.

Tab. 2.6 Summary of the calculated pK_a values and site densities from potentiometric titration for LPS from *P. aeruginosa.*

pK_a	**Site density [mmol/g LPS]**	**Functionality**
5.56 ± 0.28	0.32 ± 0.12	Carboxyl
6.96 ± 0.24	0.31 ± 0.09	Phosphoryl
8.90 ± 0.56	0.63 ± 0.42	Amine
> 10	> 1.5	Hydroxyl

Peptidoglycan [38]

Fig. 2.18 shows the structure of a single PG unit of *Bacillus subtilis*. The PG macromolecule consists of repeating *β*(1-4)-linked *N*-acetylglucosaminyl-*N*-acetylmuramyl (NAG, NAM) dimers with a short stem of four amino acids (Fig. 2.18). The peptide chains are cross-linked through D-alanyl-diaminopimelyl bonds. The average degree of peptide cross-linking is 30-35 % [43]. Whereas LPS contains all functional groups of reactions (15) – (18), phosphoryl groups are missing in PG. Here are only the deprotonation reactions (15), (17), and (18) possible. Glutamic acid and diaminopimelic acid contain the free carboxyl groups of interest for metal ion complexation. Furthermore, amino groups of not cross-linked amino acids or even amides and also hydroxyl groups from the sugars NAG and NAM are potential coordination functionalities for metal ions.

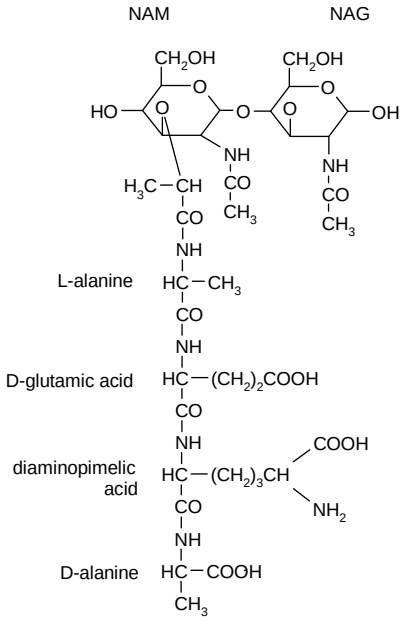

Fig. 2.18 Structure of a peptidoglycan chain, based on literature [44]. NAM = N-acetylmuramic acid; NAG = N-acetylglucosamine.

Tab. 2.7 Summary of the calculated pK_a values and site densities from potentiometric titration for PG from *B. subtilis*.

pK_a	**Site density [mmol/g]**	**Functionality**
4.55 ± 0.02	0.65 ± 0.17	Carboxyl (glutamic acid)
6.31 ± 0.01	0.76 ± 0.02	Carboxyl (diaminopimelic acid)
9.56 ± 0.03	1.45 ± 0.23	Amine / hydroxyl

The best fit for all titration curves of PG was obtained with a three site model. The results are summarized in Tab. 2.7. The pK_a values of 4.55 and 6.31 with nearly equal site densities can be dedicated both to carboxyl groups. The PG molecule offers two different free carboxyl groups, from the glutamic acid and the diaminopimelic acid. The pK_a values of the second carboxyl groups of glutamic acid (4.15) [45] and pimelic acid (5.08) [45] are within the same range. The third pK_a of 9.56 can be dedicated to both, amino and hydroxyl groups. Related $pK_a(NH_3)$ of glutamic acid (9.58) [45] or diaminohexanoic acid (lysine, 9.15 and 10.66) [45] and the $pK_a(NH_3)$ for *Shewanella putrefaciens* (10.04) [46] or pK_a(OH) for *B. subtilis* cell walls (9.4) [47] are within the same range. Hence, we assume that in contrast to the two specifiable carboxyl groups the amino and hydroxyl groups are not distinguishable. We can only determine an average value. Thus, the high site density is the sum of both functional groups.

3 Studies on the interaction of pyoverdin model compounds with actinides (U(VI), Cm(III), Np(V))

Pyoverdins have three functional domains: a chromophore, a peptide chain localized on the N-terminal end of the chromophore and an acyl chain localized on the C-3 atom of the chromophore. Preferred binding places for metals are the hydroxamic acid groups on the peptide chain and the catechol functionality of the chromophore. The model ligands used in this work, SHA, BHA and DFO simulate the hydroxamic acid function whereas 6-HQ and NAP simulate the catechol functionality of the pyoverdins.

At this time, the complexation of uranium(VI) with hydroxamic acids is rarely investigated. Khairy et al. [32] studied the uranyl complexes with salicylhydroxamic acid. They determined the protonation constants of hydroxamic acids and the complex formation constants by potentiometric titrations in a pH range from 2 to 11 and an ionic strength of 0.1 M $NaNO_3$. Uranylsalicylhydroxamate complexes of the stoichiometry 1:1 and 1:2 (metal ion:ligand) were identified. The determined complex formation constants are $\log \beta_{110} = 11.93 \pm 0.03$ and $\log \beta_{120} = 17.78 \pm 0.06$. In 1965 Baroncelli et al. [48] investigated the complex formation between benzohydroxamic acid and zirconium, iron(III) and uranium(VI). They observed the formation of 1:1 and 1:2 complexes and determined the complex formation constants by potentiometric titration from pH 2 to 4 at an ionic strength of 0.1 M KOH. The formation constants are $\log \beta_{110} = 8.71$ and $\log \beta_{120} = 16.77$. Khairy et al. [32] also studied the complexation between benzohydroxamic acid and uranium by potentiometric titration in a pH range from 2 to 11 and an ionic strength of 0.1 M $NaNO_3$. The stability constants are $\log \beta_{110} = 7.42 \pm 0.01$ and $\log \beta_{120} = 14.19 \pm 0.01$. The discrepancies in the formation constants between both papers show the need of a reinvestigation of the U(VI)–BHA system with other experimental techniques to get a consistent picture of the complex formation reactions. Recently Mullen et al. reinvestigated the UO_2^{2+} complexation with DFO by spectrophotometric titration [49]. They described three 1:1 complexes: $UO_2[H_2DFO]$, $UO_2[HDFO]$, and $UO_2[OHDFOH]$ with stability constants of $\log \beta_{111} = 22.93 \pm 0.04$, $\log \beta_{110} = 17.12 \pm 0.35$, and $\log \beta_{11-1} = 22.76 \pm 0.34$, respectively. This study shows the high potential of the trihydroxamate DFO to complex besides Fe^{3+} also UO_2^{2+}. However, the stoichiometry of the described U(VI)–DFO species remains doubtful. Brainard et al. report a $\log K = 18$ for the formation of the species UO_2HDFO [50]. The knowledge in the literature concerning U(VI) interactions with the chromophore models is very limited. Two uranyl

complexes having a 1:1:1 and a 1:2:1 stoichiometry were found in the NAP system by potentiometric titration with a pH range between 3.5 and 7.5 [36]. Nothing is known about the spectroscopic properties of soluble uranyl(VI)–NAP species. Up to now, NAP species with the higher actinides neptunium and curium are unknown. To the best of our knowledge, no aqueous uranyl species with 6-HQ are described in the literature. At present, no results are available about the complex formation of the hydroxamate and chromophore models with curium(III) and neptunium(V). Therefore, one aim of this project is to close this gap by the determination of stability constants and the spectroscopic properties of the identified species. Due to the unique luminescence properties of curium(III), TRLFS is an established experimental technique for characterizing those complexes with inorganic and organic ligands [51]. The evaluation of those luminescence sum spectra is based on a quantification of the curium(III) species by deconvoluting the total emission spectra. The emission bands of inner-sphere complexes of curium(III) with organic ligands in aqueous solution are generally red-shifted compared to the Cm^{3+} aquo ion. Many speciation studies of Np(V) in a variety of organic, e.g., polyaminocarboxylates [52]; humates [53-57]; EDTA [58, 59]; hydroxycarboxylates [60]; pyridinemonocarboxylates [61]; dicarboxylates [62]; gluconate [63]; citrate [64]; aposerumtransferrin [65] as well as inorganic, e.g., hydroxide and carbonate [66, 67] systems applied the spectrophotometric titration method. All these investigations demonstrated that the characteristic absorption band of Np(V) at 980 nm is sensitive to changes in its first coordination sphere. Hence this technique was used as a direct speciation method in this project to explore Np(V) complex formation constants in the mM concentration range.

3.1 Experimental

Preparation of actinide ligand solutions

All experiments were made in an ionic medium in which the sodium concentration was kept constant at 0.1 M by adding analytical grade $NaClO_4$ (Merck, Darmstadt, Germany). To prevent the carbonate complexation of the actinides, carbonate-free water was used. The pH was measured using an InLab 427 combination pH puncture electrode (Mettler-Toledo, Giessen, Germany) calibrated with standard buffers. The pH was changed by adding analytical grade NaOH or $HClO_4$ with an accuracy of ± 0.05 units. The stock solutions of the ligands were freshly prepared for each experiment. The Cm(III) and Np(V) experiments were performed in a glove box under an N_2 atmosphere at 25ºC.

A stock solution of 0.1 M uranium(VI) perchlorate was used. The solution was prepared by dissolving appropriate amounts of $UO_3 \times 0.77\ H_2O$ in 0.3 M $HClO_4$ and was analyzed using ICP-MS. The UV-vis experiments were carried out at a fixed uranyl concentration of 0.001 M while varying the ligand concentrations between 1×10^{-4} M and 0.05 M within pH 2 and 4. The TRLFS measurements were performed at a lower uranyl concentration of 5×10^{-5} M while varying the ligand concentrations between 1×10^{-5} M and 1×10^{-3} M at pH 3 and 4.
Three series of fs-TRLFS experiments were performed in the U(VI)–NAP system. In runs one and two, we varied the U(VI) concentration, 10^{-6} M to 5×10^{-3} M, at [NAP] of 5×10^{-5} M at fixed pH of 2.1 and 4.1; in the third run, [NAP] and [U(VI)] were kept constant at 1×10^{-4} and 2×10^{-5} M, respectively, while varying the pH between 2.0 and 12.0.

A stock solution of the long-lived curium isotope ^{248}Cm ($t_{1/2} = 3.4\times10^5$ years) was used. This solution had the following composition: 97.3% ^{248}Cm, 2.6% ^{246}Cm, 0.04% ^{245}Cm, 0.02% ^{247}Cm, and 0.009% ^{244}Cm in 1.0 M $HClO_4$. The curium(III) concentration was fixed at 3×10^{-7} M in all TRLFS measurements. The concentration of SHA and BHA was varied between 1×10^{-5} and 1×10^{-3} M, while the pH was changed between 2 and 9. In the Cm(III)–DFO system the DFO concentrations were varied between 3×10^{-5} and 6×10^{-4} M, while varying the pH between 1.6 and 11.0. In the Cm(III)–NAP system the NAP concentrations were changed between 1.5×10^{-6} and 3×10^{-4} M, while varying the pH between 1.9 and 12.0. In the Cm(III)–6-HQ system the 6-HQ concentrations were changed between 3.1×10^{-5} and 3.45×10^{-4} M, while varying the pH between 3.0 and 10.6. At least two different series of TRLFS experiments were performed with each ligand.

Aliquots of a Np(V) stock solution (^{237}Np, 0.034 M, 0.1 M HNO_3) were added to the test solutions. The neptunium(V) concentration was fixed at 1.8×10^{-4} M in all spectrophotometric titrations (2.7×10^{-4} M in the 6-HQ system). In the Np(V)–BHA system, two Np(V)-to-ligand ratios of 1:2 and 1:20 were chosen whereas the pH was varied between 3 and 9. The Np(V)-SHA experiments were performed at three Np(V)-to-ligand ratios of 1:2, 1:18, and 1:30 as a function of pH (3-9). The experiments in the Np(V)–NAP system were carried out at Np(V)-to-ligand ratios of 1:2, 1:2.5, and 1:10 by varying the pH between 3 and 10.3. In the Np(V)–DFO system ligand concentrations of 7.5×10^{-5}, 2.0×10^{-4}, 7.6×10^{-4}, 2.0×10^{-3}, and 4.2×10^{-3} M were used. The pH in those test solutions was usually changed between 3.1 and

9.7. The experiments in the Np(V)–6-HQ system were carried out at Np(V)-to-ligand ratios of 1:1.3 and 1:15 by varying the pH between 3 and 9.6.

Experimental setup of the applied spectroscopic techniques

The complexation of UO_2^{2+} with *P. fluorescens* (CCUG 32456) pyoverdins was investigated using UV-vis and fs-TRLFS. The experimental details of both techniques are summarized in chapter 2.1.2.1. The U(VI) TRLFS spectra were recorded at 25 ± 2 °C using a pulsed Nd:YAG laser system. The excitation wavelength of the uranyl fluorescence was 266 nm with a pulse energy of 100-200 μJ. The TRLFS spectra were measured from 361.08 to 678.95 nm, averaging three spectra with 100 laser pulses each and a gate time of 2 μs. The time-resolved fluorescence emission was recorded using a delay generator and a gated array spectrometer. Delay times varied from 50 to 50500 ns after fragmentation of the laser pulse in increments as follows: a) 50 ns between 50 and 500 ns, 100 ns between 500 and 1500 ns and 500 ns higher than 1500 ns for pH 3 and b) 50 ns between 50 and 500 ns, 500 ns between 500 and 5500 ns and 5000 ns higher than 5500 ns for pH 4. The spectral intensity from 450 to 625 nm was obtained by integration using the codes ORIGIN 7.5G (OriginLab Corporation, USA) and PeakFit (Microcal Software Inc., USA).

The Cm(III) TRLFS spectra were recorded at 25 °C using a pulsed flash lamp pumped Nd:YAG-OPO laser system (Powerlite Precision II 9020 laser equipped with a Green PANTHER EX OPO from Continuum, Santa Clara, CA, USA) [17]. The optical parametrical oscillator (OPO) used to tune the wavelength of the emitted laser beam was pumped by the second harmonic oscillation of the Nd:YAG laser (532 nm). The doubled signal output wavelength can be varied between 330 and 500 nm. The laser pulse energy, which was between 1 and 5 mJ depending on the excitation wavelength used, was monitored using a photodiode. The luminescence emission spectra were detected using an optical multi-channel analyzer-system, consisting of an Oriel MS 257 monochromator and spectrograph with a 300 or 1200 line mm^{-1} grating and an Andor iStar ICCD camera (Lot-Oriel Group, Darmstadt, Germany). The curium(III) emission spectra were recorded in the 500–700 nm (300 line mm^{-1} grating) and 570–650 nm (1200 line mm^{-1} grating) ranges. A constant time window of 1 ms was applied at an excitation wavelength of 395 nm. Additional experiments were performed with excitation wavelength of 360 and 400 nm. For time-dependent emission decay measurements, the delay time between laser pulse and camera grating was scanned with time intervals between 10 and 20 μs. To measure the excitation spectra of the main components, the excitation wavelength was scanned usually in the 340–450 nm range.

The spectrophotometric Np(V) titrations were carried out at room temperature (25±1 ºC) using a Cary-5G UV / Visible / Near IR spectrophotometer (Varian, Inc.) with 1 cm path length locked quartz cuvette. The spectra were obtained between 920 and 1070 nm with a resolution of 0.1 nm. The neptunium(V) concentration in all acidic test solutions without adding a ligand was determined by spectrophotometric analysis at 980 nm using a molar extinction coefficient of 395 L mol^{-1} cm^{-1} [68].

The individual scans measured for each sample were averaged and baseline corrected using ORIGIN 6.1G software (OriginLab, Northhampton, MA, USA). The complex formation constants were calculated based on the variations in the measured spectra using the factor analysis program SPECFIT [20]. The speciation calculations were made using SOLGASWATER software [19].

3.2 Results and discussion

3.2.1 Interaction of actinides with hydroxamate models (SHA, BHA, DFO)

3.2.1.1 U(VI) and hydroxamates

The U(VI)–SHA, BHA systems

Fig. 3.1 shows the measured absorption spectra at a uranium concentration of 0.001 M at pH 4 as a function of the SHA and BHA concentration (data at pH 3 are similar and not shown here). In the spectra of the U(VI)–SHA system an increase in the absorbance and a blue shift of the absorption maxima in comparison to the bands of the free uranyl ion of 21 nm (at pH 3) and 24 nm (at pH 4), indicate the formation of UO_2^{2+}-salicylhydroxamate species. Mainly a 1:1 complex formation reaction was identified. At pH 4 we found evidence for a second species, which could be best described with a 1:2 complex using SPECFIT. The existence of a 1:2 complex is described in the literature [32] and confirmed the determination of this complex by SPECFIT. The single component spectra of the identified species are shown in Fig. 3.2A. Both species show very similar properties in the UV-vis spectra (see Fig. 3.2A). Therefore a clear separation of these species is not possible. The molar absorption coefficient at the main absorption bands for the 1:1 and the postulated 1:2 complex are 436 (at 392 nm) and 165 L mol^{-1} cm^{-1} (at 390 nm), respectively, in difference to the uranyl ion, which has at 414 nm a molar absorption coefficient of 6.6 L mol^{-1} cm^{-1}. The variations observed in the UV-vis spectra could be described by the following equilibrium:

$$UO_2^{2+} + OC_6H_4CONHO^{2-} + H^+ \rightleftharpoons UO_2[HOC_6H_4CONHO]^+ \qquad \log \beta_{111} \qquad (19)$$

The stability constants for the 1:1, $UO_2[HOC_6H_4CONHO]^+$, complex was determined to be $\log \beta_{111} = 17.12 \pm 0.10$ at an ionic strength of 0.1 M.

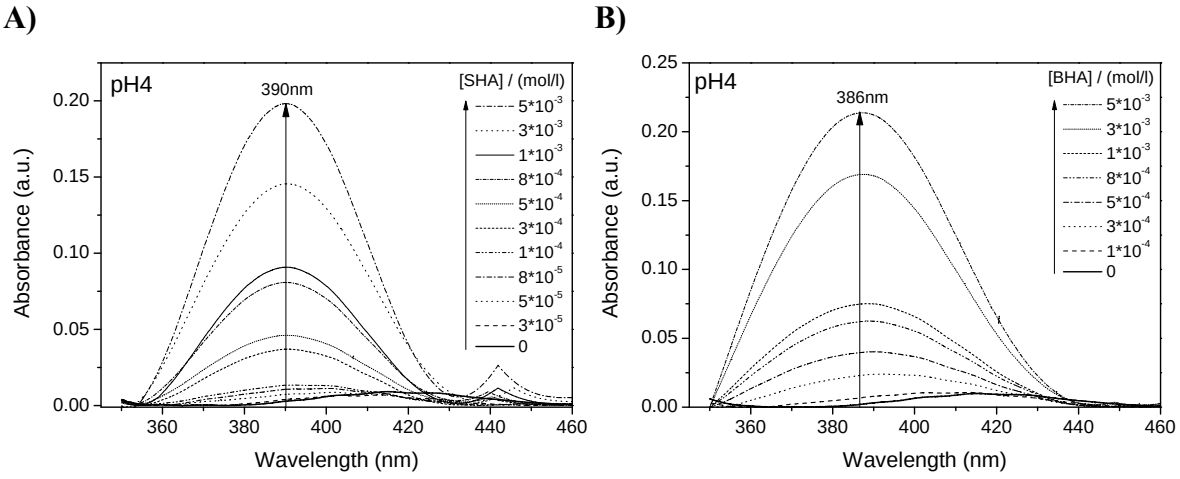

Fig. 3.1 Measured absorption spectra of 1×10^{-3} M UO_2^{2+} in 0.1 M $NaClO_4$ at pH 4 as a function of the A) SHA concentration and B) BHA concentration.

Only a rough estimate of the logarithmic value of the formation constant of the $UO_2[HOC_6H_4CONHO]_2$ complex, $\log \beta_{122} \sim 30$, is possible. The determined complex formation constant for the $UO_2[HOC_6H_4CONHO]^+$ complex is higher than reported in literature [32] ($\log \beta_{110} = 11.93 \pm 0.03$). Reasons might cause from differences in the assumed stoichiometry and the influence of the 1:2 complex. Khairy et al. assumed a complexation of uranyl with the doubled deprotonated form of SHA [32]. This is unlikely to happen in the acidic pH range investigated in this study.

Like in the U(VI)–SHA system the spectra in the U(VI)–BHA system show an increase in the absorbance and a blue shift of 26 and 28 nm at pH 3 and pH 4, respectively. These are indications for a formation of uranylbenzohydroxamate species. The single component spectra of the uranylbenzohydroxamate species are shown in Fig. 3.2B. The molar absorption coefficient for the 1:1 and 1:2 complex are 146 (at 390 nm) and 304 L mol^{-1} cm^{-1} (at 386 nm), respectively. They are much higher than the molar absorption coefficient of the uranyl ion, 6.6 L mol^{-1} cm^{-1} at a wavelength of 414 nm. The complexation reactions can be described as follows:

$$UO_2^{2+} + C_6H_4CONHO^{2-} \rightleftharpoons UO_2[C_6H_4CONHO]^+ \qquad \log \beta_{110} \qquad (20)$$

$$UO_2^{2+} + 2\ C_6H_4CONHO^{2-} \rightleftharpoons UO_2[C_6H_4CONHO]_2 \qquad \log \beta_{120} \qquad (21)$$

The stability constants for $UO_2[C_6H_4CONHO]^+$ and $UO_2[C_6H_4CONHO]_2$ are $\log \beta_{110} = 7.96 \pm 0.05$ and $\log \beta_{120} = 15.25 \pm 0.11$ at an ionic strength of 0.1 M, respectively. These values determined using UV-vis spectroscopy are in good agreement with the constants determined by Khairy et al. [32] by potentiometric titration ($\log \beta_{110} = 7.42 \pm 0.01$ and $\log \beta_{120} = 14.19 \pm 0.01$).

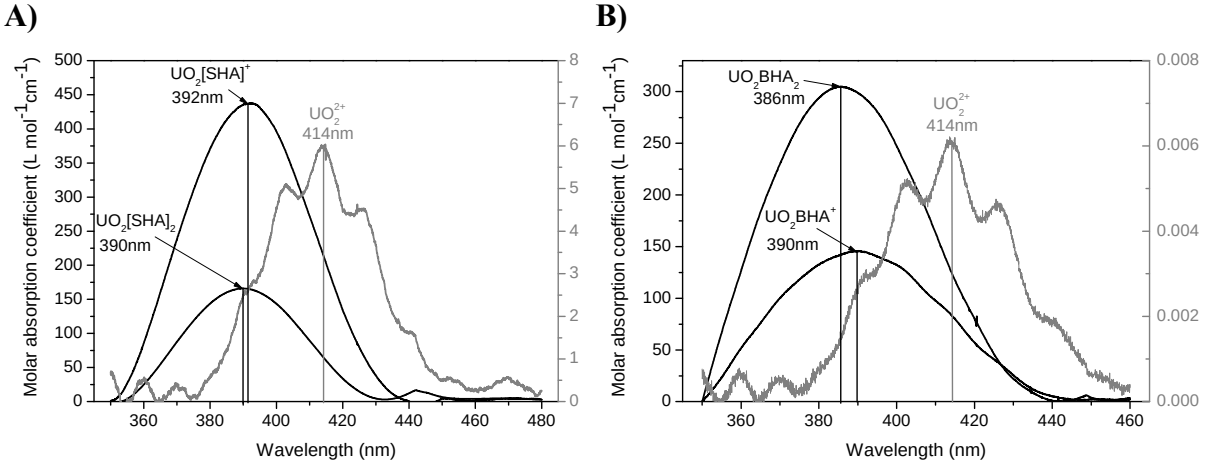

Fig. 3.2 Absorption spectra of the single components in the A) U(VI)-SHA system and B) U(VI)-BHA system.

Fig. 3.3 shows the measured luminescence spectra at 5×10^{-5} M UO_2^{2+} as a function of the ligand concentration in the U(VI)–SHA and U(VI)–BHA system at pH 3.

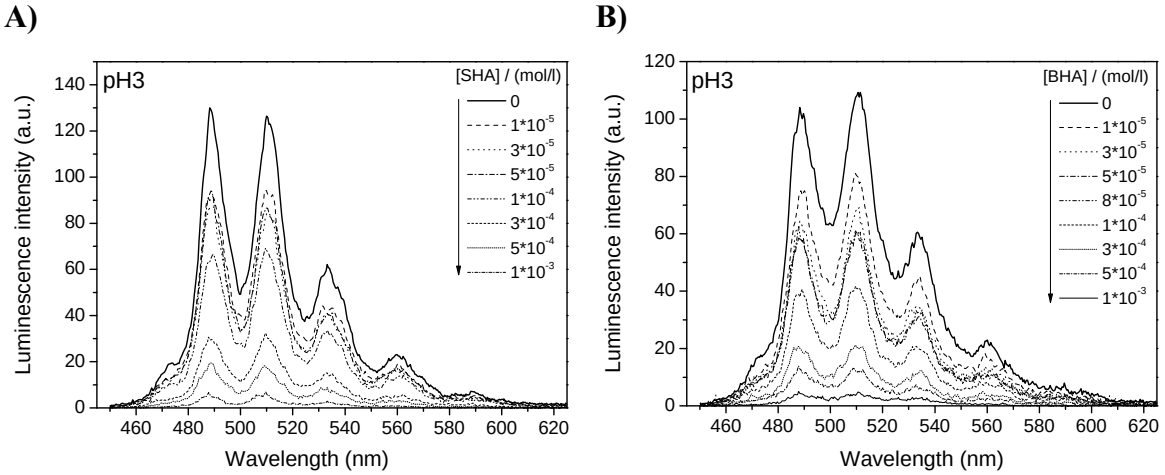

Fig. 3.3 Luminescence spectra of 5×10^{-5} M UO_2^{2+} in 0.1 M $NaClO_4$ at pH 3 as a function of the A) SHA concentration and B) BHA concentration.

In both systems a decrease in the luminescence intensity with increasing ligand concentration was observed at pH 3. This behavior is typical for static luminescence quenching. The luminescence decay was mono-exponential indicating the presence of the free uranyl ion with a lifetime of 1.30 ± 0.05 µs (SHA system) and 1.1 ± 0.1 µs (BHA system). The lifetime

decreases with increasing ligand concentration indicating additional dynamic quenching. In both cases the complexed uranyl ligand species emit no luminescence light.

To determine the stability constants and to estimate the stoichiometry of the complex formation reactions a slope analysis was made. In the U(VI)–SHA system a slope of 1.07 ± 0.14 indicates a predominant formation of the 1:1 complex $UO_2[HOC_6H_4CONHO]^+$. The stability constant log β for the 1:1, $UO_2[HOC_6H_4CONHO]^+$, complex was determined to $\log \beta_{111} = 17.34 \pm 0.06$. In the BHA system a slope of 0.70 ± 0.04 was calculated indicating the formation of a 1:1 complex. The stability constant of the 1:1 complex, $UO_2[C_6H_4CONHO]^+$, results to $\log \beta_{110} = 7.92 \pm 0.11$.

Fig. 3.4 depicts the measured luminescence spectra at 5×10^{-5} M UO_2^{2+} at pH 4 as a function of the ligand concentration in the U(VI)–SHA and U(VI)–BHA system.

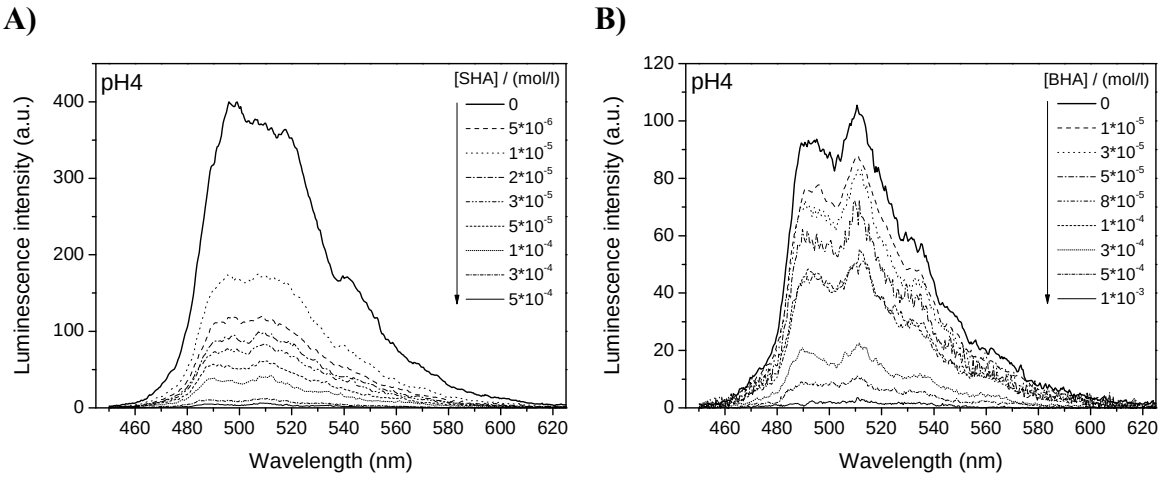

Fig. 3.4 Luminescence spectra of 5×10^{-5} M UO_2^{2+} in 0.1 M $NaClO_4$ at pH 4 as a function of the A) SHA concentration and B) BHA concentration.

Just like in the measurements at pH 3 both a static and dynamic quench process was observed in the U(VI)–SHA and U(VI)–BHA system. The luminescence spectra at pH 4 show bi-exponential decay indicating a mixture of the free uranyl ion with a lifetime of 1.2 ± 0.5 µs (SHA system) and 1.1 ± 0.08 µs (BHA system) and a uranyl hydroxide species most likely $(UO_2)_2(OH)_2^{2+}$ with a lifetime of 13 ± 0.5 µs (SHA system) and 15 ± 8 µs (BHA system), respectively. In both systems the complexed uranyl ligand species show no luminescence properties. The spectra had to be corrected for the uranyl hydroxide species, which shows very high luminescence intensities even at very low concentrations. Using a peak deconvolution procedure (method of least squares) the spectrum of the uranyl hydroxide complex was subtracted from the measured sum spectrum. The evaluation of the spectra was made with the slope analysis. In both systems a slope of 1.57 ± 0.18 (SHA) and 1.2 ± 0.11

(BHA) gives evidence for the formation of a second species most likely a 1:2 complex. Because of the occurrence of two complex species it is not possible to determine the stability constants of the complexes with the slope analysis. On this account the factor analysis program SPECFIT was used to determine the stability constants. The stability constant of the 1:2 complex $UO_2[HOC_6H_4CONHO]_2$ in the U(VI)–SHA system was determined to be $\log \beta_{122} = 35.0 \pm 0.11$ and of the 1:2 complex $UO_2[C_6H_4CONHO]_2$ in the U(VI)–BHA system to $\log \beta_{120} = 16.88 \pm 0.49$.

For both hydroxamate model ligands, SHA and BHA, the stability constants determined with TRLFS agree well with the constants determined using UV-vis spectroscopy. A larger difference was observed by comparing the spectroscopy based constants with those calculated from potentiometric titrations. In general the values resulting from the potentiometric titration are lower than the stability constants determined by both spectroscopic techniques. Reasons might cause from differences in the assumed stoichiometry of the formed species like in the U(VI)–SHA system. The complex formation constants suggest that SHA and BHA form complexes of similar strength. The tendency found with other metals [69-72], e.g., Fe(III) and Cu(II) that SHA species are more stable than BHA species was not observed for U(VI).

The U(VI)–DFO system

Fig. 3.5 shows the measured absorption spectra of 1×10^{-3} M UO_2^{2+} in 0.1 M $NaClO_4$ as a function of the DFO concentration at pH 3 (data at pH 4 are similar and not shown here) and the absorption spectra of the single components in the U(VI)–DFO system calculated with the factor analysis program SPECFIT. In the measured spectra an increase of the absorbance with increasing DFO concentration and a shift of the absorption maxima in comparison to the bands of the free uranyl ion to lower wavelengths of 24 nm was observed. These are indications for the formation of U(VI)–DFO complex species. The blue shift of the absorption maxima verified the results of the investigations with SHA and BHA. Thus, the coordination of the uranyl ion to hydroxamate ligands results in a blue shift of the absorption maxima. The formation of a 1:1 complex could be clearly identified. However, it was not possible to determine the number of protons involved in the complex formation. The complex formation can be described by the following equilibria:

$$UO_2^{2+} + DFO^{3-} + H^+ \rightleftharpoons UO_2[HDFO] \qquad \log \beta_{111} \qquad (22)$$

$$UO_2^{2+} + DFO^{3-} + 2\,H^+ \rightleftharpoons UO_2[H_2DFO]^+ \qquad \log \beta_{112} \qquad (23)$$

$$UO_2^{2+} + DFO^{3-} + 3\ H^+ \rightleftharpoons UO_2[H_3DFO]^{2+} \qquad \log \beta_{113} \qquad (24)$$

Formation constants for reactions (22) to (24) were determined to be $\log \beta_{111} = 30.96 \pm 0.06$, $\log \beta_{112} = 34.46 \pm 0.06$, and $\log \beta_{113} = 37.96 \pm 0.06$, respectively.

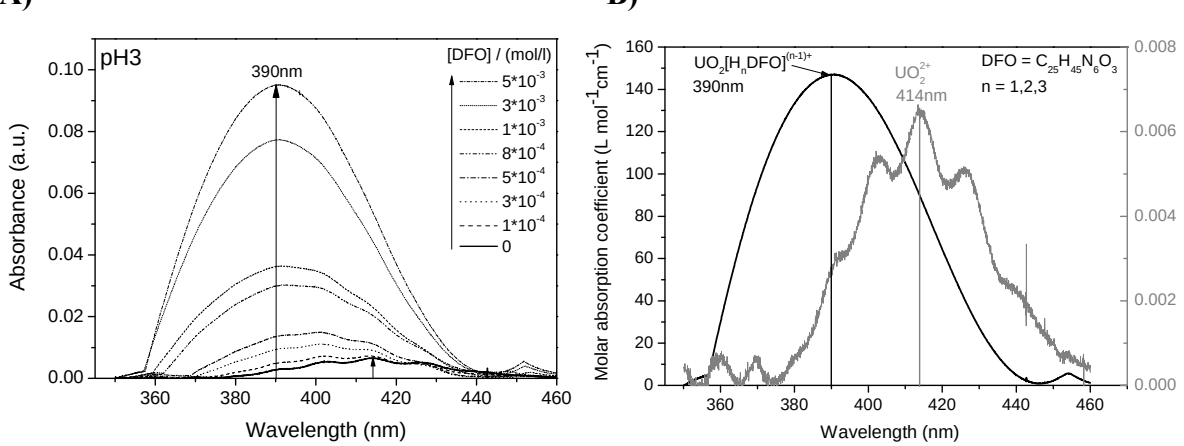

Fig. 3.5 A) Absorption spectra of 1×10^{-3} M UO_2^{2+} in 0.1 M $NaClO_4$ as a function of the DFO concentration at pH 3. B) Absorption spectra of the single components in the U(VI)–DFO system.

It must be pointed out that only one of the postulated complex species is formed. Because the absorption properties of the complexes are too similar, it was not possible to determine the exact stoichiometry of the formed 1:1 complex. Therefore, the absorption spectra of the 1:1 complexes with the three possible stoichiometries are equal and shown in Fig. 3.5B.

The complex formation of DFO and U(VI) was additionally investigated with laser luminescence measurements. Fig. 3.6 summarizes the luminescence spectra of 5×10^{-5} M UO_2^{2+} as a function of the DFO concentration at pH 3 and 4. The spectra show at both pH values a decrease of the luminescence intensity with increasing DFO concentration, which is typical for static luminescence quenching due to the complex formation. At pH 3 the luminescence decay is mono-exponential indicating the presence of the free uranyl ion with a lifetime of 1.4 µs. At pH 4 bi-exponential decay was observed with lifetimes of 1.4 µs for the free uranyl ion and 24 µs for a uranyl hydroxide species most likely $(UO_2)_3(OH)_5^+$. The lifetimes also decrease with increasing ligand concentration indicating additional dynamic quenching. It can be concluded that the formed U(VI)–DFO species show no luminescence properties. The spectra at pH 4 had to be corrected for the uranyl hydroxide species using a peak deconvolution procedure. The following slope analysis results in a slope of 0.9, which indicates clearly the formation of a 1:1 complex. Just like in the investigation of the complex formation with absorption spectroscopy also in the luminescence experiments it was not

possible to determine the number of protons involved in the complex formation. The complex formation reaction can be occurring according to the reactions (22) to (24). The stability constants of the possible complexes are calculated to $\log \beta_{111} = 31.08 \pm 0.54$, $\log \beta_{112} = 34.58 \pm 0.21$, and $\log \beta_{113} = 38.08 \pm 0.54$, respectively.

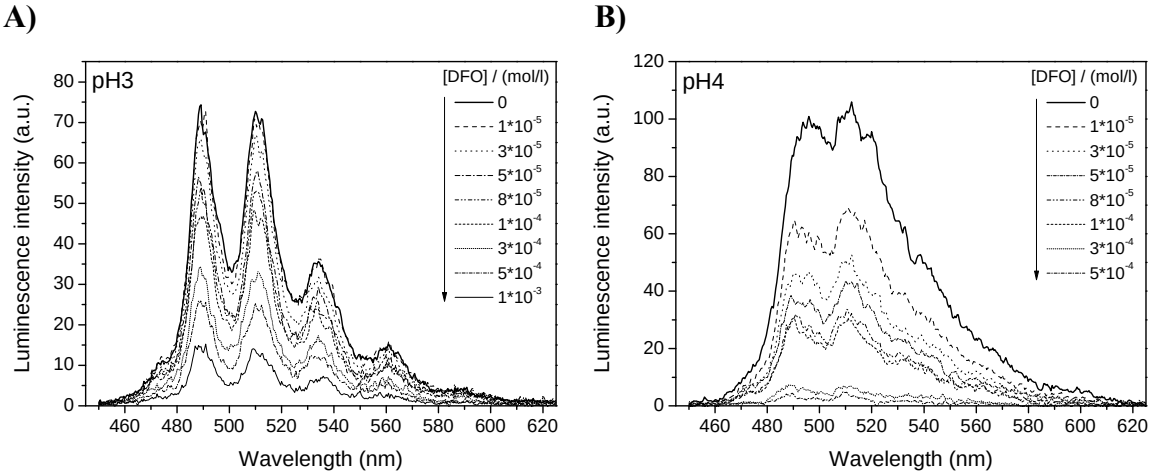

Fig. 3.6 Luminescence spectra of 5×10^{-5} M UO_2^{2+} in 0.1 M $NaClO_4$ as a function of the DFO concentration at A) pH 3 and B) pH 4**.**

The constants determined with TRLFS are in good agreement with those determined with UV-vis spectroscopy. It was not possible to determine the exact stoichiometry of the formed 1:1 complex species. Because the failure of the stability constant of the 112-complex is smaller than the others, it can be concluded that the formation of this complex is favored. First ATR-FTIR measurements performed in the U(VI)–DFO system confirm the hypothesis of a favored formation of the 112-complex. The stability constants und the stoichiometry of the determined complexes differ strong from the values determined by Mullen et al., which described three U(VI)–DFO complexes with stability constants of $\log \beta_{111} = 22.90 \pm 0.10$, $\log \beta_{110} = 17.10 \pm 0.40$, and $\log \beta_{11\text{-}1} = 22.80 \pm 0.30$ [49].

3.2.1.2 Cm(III) and hydroxamates

The Cm(III)–SHA, BHA systems

The luminescence emission spectra of 3×10^{-7} M Cm(III) with 3.26×10^{-4} M SHA in the pH range 2-9 are shown in Fig. 3.7. The spectra are recorded at excitation wavelengths of 395 nm and 360 nm. The Cm^{3+} aquo ion has a characteristic luminescence emission band maximum of 593.8 nm at an excitation wavelength of 395 nm. As known from previous studies [17, 73-75] the luminescence emission of complexes between Cm(III) and organic ligands can be

generated either by direct excitation of the Cm(III) luminescence or by excitation of the ligand followed by an energy transfer from the ligand molecule to the Cm(III) ion (indirect excitation). Therefore, the luminescence properties of the Cm(III)–hydroxamate complex species can be also determined by an excitation wavelength of 360 nm.

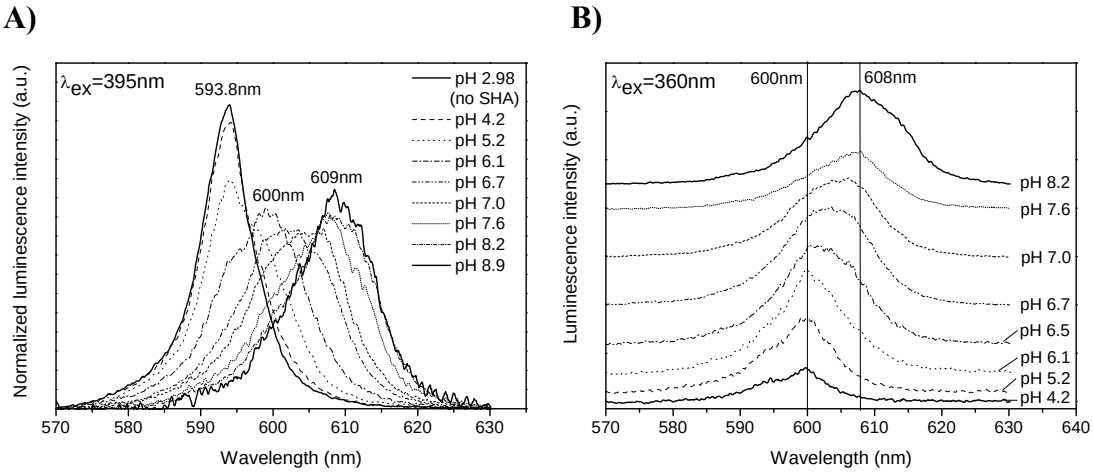

Fig. 3.7 Luminescence spectra of 3×10^{-7} M Cm^{3+} and 3.26×10^{-4} M SHA as a function of pH at an excitation wavelength of A) 395 nm (direct excitation mode) and B) 360 nm (indirect excitation mode). The spectra at an excitation wavelength of 395 nm are scaled to the same peak area; the spectra at excitation wavelength of 360 nm are energy corrected.

The measured luminescence emission spectra of Cm(III) with SHA in the pH range 4-8 at an excitation wavelength of 395 nm show a red shift of the emission maxima with increasing pH from the characteristic emission maximum of Cm(III) at 593.8 nm via 600 nm to an emission maximum at 608 nm indicating the complex formation between Cm(III) and SHA. In the luminescence spectra at an excitation wavelength of 360 nm also a red shift of the emission maxima and an increase of the luminescence intensity with increasing pH were observed. From this it can be concluded that the concentration of the Cm(III)–hydroxamate species increased with increasing pH. A comparison of the spectra at the two excitation wavelengths in dependence of the pH is shown in Fig. 3.8. At an excitation wavelength of 395 nm and pH 4, the spectrum shows no influence of the beginning complex formation. In contrast to this, the spectrum measured at an excitation wavelength of 360 nm exhibits clearly a peak at 600 nm corresponding to the formation of the first complex. With increasing pH, the formation of Cm(III)–SHA species influences strongly the measured sum luminescence spectra using the indirect excitation mode in contrast to the spectra at 395 nm. At pH 8, where no uncomplexed Cm(III) species exist, the measured spectra exhibit the same peak maxima at both excitation wavelengths.

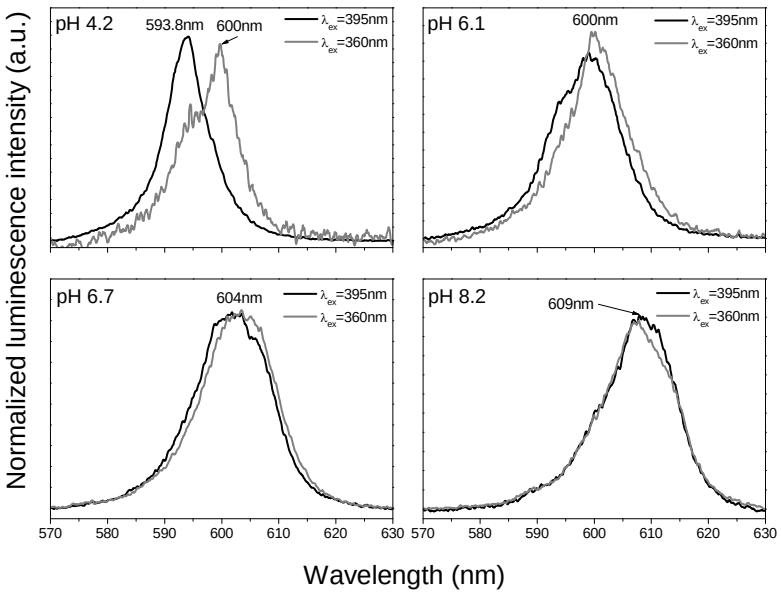

Fig. 3.8 Direct comparison of luminescence spectra of the Cm(III)–salicylhydroxamate system measured at excitation wavelengths of 360 (indirect excitation mode) and 395 nm (direct excitation mode).

The complexation is accompanied by an increase of the luminescence emission lifetime. At pH values less than 7, the luminescence lifetime increased from 65 µs for the Cm^{3+} aquo ion to 80 µs showing mono-exponential decay. At pH values greater than 7, a bi-exponential decay was measured with lifetimes of 80 and 200 µs. In the pH range 4-7, a second Cm(III) species besides the Cm^{3+} aquo ion with a peak maximum at 600 nm dominates more and more the sum luminescence spectrum. Above pH 7 a third Cm(III) species appeared with a peak maximum at 609 nm. These experimental findings, the two identified peak maxima and the two identified lifetimes give clear evidence for the formation of two different Cm(III)–SHA species.

As a result of the SPECFIT calculations, the variations observed in the luminescence emission spectra can be described by the following equilibria [76]:

$$Cm^{3+} + OC_6H_4CONHO^{2-} + H^+ \rightleftharpoons Cm[HOC_6H_4CONHO]^{2+} \qquad \log\beta_{111} \quad (25)$$

$$Cm^{3+} + 2\ OC_6H_4CONHO^{2-} + H^+ \rightleftharpoons Cm[HOC_6H_4CONHO,OC_6H_4CONHO] \qquad \log\beta_{121} \quad (26)$$

The stability constants were determined at both excitation wavelengths. At an excitation wavelength of 395 nm the stability constant for the 1:1 complex, $Cm[HOC_6H_4CONHO]^{2+}$, was determined to be $\log \beta_{111} = 16.52 \pm 0.14$ and for the 1:2 complex, $Cm[HOC_6H_4CONHO,OC_6H_4CONHO]$, $\log \beta_{121} = 23.92 \pm 0.23$ at an ionic strength of 0.1 M. The stability constants at an excitation wavelength of 360 nm are $\log \beta_{111} = 16.14 \pm 0.15$ and $\log \beta_{121} = 23.76 \pm 0.21$. The stability constants determined either by indirect (360 nm) or

direct (395 nm) excitation of the Cm(III) luminescence are consistent. The corresponding single component spectra of the Cm(III)–salicylhydroxamate species at both wavelengths are shown in Fig. 3.9. The emission maxima of both complex species are in agreement measured either with direct or indirect excitation.

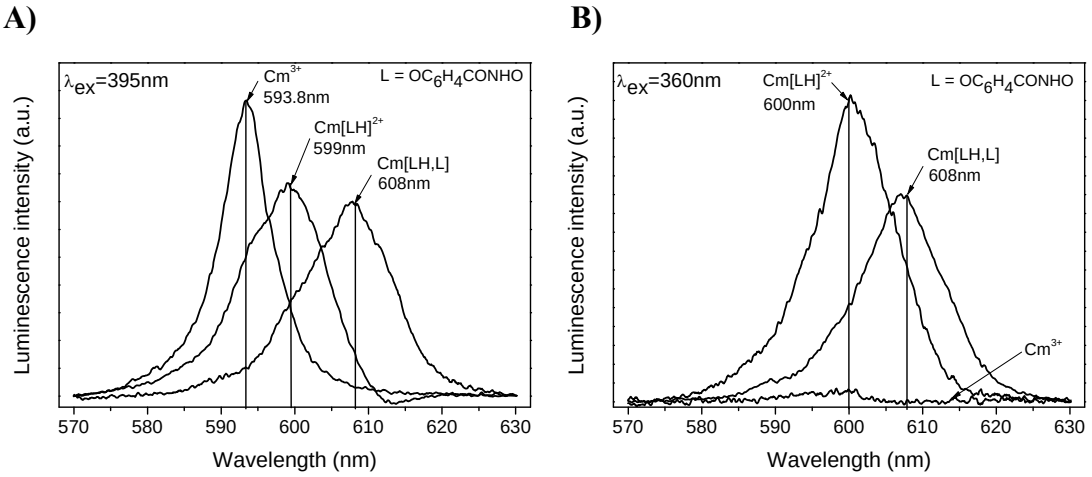

Fig. 3.9 Luminescence spectra of the single components in the Cm^{3+}–SHA system at an excitation wavelength of A) 395 nm and B) 360 nm.

The 1:2 complex is a mixed complex consisting of two different deprotonated ligand molecules ($HOC_6H_4CONHO^-$ and $OC_6H_4CONHO^{2-}$) and a Cm^{3+} ion. There are evidences that the phenolic OH-group of one of the ligand molecules is deprotonated through the complexation.

The measured luminescence emission spectra of Cm(III) with BHA in the pH range 2-9 (spectra are similar to those of SHA and not shown here) at an excitation wavelength of 395 nm show a red shift of the emission maxima with increasing pH from the characteristic emission maximum of Cm(III) at 593.8 nm via 600 nm to an emission maximum at 609 nm indicating the complex formation between Cm(III) and BHA. Two different Cm(III)–BHA species are formed. The first complex species appears in the pH range 2-7 with a peak maximum of 600 nm and a lifetime of 85 µs; the second species with a lifetime of 150 µs and a peak maximum of 609 nm occurs at pH values greater than 8. The complexation reactions can be expressed as follows [76]:

$$Cm^{3+} + C_6H_4CONHO^{2-} \rightleftharpoons Cm[C_6H_4CONHO]^{2+} \qquad \log\beta_{110} \qquad (27)$$

$$Cm^{3+} + 2\ C_6H_4CONHO^{2-} \rightleftharpoons Cm[C_6H_4CONHO]_2^{+} \qquad \log\beta_{120} \qquad (28)$$

The stability constants were determined at both excitation wavelengths. At an excitation wavelength of 395 nm the stability constant for the 1:1 complex, $Cm[C_6H_4CONHO]^{2+}$, was

determined to be $\log \beta_{110} = 6.42 \pm 0.11$ and for the 1:2 complex, $Cm[C_6H_4CONHO]_2^+$, $\log \beta_{120} = 11.25 \pm 0.36$ at an ionic strength of 0.1 M. The stability constants at an excitation wavelength of 360 nm are $\log \beta_{110} = 6.61 \pm 0.21$ and $\log \beta_{120} = 11.95 \pm 0.35$. The stability constants determined either by indirect (360 nm) or direct (395 nm) excitation of the Cm(III) luminescence are consistent.

Luminescence lifetime measurements were used to obtain information about the composition of the first coordination sphere of curium(III). In 1994 Kimura and Choppin [77] found a linear relationship between the lifetime τ and the number of water molecules n_{H2O} in the first coordination sphere of Cm(III). The relationship can be expressed as follows:

$$n_{H2O} = 0.65/\tau - 0.88$$

The Cm^{3+} aquo ion is characterized by a measured lifetime of 68 ± 1 µs, which corresponds to nine water molecules, while the value of 1370 µs measured in D_2O [78] corresponds to zero water molecules in the first coordination sphere of curium(III). In case of a complex formation of the Cm^{3+} aquo ion, the lifetimes of the Cm(III) species increase indicating the exclusion of water molecules out of the first coordination sphere. In all samples with pH values up to 5 a mono-exponential decay was measured with an averaged lifetime of 80 µs in the Cm(III)–SHA system and 85 µs in the Cm(III)–BHA system. This lifetime might correspond to the 1:1 Cm(III)–hydroxamate complexes. In samples with pH values above 5, a bi-exponential decay was detected with average lifetimes of 80 and 200 µs for SHA and 85 and 150 µs for BHA, respectively. The second larger lifetime could correspond to the 1:2 complexes. The average number of water molecules in the first coordination sphere calculated with the determined luminescence lifetimes is 7.3 (SHA) and 6.8 (BHA) for the 1:1 complex and 2.4 (SHA) and 3.5 (BHA) for the 1:2 complex, respectively. During the formation of the 1:1 complex with both hydroxamic acids 2 water molecules are excluded out of the first coordination sphere. This is in good agreement with the complex stoichiometry found with SPECFIT. In a first assumption also caused by the lack of information regarding the structure of Cm(III)–hydroxamate compounds, it can be assumed that the complex stoichiometry and structure of the 1:1 complexes are similar to the U(VI)–SHA and –BHA complexes. The coordinating atoms in the complexes are the hydroxamic acid oxygens ([O,O]-mode), the other reasonable coordination mode via the phenolic oxygen and the nitrogen atom ([N,O']-mode) could be excluded according to reference [79]. So, the Cm^{3+} aquo ion binds like the UO_2^{2+}-ion to the hydroxamic acids via the two hydroxamate oxgens. As a result of the formation of the 1:2 Cm(III)–SHA complex 6-7 water molecules leave the first coordination sphere. The outcome of the SPECFIT calculation points to a five- or six- coordinated Cm(III)

atom depending if the phenolic OH-groups are involved in the complex formation or not. Six released water molecules suggest that the protonated OH-group is concerned in the complexation. In the Cm(III)–BHA system the luminescence lifetime of the 1:2 complex suggest that 5 water molecules are released. The bidentate coordination of two hydroxamate groups of BHA to Cm(III) would result in 5 remaining water molecules. The observed difference could be explained by additional interactions with the π –system of the ring. In case of the 1:1 complexes with the hydroxamic acids the relationship between the lifetime and the number of released water molecules agree well with the stoichiometry of the complexes found with SPECFIT. However, quench mechanism during the complexation via the organic ligands can not be excluded, which might cause that the linear relationship of Kimura and Choppin would be inapplicable. On that account the luminescence decay was used for comparison and to give evidences for the structure of the formed complexes.

The Cm(III)–DFO system

An overview of the emission spectra of 3×10^{-7} M curium(III) in 0.1 M $NaClO_4$ measured in the DFO system is presented in Fig. 3.10A. The spectral variations depicted in Fig. 3.10A; (a) as a function of the DFO concentration at pH 5 and (b) as a function of pH at a fixed DFO concentration; are clear indications for a strong interaction with aqueous DFO species and Cm^{3+}. The emission maximum of Cm^{3+} at 593.8 nm decreased with: (a) increasing DFO amounts at fixed pH and (b) increasing pH at fixed [DFO]. No influence of the Cm^{3+} aquo ion could be detected in the measured sum TRLFS spectra at pH $\geq$ 6.2. At the same time, the amount of a first Cm(III)–DFO species increased having an emission maximum at approximately 600 nm. The formation of the second Cm(III)–DFO species is shown by the strong changes in the emission spectra between pH 5.8 and 6.2 (see Fig. 3.10A). Then the spectra are independent from pH until pH 8.7. The again red shifted emission maximum at pH 9.8 indicates the increased influence of the third Cm(III)–DFO complex.

In light of relevant complexation studies of DFO with metals [49, 50, 80], and taking into consideration the deprotonation of the DFO molecule, possible curium(III)–DFO species of the $M_pH_qL_r$ type were introduced into the data analysis procedure. The variations observed in the emission data (see Fig. 3.10A) could be described by the following equilibria:

$$Cm^{3+} + DFO^{3-} + 2H^{+} \rightleftharpoons CmH_2DFO^{2+} \qquad \log \beta_{121} \qquad (29)$$

$$Cm^{3+} + DFO^{3-} + H^{+} \rightleftharpoons CmHDFO^{+} \qquad \log \beta_{111} \qquad (30)$$

$$Cm^{3+} + DFO^{3-} \rightleftharpoons CmDFO \qquad \log \beta_{101} \qquad (31)$$

Formation constants for reactions (29) to (31) were calculated to be log $\beta_{121} = 31.62 \pm 0.23$, log $\beta_{111} = 25.73 \pm 0.17$, and log $\beta_{101} = 16.80 \pm 0.40$, respectively [81].

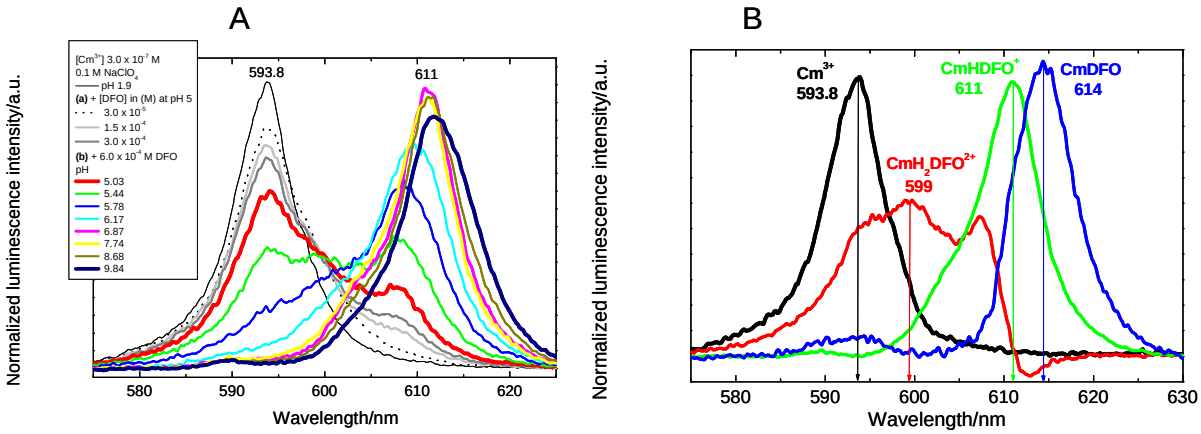

Fig. 3.10 A) Luminescence spectra of 3×10^{-7} M curium(III) in 0.1 M $NaClO_4$ measured as a function of the DFO concentration at pH 5.0 (not all data shown) and at a fixed DFO concentration of 6×10^{-4} M as a function of pH (not all data shown). B) Luminescence spectra of the single components in the Cm^{3+}–DFO system, as derived by peak deconvolution using SPECFIT. The spectra are scaled to the same peak area.

These results indicate that DFO forms strong 1:1 complexes with curium(III). No published data exist for curium(III) to provide a basis for comparison. The corresponding single-component spectra of the individual species are summarized in Fig. 3.10B. The spectrum of the 1:2:1 species shows a complex structure with a maximum at 599 nm and two shoulders at 595 and 607 nm. The two other species, $CmHDFO^+$ and CmDFO, are characterized by single emission peaks at 611 and 614 nm, respectively. The single component spectrum of the CmDFO species shows in addition a small and broad maximum at 594 nm. This feature is rather a result of the SPECFIT analysis than a contribution of the uncomplexed Cm^{3+} aquo ion, because no free Cm(III) exists under the experimental conditions (e.g., DFO concentration and pH) where CmDFO is formed. This explanation is supported by our experiments applying the indirect excitation mode of the Cm(III) luminescence [81]. The spectroscopic speciation determined at 360 (indirect excitation mode) and 395 nm (direct excitation mode) is in agreement.

The complexation is accompanied by an increase of the luminescence lifetime. The linear relation-ship between the decay rate and the number of H_2O molecules in the first coordination sphere of curium(III) found by Kimura and Choppin [77] was used for an approximate insight into the structure of the formed Cm(III)–DFO species. In all samples in which the Cm^{3+} aquo ion and the first DFO complex, CmH_2DFO^{2+}, are present, a mono-exponential decay was measured with an average lifetime of 85 µs; this lifetime could

correspond to the CmH_2DFO^{2+} species. Between pH 6 and 8.5, again a mono-exponential decay with an average lifetime of 123 µs was observed. This lifetime can be attributed to the $CmHDFO^{+}$ species. At pH values greater than 8.5, a bi-exponential decay was measured with lifetimes of 124 and 319 µs. The latter might correspond to the third Cm(III)–DFO species, CmDFO. The increasing lifetimes of the Cm(III)–DFO species reflect the exclusion of water molecules from the first coordination sphere of curium(III), due to the identified complex formation reactions. The average number of water molecules in the first coordination sphere of CmH_2DFO^{2+}, $CmHDFO^{+}$, and CmDFO, calculated with the determined luminescence lifetimes are 6.8 (5), 4.4 (3) and 1.2 (2), respectively. The numbers of water molecules estimated from the stoichiometry found with SPECFIT are given in parenthesis and were calculated as follows. Due to the lack of information regarding the structure of Cm(III) complexes with DFO, we postulate a bidentate coordination by the hydroxamate oxygens ([O,O]-mode) according to the 1:1 complex of U(VI) with SHA [79]. In the CmH_2DFO^{2+} complex two hydroxamate groups of the DFO molecule are deprotonated and coordinated in a bidentate fashion via their oxygen atoms to the Cm(III) center. This results in a release of four water molecules from the first coordination sphere of Cm(III). Hence the CmH_2DFO^{2+} complex contains five water molecules. A bidentate coordination of three deprotonated hydroxamate groups of DFO results in three remaining water molecules in the $CmHDFO^{+}$ complex. Two remaining water molecules in the CmDFO complex can be explained by a bidentate coordination of the three deprotonated hydroxamate groups and an additional interaction of Cm(III) with the amine group of the DFO molecule. The measured lifetimes represent sum values of all luminescence emitting species present in the individual test solutions. Due to the overlapping area of existence of all Cm(III) species in the DFO system, the preparation of samples with only one Cm(III) species is hampered. This might explain the discrepancies in the number of remaining water molecules especially for the 1:1:2 and the 1:1:1 species determined with the Kimura-Choppin relation and with SPECFIT. The lower number of remaining water molecules in the CmDFO species could be explained by an additional interaction with one amide group of the DFO molecule.

This study shows that curium(III)–DFO species dominate over a wide curium concentration and pH range. Hence, strong Cm^{3+}-DFO species are formed, indicating the great potential of trihydroxamate siderophores to mobilize curium(III) in the biologically relevant pH range. The results of the presented work contribute to an improved understanding of the chemistry of curium(III) coordination with natural trihydroxamate siderophores in aqueous solution.

3.2.1.3 Np(V) and hydroxamates

The Np(V)–SHA, BHA systems

The results of the spectrophotometric titrations of the NpO_2^+ test solutions in the SHA and BHA system are shown in Fig. 3.11. To the best of our knowledge spectrophotometric titrations of NpO_2^+ with BHA and SHA were not reported before. Neptunyl(V) forms strong complexes with the selected simple hydroxamate ligands. The NIR absorption spectra of the corresponding single components are summarized in Fig. 3.12.

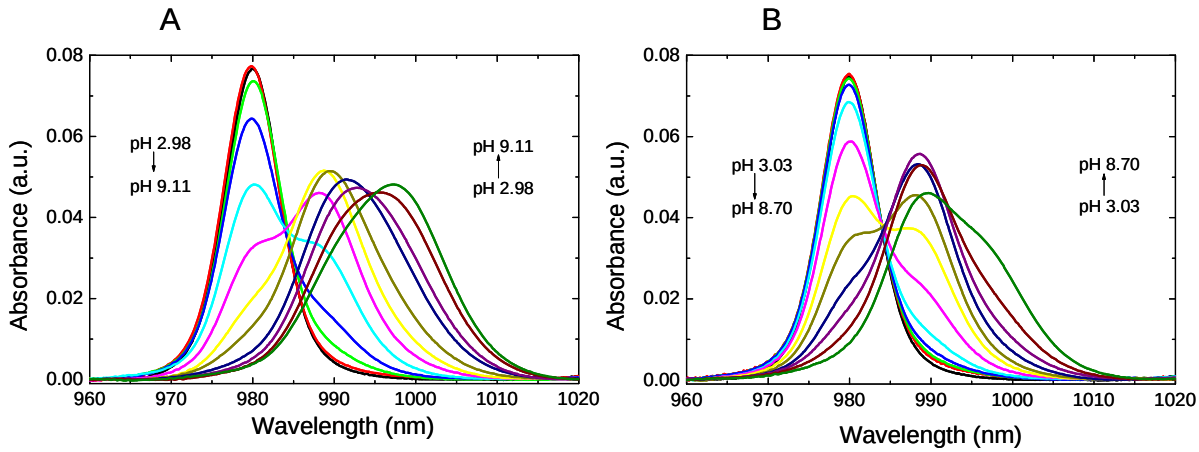

Fig. 3.11 Spectrophotometric titrations of 1.8×10^{-4} M NpO_2^+-bioligand solutions in 0.1 M $NaClO_4$. (A) 5.40×10^{-3} M SHA; (B) 3.69×10^{-3} M BHA.

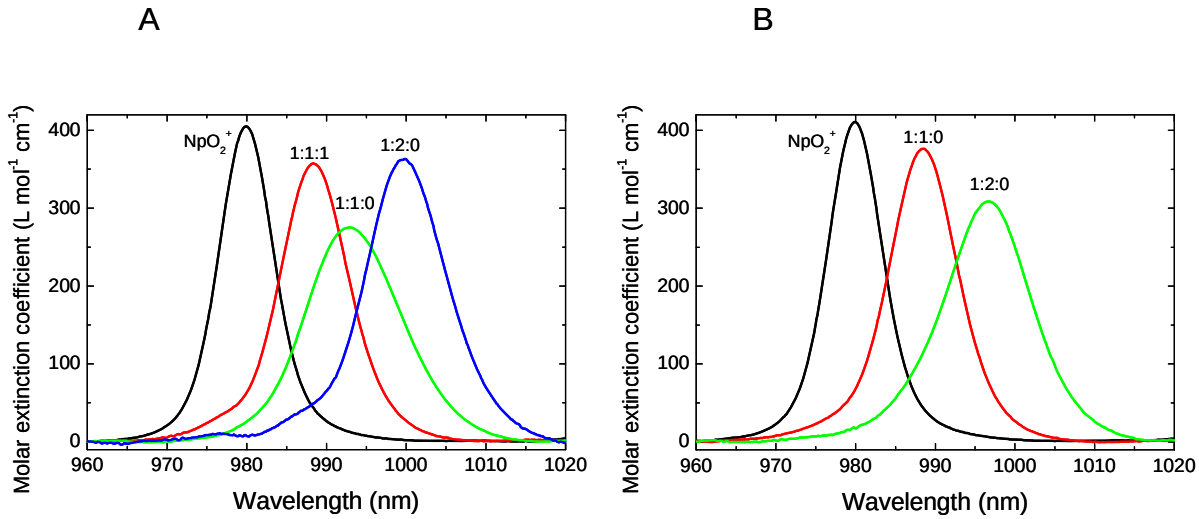

Fig. 3.12 NIR absorption spectra of the single components in the NpO_2^+–SHA and –BHA system, as derived by peak deconvolution using SPECFIT.

Within the SHA system two different 1:1 species, 1:1:1 and 1:1:0, were identified. At a metal-to-ligand ratio of 1:30 in addition the formation of a 1:2:0 species could be confirmed. The following Np(V)–SHA stability constants were calculated: $\log \beta_{111} = 13.68 \pm 0.05$,

log $\beta_{110} = 6.09 \pm 0.10$, and log $\beta_{120} = 9.32 \pm 0.20$ [18]. The deprotonated BHA molecule forms two neptunyl(V) species with metal-to-ligand ratios of 1:1 and 1:2 and stability constants of log $\beta_{110} = 4.57 \pm 0.01$, and log $\beta_{120} = 7.59 \pm 0.05$ [18]. The difference between SHA and BHA is the phenolic OH group next to the hydroxamate group in SHA. Interestingly, this structural difference is also pronounced in the spectrophotometric titration results. A direct comparison of the 1:1 and 1:2 species (λ_{max}, log β) indicate an involvement of the phenolic OH group in the binding of Np(V) to SHA. Similar indications were observed in our Cm(III) speciation study with SHA and BHA (see 3.2.1 and [76]). However, the larger SHA formation constants can be also the results of the stabilizing effect of the OH group (e.g., increase of the electron density of the hydroxamate group).

The Np(V)–DFO system

The results of the spectrophotometric titrations of the NpO_2^+ test solutions in the DFO system are shown in Fig. 3.13A. To the best of our knowledge spectrophotometric titrations of NpO_2^+ with the trihydroxamate siderophore DFO were not reported before.

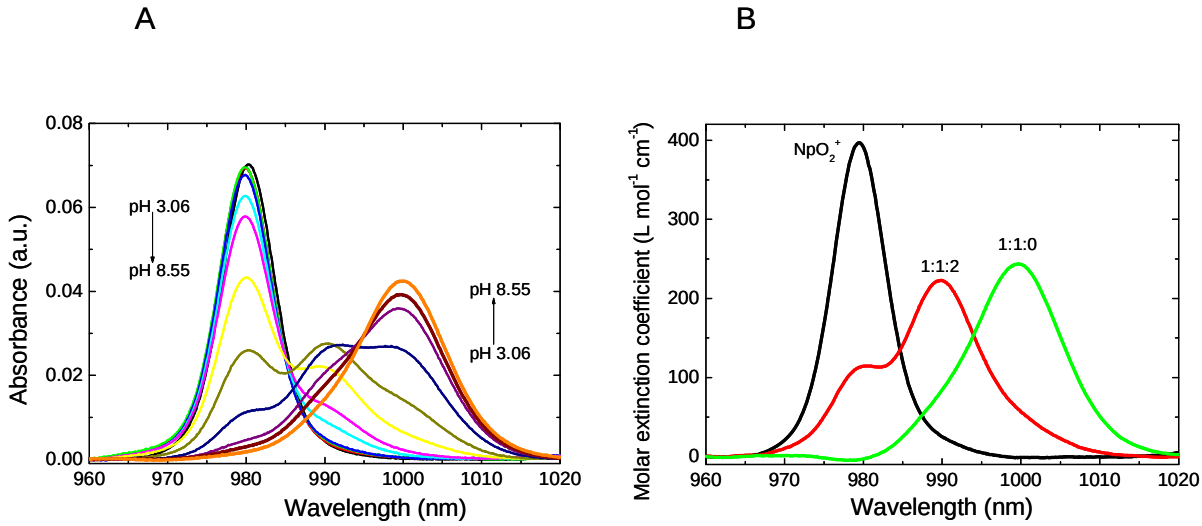

Fig. 3.13 (A) Spectrophotometric titrations of 1.8×10^{-4} M NpO_2^+ with 2.0×10^{-3} M DFO in 0.1 M $NaClO_4$. (B) NIR absorption spectra of the single components in the NpO_2^+–DFO system, as derived by peak deconvolution using SPECFIT.

As depicted in Fig. 3.13 neptunyl(V) forms strong complexes with aqueous DFO species. The NIR absorption spectra of the identified single components are summarized in Fig. 3.13B. Within the DFO system two different 1:1 species, 1:1:2 and 1:1:0, were isolated based on the variations in the absorption spectra (Fig. 3.13A). The following Np(V)–DFO stability constants were calculated: log $\beta_{112} = 27.23 \pm 0.35$, and log $\beta_{110} = 11.61 \pm 0.78$. Interestingly,

the spectrum of the 1:1:2 species shows a complex structure with two maxima at 980 nm and 990 nm. As a result of the SPECFIT calculations, the contribution at 980 nm depends on the number of coordinated protons in this complex and to less extend on the value of log β_{110}. The best results were obtained if this complex contains two protons. It is interesting to mention that the corresponding Cm(III) complex shows also a complex structure in his luminescence emission spectrum. The NpO_2DFO^{2-} species is characterized by single absorption peaks at 999.9 nm.

A direct comparison of the 1:1 neptunyl(V) complexes formed with the hydroxamate models shows an increased magnitude of the stability constants in the order BHA, SHA and DFO. Hence DFO forms the strongest neptunyl hydroxamate complexes in aqueous solution. This can be explained by the occurrence of three hydroxamate groups in DFO. The stability constant of NpO_2BHA ($\log \beta = 4.57$) which has only one hydroxamate group is approximately three times smaller than those measured for NpO_2DFO^{2-} ($\log \beta = 11.61$).

3.2.2 Interaction of actinides with chromophore models (6-HQ, NAP)

3.2.2.1 U(VI) and chromophore models

The U(VI)–6-HQ system

Fig. 3.14A illustrates the measured absorption spectra of 6-HQ as a function of the UO_2^{2+} concentration at pH 1.

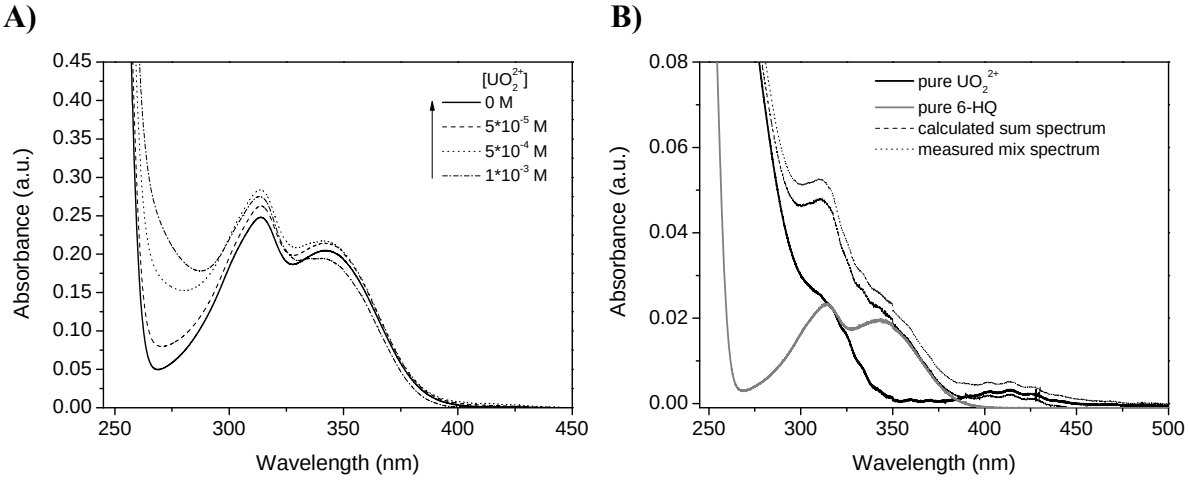

Fig. 3.14 A) Absorption spectra of 5×10^{-5} M 6-HQ in 0.1 M $NaClO_4$ as a function of the UO_2^{2+} concentration at pH 1. B) Comparison of the measured absorption spectrum of a mixing solution of 6-HQ and UO_2^{2+} with the calculated sum spectrum of the pure single components.

Clearly visible is the overlap of the spectrum of the UO_2^{2+} in the 450-350 nm range with the spectrum of the 6-HQ. Therefore, the determination of the complex formation can not be carried out using the absorption properties of the metal ion. The absorption properties of the ligand were only negligibly changed. The spectra are a linear combination of the single component spectra of the free uranyl ion and the ligand (Fig. 3.14B). Measurements at higher pH values addicted also no analyzable results. Therefore, absorption spectroscopy is not appropriated to determine the stability constants of the complex formation of 6-HQ with U(VI).

The complex formation of 6-HQ and U(VI) was also investigated with laser fluorescence measurements in order to determine the complex formation reactions. Fig. 3.15 shows the luminescence spectra of 1×10^{-5} M UO_2^{2+} as a function of the ligand concentration at pH 3 and 4.

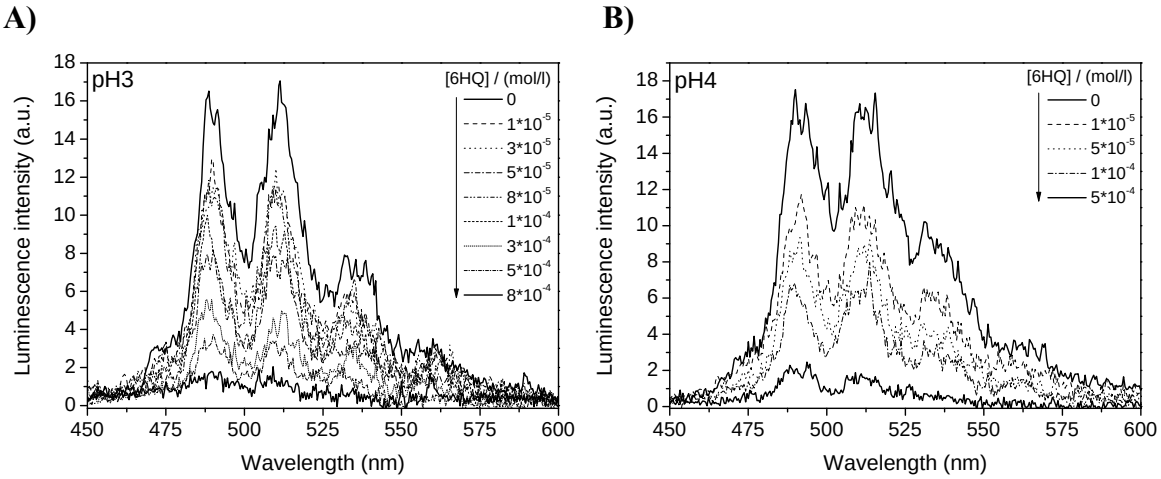

Fig. 3.15 Luminescence spectra of 1×10^{-5} M UO_2^{2+} in 0.1 M $NaClO_4$ as a function of the 6-HQ concentration at A) pH 3 and B) pH 4.

The evaluation of the spectra was carried out with the spectra recorded after 201 ns due to the luminescence properties of the ligand. At this time the luminescence of 6-HQ is completely decayed. The spectra at pH 3 and 4 show a decrease of the luminescence intensity with increasing ligand concentration. This behavior is typical for static luminescence quenching. At pH 3 the decay was bi-exponential indicating a mixture of the free uranyl ion with a lifetime of 1.3 µs and the 6-HQ with a lifetime of 25 ns. The spectra at pH 4 show tri-exponential decay. The first lifetime of 37 ns can be assigned to the ligand 6-HQ, the second lifetime of 1.3 µs to the free uranyl ion and the third lifetime of 35 µs to a uranyl hydroxide species most likely UO_2OH^+. The lifetimes of the different species decrease with increasing ligand concentration indicating additional dynamic quenching. The spectra at pH 4 had to be

corrected for the uranyl hydroxide species, which shows very high luminescence intensities even at very low concentrations.

The evaluation of the spectra and the calculation of the stability constant were carried out with both the slope analysis and the factor analysis program SPECFIT. The examination with the slope analysis results in a slope of 1.13 at pH 3 and 1.03 at pH 4, respectively. These slopes indicate clearly the formation of a 1:1 complex. The SPECFIT calculations show that the complex formation of UO_2^{2+} occurs with the anionic species of 6-HQ. The SPECFIT fit with the cationic species achieved worse results than those with the anionic species. The complex formation reaction can be expressed as follows:

$$UO_2^{2+} + C_9H_5NO^- \rightleftharpoons UO_2[C_9H_5NO]^+ \qquad \log \beta_{110} \qquad (32)$$

The stability constant for the 1:1 complex $UO_2[C_9H_5NO]^+$ was determined to be $\log \beta_{110} = 9.67 \pm 0.13$. At present, no literature data are available about the complex formation of 6-HQ with comparable metal ions.

The U(VI)–NAP system

Fig. 3.16 depicts the measured emission spectra of 1×10^{-4} M UO_2^{2+} in 0.1 M $NaClO_4$ as a function of the NAP concentration at pH 2 and 4.

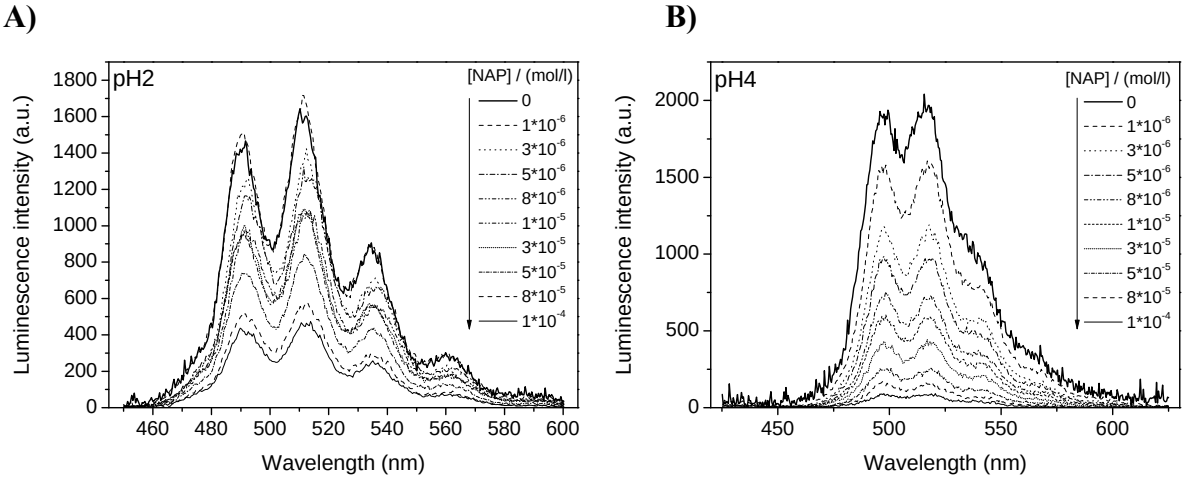

Fig. 3.16 Luminescence spectra of 1×10^{-4} M UO_2^{2+} in 0.1 M $NaClO_4$ as a function of the NAP concentration at A) pH 2 and B) pH 4.

The spectra at pH 2 and 4 show a decrease in the luminescence intensity with increasing ligand concentration and a slightly shift of the emission maxima of 1-2 nm to higher wavelengths. This is typical for static luminescence quenching due to the complex formation.

The spectra at pH 2 show mono-exponential decay with an averaged lifetime of 631 ns, the spectra at pH 4 bi-exponential decay with lifetimes of 417 ns and 2019 ns. The lifetimes are independent of the NAP concentration and were not changed. Additional dynamic quenching is not existent. The determined lifetimes are very short and can not be clearly assigned to the different species. Reasons therefore are unknown at this time. However, the lifetimes are not of importance for the further evaluation of the spectra due to the absence of dynamic quenching.

The evaluation of the emission spectra with the slope analysis delivers no utilizable results. Therefore, the evaluation of the spectra was made with the factor analysis program SPECFIT. At both pH a 1:1 complex $UO_2[C_{10}H_6O_2H]^+$ with an averaged stability constant of $\log \beta_{111} = 23.18 \pm 1.19$ was determined.

Furthermore, fs-TRFLS measurements were performed to investigate the complex formation based on the luminescence properties of NAP. Fig. 3.17 shows the measured fs-TRLFS spectra of 2×10^{-5} M UO_2^{2+} and 1×10^{-4} M NAP in 0.1 M $NaClO_4$ as a function of the pH and the integral luminescence intensity with and without U(VI) as a function of the pH.

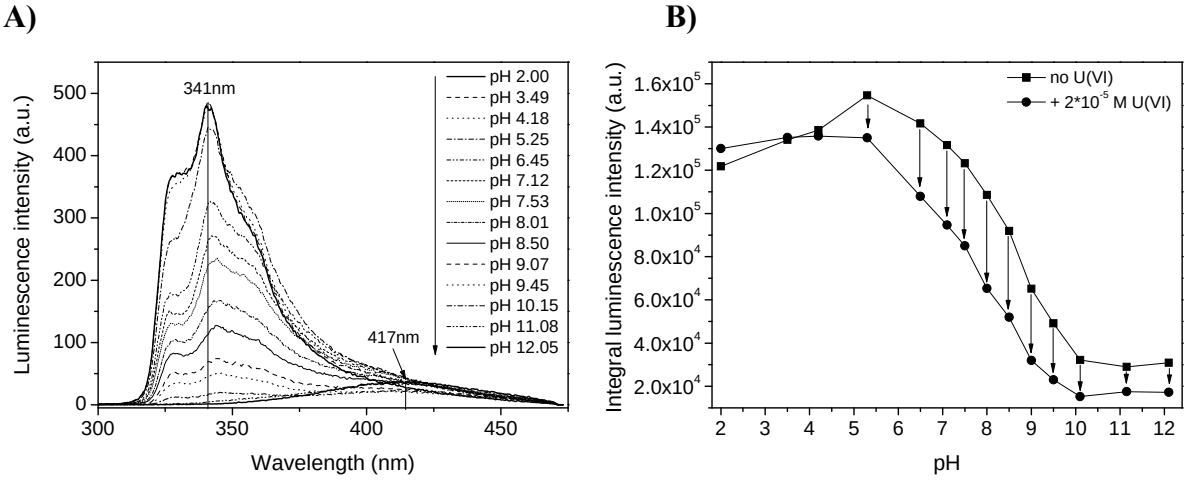

Fig. 3.17 A) fs-TRLFS spectra of 2×10^{-5} M UO_2^{2+} and 1×10^{-4} M NAP in 0.1 M $NaClO_4$ as a function of the pH. B) Integral luminescence intensity of the spectra without and with UO_2^{2+} as a function of the pH.

In all samples at pH values above 4 a strong quenching of the NAP luminescence intensity was observed. It follows that the formed U(VI)–NAP complexes emit no luminescence light. The luminescence lifetimes were not influenced within the investigated pH range. Static luminescence quenching was observed during the complex formation, additional dynamic quenching is not existent. Two U(VI)–NAP complexes could be identified using SPECFIT, which can be described by following equilibria:

$$UO_2^{2+} + NAP^{2-} + H^+ \rightleftharpoons UO_2[NAPH]^+ \qquad \log \beta_{111} \qquad (33)$$

$$UO_2^{2+} + 2NAP^{2-} + H^+ \rightleftharpoons UO_2[NAP]_2H^- \qquad \log \beta_{121} \qquad (34)$$

Stability constants for the reactions (33) and (34) were determined to be $\log \beta_{111} = 20.50 \pm 1.40$ and $\log \beta_{121} = 29.90 \pm 0.50$.

Bartusek studied in 1967 the complex formation of U(VI) and NAP with potentiometric titration and determined two complex species with stability constants of $\log \beta_{110} = 15$ and $\log \beta_{120} = 25.80$ [36]. These values are different from those determined with spectroscopic measurements. A reason therefore is the different stoichiometry of the determined complexes.

3.2.2.2 Cm(III) and chromophore models

The Cm(III)-NAP system

Fig.3.18A presents an overview of the emission spectra of 3×10^{-7} M curium(III) in 0.1 M $NaClO_4$ measured in the NAP system.

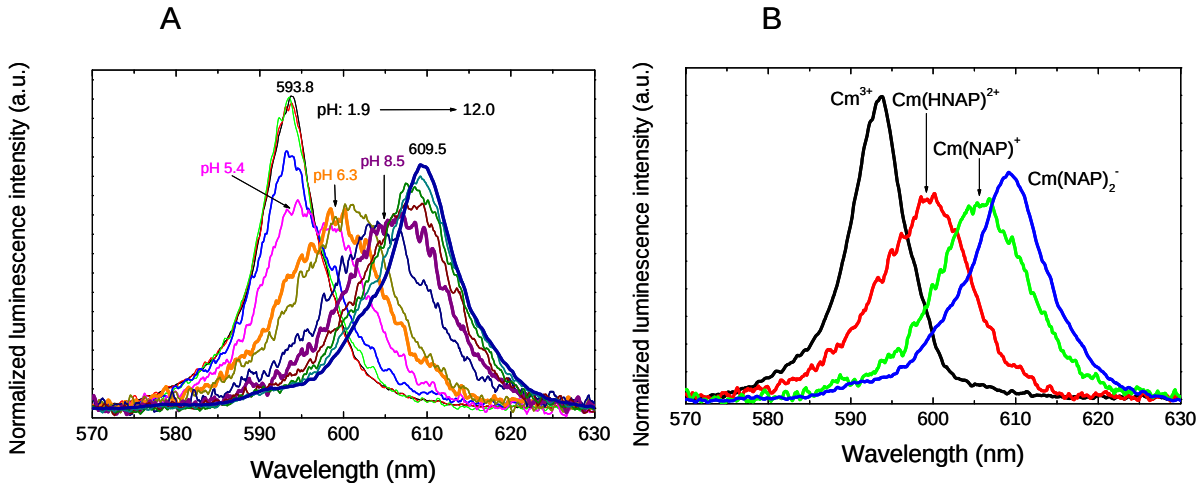

Fig. 3.18 A) Luminescence spectra of 3×10^{-7} M curium(III) in 0.1 M $NaClO_4$ at a fixed NAP concentration of 1.5×10^{-4} M as a function of pH. B) Luminescence spectra of the single components in the Cm^{3+}–NAP system, as derived by peak deconvolution using SPECFIT. The spectra are scaled to the same peak area.

The spectral variations depicted in Fig. 3.18A as a function of pH at a fixed NAP concentration are clear indications for a strong interaction of aqueous NAP species and Cm^{3+}. The emission maximum of Cm^{3+} at 593.8 nm decreased with increasing pH at fixed NAP concentration. The interaction between NAP and Cm(III) was already visible at pH 4.5. The shoulder at 598 nm observed at pH 5.4 underlines the formation of a first Cm(III)-NAP

species. No influence of the Cm^{3+} aquo ion could be detected in the measured sum TRLFS spectra at pH ≥ 7.95. The formation of the second Cm(III)–NAP species is shown by the changes in the emission spectra between pH 6.9 and 8.5 (see Fig. 3.18A). Then up to pH 11.9 the spectra are again red shifted with an emission maximum at 609 nm indicating the increased influence of the third Cm(III)–NAP complex. To the best of our knowledge both no complexation constants of Cm(III) with NAP as well as no spectroscopic characteristics of those species are reported. The variations observed in the emission data (see Fig. 3.18A) could be described by the following equilibria:

$$Cm^{3+} + NAP^{2-} + H^{+} \rightleftharpoons CmHNAP^{2+} \qquad \log \beta_{111} \qquad (35)$$

$$Cm^{3+} + NAP^{2-} \rightleftharpoons CmNAP^{+} \qquad \log \beta_{110} \qquad (36)$$

$$Cm^{3+} + 2NAP^{2-} \rightleftharpoons Cm[NAP]_2^{-} \qquad \log \beta_{120} \qquad (37)$$

Formation constants for reactions (35) to (37) were calculated using SPECFIT to be $\log \beta_{111} = 18.70 \pm 1.0$, $\log \beta_{110} = 11.50 \pm 0.67$, and $\log \beta_{120} = 19.21 \pm 0.21$. These results indicate that NAP forms strong 1:1 and 1:2 complexes with curium(III). The three species, $CmHNAP^{2+}$, $CmNAP^{+}$ and $Cm[NAP]_2^{-}$, are characterized by single emission peaks at 599, 606, and 609 nm, respectively (see 3.18B).

The complexation is accompanied by an increase of the luminescence lifetime. In all test solutions a mono-exponential decay was measured. Between pH 2 and 5.4 an average lifetime of 76 µs was detected; this lifetime could correspond to the $CmHNAP^{2+}$ species. Between pH 6.3 and 8.6 an average lifetime of 90.4 µs was observed. This lifetime can be attributed to the $CmNAP^{+}$ species. At pH values greater than 9.1 also a mono-exponential decay was measured with an average lifetime of 101 µs. This parameter might correspond to the third Cm(III)–NAP species, $Cm[NAP]_2^{-}$. The increasing lifetimes of the Cm(III)–NAP species reflect the exclusion of water molecules from the first coordination sphere of curium(III), due to the identified complex formation reactions. The average number of water molecules in the first coordination sphere of $CmHNAP^{2+}$, $CmNAP^{+}$, and $Cm[NAP]_2^{-}$, calculated with the determined luminescence lifetimes using the Kimura and Choppin equation [77] are 7.7 (8), 6.3 (7) and 5.5 (5), respectively. The numbers of water molecules estimated from the stoichiometry found with SPECFIT are given in parenthesis and were calculated as follows. There is a lack of information regarding the structure of Cm(III) complexes with NAP. The preferred binding places for Cm(III) are the two neighboring OH groups of the naphthalene ring structure. In the $CmHNAP^{2+}$ complex one deprotonated OH group of the NAP molecule is coordinated in a monodentate fashion to the Cm(III) center. This results in a release of one water molecule from the first coordination sphere of Cm(III). Hence the $CmHNAP^{2+}$ complex

contains eight water molecules. A bidentate coordination of the two deprotonated hydroxyl groups of NAP results in seven remaining water molecules in the $CmNAP^{+}$ complex. The large increase of the stability constant compared to those from the 1:1:1 species suggest the formation of a four-membered chelate ring structure. Five remaining water molecules in the $Cm[NAP]_2^{-}$ complex can be explained by a bidentate coordination of two deprotonated NAP molecules. The stoichiometry of the Cm(III)–NAP species obtained by both methods (Kimura & Choppin equation and SPECFIT) is in fair agreement.

The Cm(III)–6-HQ system

Fig. 3.19A depicts the summary of the emission spectra of 3×10^{-7} M curium(III) in 0.1 M $NaClO_4$ measured in the 6-HQ system. The spectra were obtained using an excitation wavelength of 400 nm and are corrected for the actual laser energy. The changes in the luminescence intensity combined with a red shift of the emission maxima depicted in Fig. 3.19A as a function of pH at a fixed 6-HQ concentration, are clear indications for complexation reactions between aqueous 6-HQ species and Cm^{3+}. Within pH 3.2 and 7.2, we measured an increase in the luminescence intensity together with a red shift of the emission maximum from 594 nm (free Cm^{3+} ion) to 600.6 nm. Both are indications for the formation of a first Cm(III)–6-HQ species. Then up to pH 10.4 the spectra show a continuous red shift to 606.1 nm in combination with a decrease of the luminescence intensity. This indicates that the second Cm(III)–6-HQ species exhibits a lower luminescence yield.

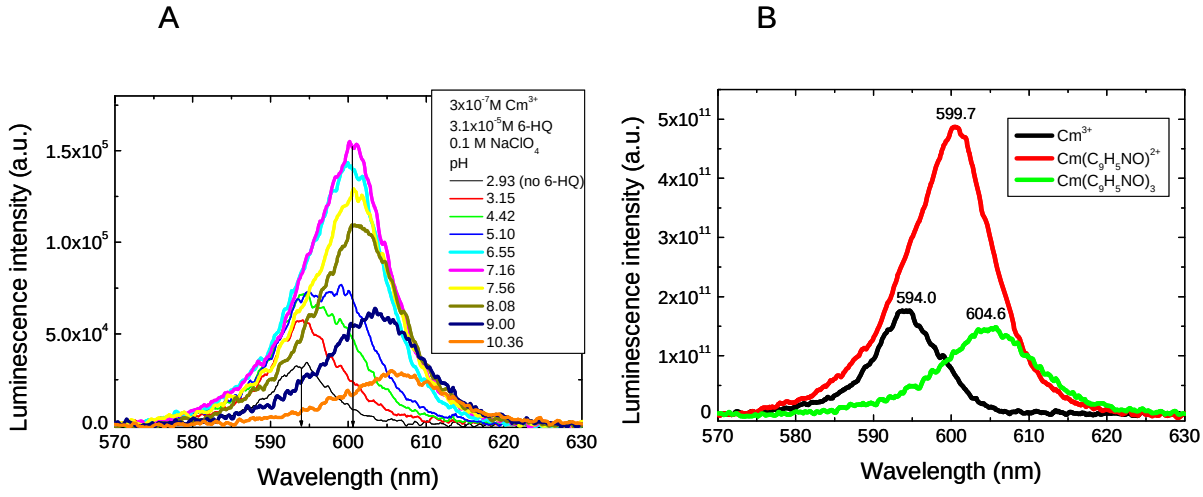

Fig. 3.19 A) Luminescence spectra of 3×10^{-7} M curium(III) in 0.1 M $NaClO_4$ at a fixed 6-HQ concentration of 3.1×10^{-5} M as a function of pH measured at an excitation wavelength of 400 nm. B) Luminescence spectra of the single components in the Cm^{3+}–6-HQ system, as derived by peak deconvolution using SPECFIT.

To the best of our knowledge both no complexation constants as well as no spectroscopic characteristics of Cm(III) hydroxyquinoline species are reported. The variations observed in the emission data (see Fig. 3.19A) could be described by the following equilibria:

$$Cm^{3+} + C_9H_5NO^- \rightleftharpoons Cm[C_9H_5NO]^{2+} \qquad \log \beta_{110} \qquad (38)$$

$$Cm^{3+} + 3\ C_9H_5NO^- \rightleftharpoons Cm[C_9H_5NO]_3 \qquad \log \beta_{130} \qquad (39)$$

Formation constants for reactions (38) and (39) were calculated using SPECFIT to be $\log \beta_{110} = 8.43 \pm 0.17$, and $\log \beta_{130} = 18.95 \pm 1.3$. The corresponding single-component spectra of the individual species are summarized in Fig. 3.19B. The two species, $Cm[C_6H_5NO]^{2+}$, and $Cm[C_6H_5NO]_3$, are characterized by emission peaks at 599.7 and 604.6 nm, respectively.

The complexation is accompanied by an increase of the luminescence lifetime. In all test solutions a mono-exponential decay was measured. An average lifetime of 76.4 µs was measured at pH 4.4 which could be assigned to the species $Cm[C_6H_5NO]^{2+}$. Between pH 6.5 and 10.6 an average lifetime of 96 ± 3 µs was detected. The measured lifetimes represent an average lifetime of all Cm(III)–6-HQ species in equilibrium. At pH 10.4 the influence of the first species, $Cm[C_9H_5NO]^{2+}$, should be below the detection limit of the method. Then the lifetime of 96 µs can be attributed to the $Cm[C_9H_5NO]_3$ complex. Using the Kimura&Choppin equation [77] the lifetimes of the species $Cm[C_6H_5NO]^{2+}$ and $Cm[C_9H_5NO]_3$ correspond to 7.6 (8) and 6.0 (6), respectively, water molecules in the first coordination sphere of Cm(III) in these species. The numbers of water molecules estimated from the stoichiometry found with SPECFIT is given in parenthesis and were calculated as follows. The preferred binding place for Cm(III) is the phenolic OH group located on the C6 atom of the naphthalene ring structure. If one deprotonated 6-HQ molecule is coordinated in a monodentate fashion to the Cm(III) center, this results in a release of one water molecule from the first coordination sphere of Cm(III). Hence the $Cm[C_6H_5NO]^{2+}$ complex contains eight water molecules. Consequently, the coordination of three deprotonated 6-HQ molecules results in a release of three water molecules. Interestingly, all attempts to isolate a 1:2 complex failed. The coordination of two deprotonated 6-HQ molecules to the Cm(III) center seems to be energetically less favorable than the binding of three deprotonated 6-HQ molecules.

The involvement of the N atom of the naphthalene ring structure in Cm(III) bonding seems unlikely from for instance sterical reasons. The formation of chelates should result in both larger formation constants as well as more red shifted emission maxima (please see the results obtained in the Cm(III)–NAP system for comparison). For the U(VI)–8-hydroxyquinoline

system it could be demonstrated that the phenolic OH group and the neighboring N (via one C atom from the ring) atom are involved in a bidentate coordination to uranyl [82]. This results in significant greater formation constants for instance $\log \beta_{110} = 10.05 \pm 0.02$ as determined for the Cm(III)–6-HQ species (e.g., $\log \beta_{110} = 8.43 \pm 0.17$).

3.2.2.3 Np(V) and chromophore models

The Np(V)–NAP system

The results of the spectrophotometric titrations of the NpO_2^+ test solutions in the NAP system are shown in Fig. 3.20A.

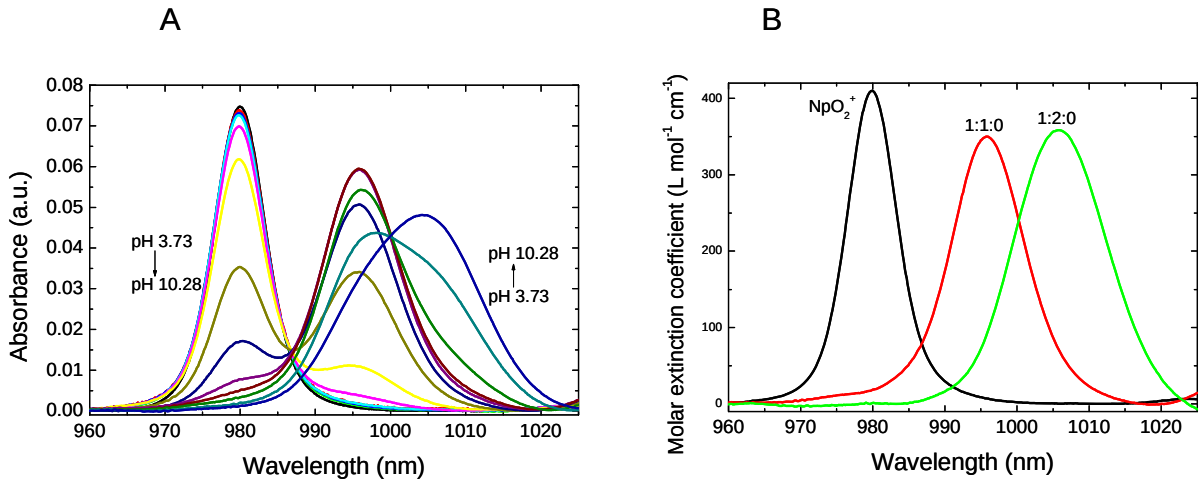

Fig. 3.20 A) Spectrophotometric titrations of 1.8×10^{-4} M NpO_2^+ in solutions containing 1.7×10^{-3} M NAP at an ionic strength of 0.1 M $NaClO_4$. B) NIR absorption spectra of the single components in the NpO_2^+–NAP system, as derived by peak deconvolution using SPECFIT.

To the best of our knowledge, spectrophotometric titrations of NpO_2^+ with NAP were not reported before. Neptunyl(V) forms strong complexes with this selected chromophore model ligand. The NIR absorption spectra of the corresponding single components are summarized in Fig. 3.20B. The identification of two isosbestic points at approximately 987 and 1000 nm points to the occurrence of two different Np(V)–NAP species. Thus two different species, 1:1:0 and 1:2:0, were identified. The following Np(V)–NAP stability constants were calculated: $\log \beta_{110} = 8.23 \pm 0.17$, and $\log \beta_{120} = 13.60 \pm 0.05$ [18]. Among the pyoverdin model systems (simple hydroxamates), NAP forms the strongest 1:1 and 1:2 complexes with Np(V). The largest red shift of the Np(V) absorption band, 996.2 nm, for a 1:1 model complex compared to those with SHA and BHA and the magnitude of the stability constant indicate the formation of a four-membered chelate ring. In this structure, Np(V) binds to both

oxygen atoms from the deprotonated phenolic OH groups. A similar structure involving two deprotonated NAP ligands can be postulated for the identified 1:2 complex.

The strength of complexation increases in the order BHA, SHA to NAP. One might conclude that the four-membered chelate ring of the NAP molecule formed with the linear neptunyl unit is more stable than those with the hydroxamate groups of SHA and BHA. It is difficult to include DFO in this discussion because this ligand contains three hydroxamate groups. The occurrence of three chelating hydroxamate groups in one molecule explains whose good Np(V) binding properties.

The Np(V)–6-HQ system

One example of spectrophotometric titrations measured in the Np(V)–6-HQ system is shown in Fig. 3.21.

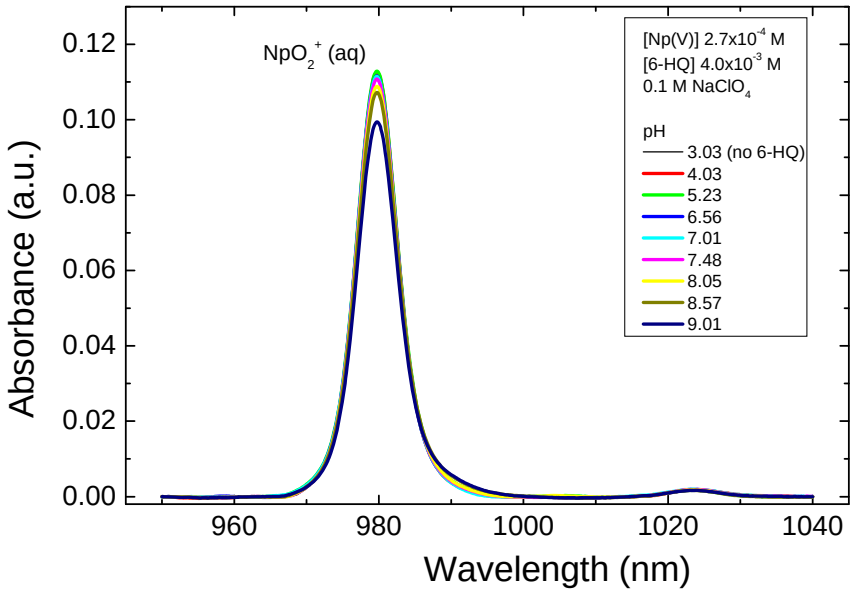

Fig. 3.21 Spectrophotometric titrations of 2.7×10^{-4} M NpO_2^+ as a function of pH in solutions containing 4.0×10^{-3} M 6-HQ at an ionic strength of 0.1 M $NaClO_4$.

To the best of our knowledge spectrophotometric titrations of NpO_2^+ with 6-HQ were not reported before. We observed by adding NaOH to the Np(V)–6-HQ test solutions only a small decrease in the intensity of the absorption peak at 980 nm (free NpO_2^+ ion). It follows that we could not detect interactions of NpO_2^+ with 6-HQ within 6-HQ concentrations of 3.4×10^{-4} M and 4.0×10^{-3} M and a wide pH range using NIR spectroscopy. The inset of greater 6-HQ concentrations is limited due to their low solubility in aqueous solution.

4 Studies on the interaction of isolated bacterial cell wall components with actinides (U(VI), Cm(III), Np(V))

The influence of microorganisms on the transport behavior of heavy metals in the environment is significant. Bacteria can immobilize or mobilize metal ions through diverse accumulation and complexation mechanisms [83]. Bacteria have the highest surface to volume ratio of any life form [84]. Therefore, soluble metal ions will interact mainly with bacterial surfaces. The main binding sites of the bacterial cell surfaces for heavy metal ions are phosphoryl, carboxyl, hydroxyl, and amino groups. Various investigations with bacteria show that the uranium ion has a high affinity to phosphoryl groups [e.g., 85-91], whereas for trivalent actinides and lanthanides carboxyl and phosphoryl groups seem to be in equal measure effective for binding [e.g., 92-98]. However, the exact mechanisms of the interactions between cell surfaces and metals remain unclear. To our knowledge, up to now either complete cell walls or even whole cells were used to study the interactions with metal ions. Therefore, we investigated in this project the complexation of the actinides U(VI), Cm(III), and Np(V) with single cell wall constituents. We chose as model compounds lipopolysaccharide (LPS), the main component of the outer membrane of Gram-negative bacteria, and peptidoglycan (PG), the main component of the cell wall of Gram-positive bacteria.

The interaction of U(VI) [37, 38] and Cm(III) with LPS [99] and PG were studied with TRLFS. Additionally the U(VI) bioligand systems were examined with potentiometric titration [37, 38]. The complexation of the biomacromolecules with Np(V) were investigated with spectrophotometric titration.

4.1 Experimental

Solutions and reagents

All experiments were made in an ionic medium in which the sodium concentration was kept constant at 0.1 M by adding analytical grade $NaClO_4$ (Merck, Darmstadt, Germany). To prevent the carbonate complexation of the actinides, carbonate-free water was used. The pH was measured using an InLab 427 combination pH puncture electrode (Mettler-Toledo, Giessen, Germany) calibrated with standard buffers. The pH was changed by adding analytical grade NaOH or $HClO_4$ with an accuracy of ± 0.05 units. Lipopolysaccharide from *P. aeruginosa* Serotyp 10 (LPS), purified by trichloroacetic acid extraction, was purchased

from SIGMA-ALDRICH. Peptidoglycan (PG) from *B. subtilis* was purchased from Fluka and used without further purification. The stock solutions were prepared freshly for each experiment. The Cm(III) and Np(V) experiments were performed in a glove box under an N_2 atmosphere at 25 ºC.

Potentiometric titrations

For uranyl LPS complexation titration (5 measurements), in each case 10 mg LPS and 50 µmol UO_2^{2+} were dissolved in 50 mL carbonate free deionized water, resulting in concentration values of 0.2 g/L LPS and 0.1 mM U(VI). For uranyl PG complexation titration (3 measurements), 3 mg PG and 3 µmol UO_2^{2+} were dissolved in 30 mL carbonate free deionized water, resulting in concentration values of 0.1 g/L PG and 0.1 mM U(VI). The solutions were acidified with $HClO_4$ (carbonate free) to obtain a starting pH of about 4 and titrated with 1 mM NaOH (carbonate free, Merck, Titrisol). The pH values were measured with a BlueLine 16 pH electrode (Schott). The electrode was calibrated for each experiment with NBS buffers (4.01 and 6.86, Schott). All samples were titrated with an automatic titrator (TitroLine alpha, Schott) and monitored by the accompanied software (TitriSoft 2.11, Schott). The titration procedure was a dynamic titration with a minimum drift of 5 mV/min. The titration curves were analyzed with the program HYPERQUAD. The pK_a values of the uranyl hydroxide species, corrected for I = 0.1 M, were included in analyzing the complex mixtures [100].

Preparation of actinide solutions with isolated bacterial cell wall components and experimental setup of the applied spectroscopic techniques

Uranyl LPS/PG system

TRLFS spectra were measured with a fixed uranyl concentration of 10^{-5} M as a function of the LPS concentration, 0.025 - 1.0 g/L. The pH values were varied between 2.5 and 9.0. Necessary pH adjustments were made with $HClO_4$ or NaOH with an accuracy of ± 0.02 units. Altogether 65 measurements with different pH values and LPS concentrations were performed and used in the interpretation and evaluation of the data. The exact uranyl concentrations at all measurements and also the amount of phosphorous were detected by ICP-MS (inductively-coupled-plasma mass-spectrometry) with an accuracy of 5 %.

In the U(VI)–PG system, TRLFS spectra were measured with a fixed uranyl concentration of 10^{-5} M. Three measurement series were carried out: First and second at fixed pH = 2.5 ± 0.1 and 4.0 ± 0.1, respectively, as a function of the PG concentration (0.01 – 0.2 g/L), and third at

fixed PG concentration (0.1 g/L) as a function of the pH (2.0 – 9.0). The samples were prepared in a glove box under inert gas atmosphere (nitrogen). Necessary pH adjustments were made with a BlueLine 16 pH electrode (Schott) using $HClO_4$ or NaOH with an accuracy of ± 0.02 units. The exact uranyl concentration at all measurements was detected.

The spectra were recorded at 22 ± 1 °C using a pulsed Nd:YAG laser system (Continuum Minilite Electro-Optics, Inc., Santa Clara, USA) with a fast pulse generator (FPG/05, EG&G Princeton Instruments, NJ, USA), and a digital delay generator (model 9650, EG&G Princeton Instruments, NJ, USA). The excitation wavelength of the uranyl fluorescence was 266 nm with pulse energy of 0.2 - 0.5 mJ. The TRLFS spectra were measured from 360 to 670 nm, averaging three spectra with 100 laser pulses each, and a gate time of 2 µs. The time-resolved fluorescence emission was detected using a detector interface (model 1471A, EG&G Princeton Instruments, NJ, USA), and a TRIAX 550 spectrograph (Jobin Yvon Horiba) with a resolution of 0.2 nm, controlled by the software V2.10 TRIAX (Jobin Yvon Horiba). All other functions of the laser spectrometer are computer controlled with home made software; a description is given elsewhere [101]. The baseline corrections, lifetime and peak maxima determinations of the spectra were done with Origin 7.5 (OriginLab, Northhampton, MA, USA). The complex stability constants were determined with SPECFIT [20]. Again the pK_a values of the uranyl hydroxide species, corrected for I = 0.1 M, were included in analyzing the complex mixtures [100].

Cm(III) LPS/PG system

The curium(III) concentration was fixed at 3×10^{-7} M in all TRLFS measurements. The Cm(III) TRLFS spectra were recorded at 25°C using a pulsed flash lamp pumped Nd:YAG-OPO laser system as described in chapter 3.1. Four series of experiments were performed to explore the complexation behavior of curium(III) with LPS. In the first three runs, we investigated the curium(III) complex formation by varying the LPS concentration between 1 and 250 mg/L at a fixed pH of 3, 6.9, and 10.6; in the fourth run, the LPS concentrations was kept constant at 50 mg/L, while varying the pH between 1.7 and 11.0.

In the Cm(III)–PG system, two series of measurements with a fixed Cm(III) concentration of 3×10^{-7} M were carried out: With fixed PG concentration of 50 mg/L and pH varying from 3.2 to 9.3 and with fixed pH (6.0) and varying PG concentration (0.1 – 50 mg/L).

Np(V) LPS/PG system

Aliquots of a Np(V) stock solution (^{237}Np, 0.034 M, 0.1 M HNO_3) were added to the test solutions. The neptunium(V) concentration was fixed at 1.8×10^{-4} M in all spectrophotometric titrations. In the Np(V)–LPS system, LPS concentrations of 0.05, 0.5, and 0.8 g/L were used. The pH in those test solutions was usually changed between 3.0 and 9.6. In the Np(V)–PG system, two PG concentrations of 0.05 and 0.3 g/L were used while varying the pH between 3 and 10. The spectrophotometric Np(V) titrations were carried out at room temperature (25 ± 1 ºC) using a Cary-5G UV / Visible / Near IR spectrophotometer (Varian, Inc.) as described in chapter 3.1. The neptunium(V) concentration in all acidic test solutions without adding a ligand was determined by spectrophotometric analysis at 980 nm using a molar extinction coefficient of 395 L mol^{-1} cm^{-1} [56].

The individual scans measured for each sample were averaged and baseline corrected using ORIGIN 6.1G software (OriginLab, Northhampton, MA, USA). The complex formation constants were calculated based in the variations in the measured spectra using the factor analysis program SPECFIT [20]. The speciation calculations were made using SOLGASWATER software [19].

4.2 Results and discussion

4.2.1 Actinide interaction with lipopolysaccharide (LPS)

4.2.1.1 U(VI) and LPS

Potentiometric titrations

The calculation procedure is based on the formal complex formation equation for discrete binding sites

$$x\ UO_2^{2+} + y\ R\text{–}A_i^{-} + z\ H^{+} \rightleftharpoons [(UO_2)_x(R\text{–}A_i)_yH_z]^{x(2x-y+z)+}, \quad (40)$$

and the appropriate mass action law, which represents the complex stability constant log β_{xyz}:

$$K = \frac{[(UO_2)_x(R-A_i)_yH_z]}{[UO_2^{2+}]^x[R-A_i]^y[H^+]^z} \quad (41)$$

As initial data for the calculation of the complex stability constants we used the pK_a values and site densities of the functional groups calculated with ProtoFit (see Table 2.6). Additionally, the stability constants of the relevant uranyl hydroxide complexes were included.

With the site densities listed in Tab. 2.6, the concentrations of carboxyl and phosphoryl groups for 0.2 g/L LPS result in about 0.06 mM each. With a uranyl concentration of 0.1 mM, we have a slight deficit in each functionality, but altogether it results in a nearly equimolar ratio of potential coordination groups. For all titration experiments with uranyl and LPS the best fits were obtained with three 1:1 complexes, one with carboxyl coordination ($R–COO–UO_2^+$) and two with phosphoryl coordination, at lower pH a protonated complex ($R–O–PO_3H–UO_2^+$), and at higher pH the deprotonated form $R–O–PO_3–UO_2$. The complex stability constants were calculated to be $\log \beta_{110} = 5.93 \pm 0.17$ for the carboxyl coordination, and $\log \beta_{110} = 7.50 \pm 0.30$ and $\log \beta_{111} = 11.66 \pm 0.30$ for the phosphoryl complexes, respectively (see Tab. 4.1).

TRLFS

Fig. 4.1 depicts a summary of the measured luminescence spectra of the UO_2^{2+}–LPS system at different pH.

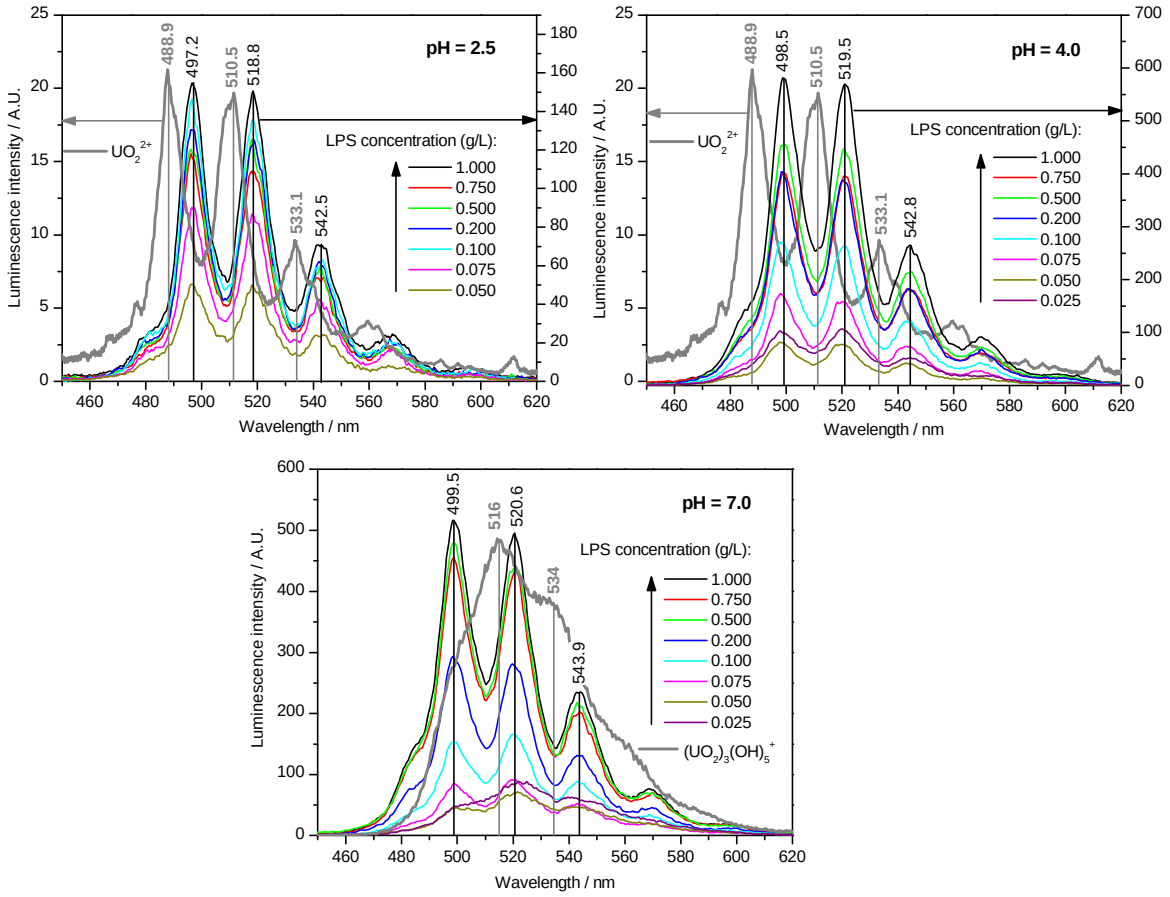

Fig. 4.1 Summary of the measured luminescence spectra at fixed uranyl concentration (10^{-5} M) and various LPS concentration at different pH.

For comparison the uranyl spectra at pH 2.5 (100% UO_2^{2+}(aq)) and pH 6.0 (main species: $(UO_2)_3(OH)_5^+$) are included. The concentrations of the functional groups (calculated out of the results from potentiometry, see Tab. 2.6) ranged from about 0.75×10^{-5} M (0.025 g/L LPS) to 3×10^{-4} M (1 g/L LPS) for each, carboxyl and phosphoryl groups. Generally a strong increase of the luminescence intensity, connected with a red shift of the peak maxima of about 8 nm at pH 2.5 and up to 11 nm at neutral pH range, compared to the free uranyl ion UO_2^{2+}(aq), was observed. At very low LPS concentration values (up to 0.05 g/L) at pH 7 uranyl hydroxide species come up, but at high LPS concentration (1 g/L) not until pH 8 formation of uranyl hydroxide species was detected. This behavior is an indicator for the high stability of UO_2^{2+}–LPS complex species at an excess of LPS.

A red shift of about 8-11 nm is very typical for uranyl phosphoryl complexes [102, 103]. Most of the uranyl carboxylate complexes normally show no luminescence behavior at room temperature as well as inorganic uranyl carbonates [102, 104, 105]. At the few exceptions, the carboxylic coordination causes a relatively small red shift of the luminescence maxima of about 5-8 nm [105, 106-108]. Inorganic phosphate causes a still stronger red shift of about 10-14 nm [109-111].

The time-resolved measurements give information about the lifetimes of the exciting state of the luminescent species in the mixture. Thus, it provides further information on the number of the luminescent species. To evaluate the number of the luminescent species and their lifetimes, the integrated luminescence signal is fitted to a sum of exponential decay functions:

$$E(t) = \sum_i E_i \cdot \exp(-1/\tau_i) \qquad (42)$$

E is the total luminescence intensity at the time t, E_i the luminescence intensity of the species i at t = 0, and τ_i the corresponding lifetime.

We observed for all measurements a bi-exponential decay according to at least two different luminescent uranyl species. At pH 2.5 to 3.3 the intensity of the first lifetime (averaged 1.5 ± 0.3 µs) decreases with increasing ligand concentration. The second lifetime (averaged 8.3 ± 0.6 µs) shows an increase in intensity with increasing ligand concentration. Therefore, we dedicate the shorter lifetime to the free uranyl ion (1.8 ± 0.2 µs[112]) and the longer one to a uranyl LPS complex species. At pH values higher than 3.5, the lifetime of the free uranyl ion is no more detectable. Now, the first lifetime of (averaged) 1.2 ± 0.4 µs is somewhat shorter than those of the free uranyl ion, and a second lifetime appears at (averaged) 13.3 ± 1.5 µs. At about pH 4 both lifetimes are detectable nearly on par, but with higher pH the longer lifetime increases and dominates near neutral pH. We dedicate both lifetimes to

uranyl LPS complexes. At pH over 8 uranyl hydroxides appear and become predominant even at a high LPS excess.

As a result, from lifetime analysis we conclude that at least three different uranyl LPS complexes are detectable with TRLFS. The quantitative investigation of the luminescence spectra we carried out with SPECFIT. The calculation procedure is based on the formal complex formation equations (40) and (41). As initial data we used again the pK_a values and site densities of the functional groups calculated earlier (see Tab. 2.6) and the stability constants of the relevant uranyl hydroxide and carbonate complexes [100]. The contribution of the $–NH_3^+$ and –OH groups to the complexation was neglected, due to their strong basic dissociation constants (see Tab. 2.6). Because the TRLFS experiments were carried out with a high LPS excess (equitable with a high phosphoryl excess) and taking in consideration the high affinity of uranyl to phosphoryl it is assumed that only the luminescence properties of uranyl phosphoryl species could be detected. Possible uranyl carboxyl species are probably restrained by the dominating uranyl phosphoryl luminescence.

Tab. 4.1 Summary of the calculated log β_{xyz} values of uranyl LPS complexes and comparison with some literature data.

Species	**Complex**	**xyz**[a]	**Log β_{xyz}**	**Method**
LPS (*P. aeruginosa*)	$R–COO–UO_2^+$	110	5.93 ± 0.17	Potentiometry
	$R–O–PO_3–UO_2$	110	7.50 ± 0.30 7.53 ± 0.25	Potentiometry TRLFS
	$R–O–PO_3H–UO_2^+$	111	11.66 ± 0.30 12.01 ± 0.10	Potentiometry TRLFS
	$(R–O–PO_3)_2–UO_2^{2-}$	120	13.80 ± 0.37	TRLFS
Bacillus subtilis[113]	$R–COO–UO_2^+$	110	5.4 ± 0.2	
	$R–POH–UO_2^{2+}$	111	11.8 ± 0.2	

At pH 2.5 a uranyl complex with a protonated phosphoryl group gave the best fit with a stability constant of log β_{111} = 12.01 ± 0.10 ($R–O–PO_3H–UO_2^+$). This value agrees well with the constant determined by potentiometry. From pH 4 two uranyl complexes with deprotonated phosphoryl groups lead to the best fit, a 1:1 and a 1:2 (metal:ligand) complex. At pH 4-5 both complexes could be fitted side by side satisfiable. At pH 6 and higher only the 1:2 complex could be calculated to obtain the best result. The stability constants were calculated to be (averaged) log β_{110} = 7.53 ± 0.25 ($R–O–PO_3–UO_2$), and

$\log \beta_{120} = 14.41 \pm 0.81$ ($[R–O–PO_3]_2–UO_2^{2-}$). The $\log \beta_{110}$ value is again in very good accordance to those calculated by potentiometry (see Tab. 4.1).

To our knowledge, only one study with binding stability constants of uranyl to bacteria is published. There, the binding stability constants of UO_2^{2+} to *Bacillus subtilis* were calculated to be $\log K = 5.4 \pm 0.2$ for carboxylic binding ($R–COO–UO_2^{+}$) and $\log K = 11.8 \pm 0.2$ for phosphoryl binding ($R–POH–UO_2^{2+}$) [113]. Both constants agree well with ours (see Tab. 4.1).

Tab. 4.2 Summary of the measured luminescence data.

Species	Peak maxima [nm]/Peak width at half height [nm]						Lifetime [µs]
UO_2^{2+} (aq) pH = 2.5		488.9	510.5	533.2	559.6	583.8	1.67 ± 0.10
UO_2^{2+} (aq) pH = 1.0[112]	471.3	488.9	510.5	533.9	559.4	585.5	1.80 ± 0.20
U(VI) (aq) pH = 6-7		502	516	534	559	588	26.6 ± 3.6
$(UO_2)_3(OH)_5^{+}$ [113]	484	498	514	534	557	583	19.8 ± 1.8
Uranyl-LPS-complexes:							
$R–O–PO_3H–UO_2^{+}$	480.4	**497.2**	**518.9**	**542.4**	567.3	595.4	8.3 ± 0.6
$R–O–PO_3–UO_2$	481.5	**498.1**	**519.6**	**542.9**	567.5	596.0	1.2 ± 0.4
$[R–O–PO_3]_2–UO_2^{2-}$	483.6	**499.7**	**521.0**	**544.3**	568.9	596.9	13.3 ± 1.4
Uranyl phosphates:[a]							
$UO_2H_2PO_4^{+}$ (10^{-5} M UO_2^{2+}, 10^{-3} M HPO_4^{2-}, pH = 2.0)		496.2	518.3	540.2	567.6	595.4	12.8 ± 0.9
UO_2HPO_4 / $UO_2PO_4^{-}$ (10^{-5} M UO_2^{2+}, 10^{-3} M PO_4^{3-}, pH = 5.0)		503.2	524.7	546.7	572.6	598.2	5.4 ± 0.9 / 20.1 ± 3.3

a: own measurements; species assignment based on [110, 115].

With SPECFIT the single spectra of the different uranyl complex species could be calculated (see Tab. 4.2). The differences in the peak maxima are quite small, but the findings in lifetime calculation and the results of potentiometry support the segmentation of the spectra into three different complex species. The calculated spectrum of the $R–O–PO_3H–UO_2^{+}$ species is consistent with the measured spectra at pH 2.5 and high ligand concentrations, whereas the spectrum of the 1:1 complex ($R–O–PO_3–UO_2$) is recognizable at pH 4. The spectrum of the

1:2 complex ($[R–O–PO_3]_2–UO_2^{2-}$) corresponds to the measured spectra at pH 6-7 and high LPS concentrations, implicating that these species predominate in each case.

The different lifetimes that were found at the varying pH values can be dedicated to the corresponding uranyl phosphoryl species. At very low pH the phosphoryl groups of the LPS molecule are mainly protonated, therefore the protonated uranyl phosphoryl complex $R–O–PO_3H–UO_2^+$ is built first; and it is associated with the lifetime of 8.3 ± 0.6 µs. With increasing pH the amount of deprotonated phosphoryl groups rises, and the two deprotonated complexes appear, primarily the 1:1 complex $R–O–PO_3–UO_2$, which is allocated to the shortest lifetime of 1.2 ± 0.4 µs, and afterwards the 1:2 complex $[R–O–PO_3]_2–UO_2^{2-}$ with the longest lifetime of 13.3 ± 1.5 µs (see Tab. 4.2).

4.2.1.2 Cm(III) and LPS

An overview of the emission spectra of 3×10^{-7} M curium(III) in 0.1 M $NaClO_4$ measured in the LPS system at an excitation wavelength of 400 nm is presented in Fig. 4.2.

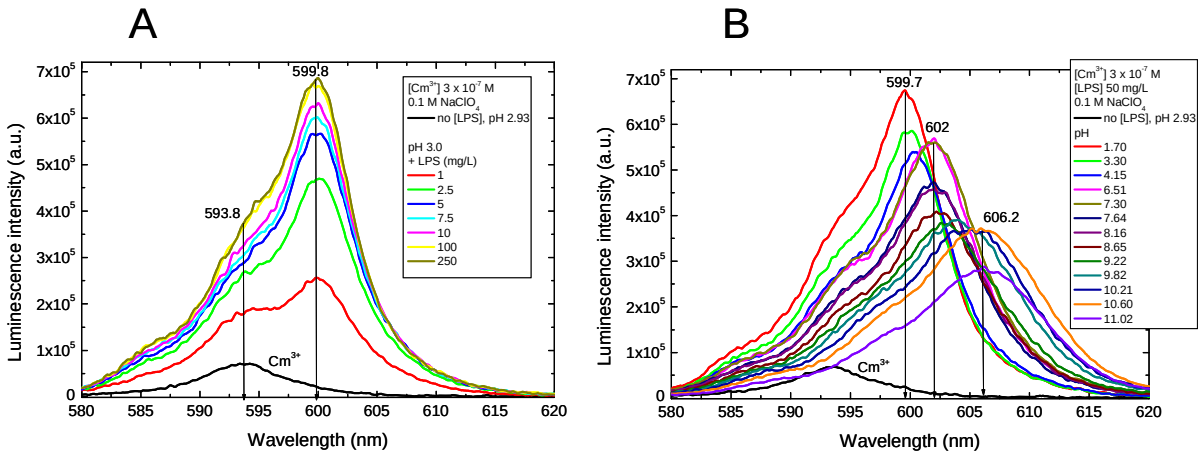

Fig. 4.2 Luminescence spectra of 3×10^{-7} M curium(III) in 0.1 M $NaClO_4$ measured at an excitation wavelength of 400 nm: A) as a function of the LPS concentration at pH 3.0; and B) at a fixed LPS concentration of 50 mg/L as a function of pH (not all data shown).

The complexation of curium(III) with LPS molecules had started even at a low LPS concentration of 1 mg/L at pH 3 (Fig. 4.2A). This LPS amount corresponds to a concentration of phosphoryl groups of 3×10^{-7} M which are most likely involved in curium bonding at this pH. With a Cm^{3+}concentration of 3×10^{-7} M, we have a nearly equimolar concentration ratio between curium and available functional groups. The changes observed in the emission spectra as a function of LPS concentration, 1–250 mg/L, at fixed pH 3 exhibit the formation

of a first Cm(III)–LPS complex. This is evidenced by the formation of the new emission band at 599.8 nm. The increase in concentration of the first Cm(III)–LPS complex is associated with a great increase in luminescence intensity. Fig. 4.2B presents the changes observed in the emission spectra at a fixed LPS concentration of 50 mg/L as a function of pH. Already at pH 1.6 and at an excess of potential coordination groups, the influence of the Cm^{3+} (aq) is very small compared to the first Cm(III)–LPS complex characterized by the emission band at 599.7 nm. At pH values greater than 6, a second complex species is formed indicated by the emission maximum at 602 nm. Then the luminescence emission maximum at 602 nm is nearly unaffected until pH 8.2. The again red shifted emission maximum, 606 nm, up to pH 10.6 indicates the formation of a third Cm(III)–LPS complex. In summary, the observed spectral changes (see Fig. 4.2) gave clear evidence for the occurrence of three different Cm(III)–LPS species.

The increased Cm(III) luminescence lifetimes in the presence of LPS are a clear indication for a replacement of water molecules by functional groups of the LPS molecule and hence for the complex formation. In the acidic pH region between pH 1.7 and 5.6, a mono-exponential decay was detected. The average lifetime 149 ± 8 µs correspond to the first Cm(III)–LPS complex. A bi-exponential luminescence decay with average lifetimes of 100 ± 9 and 214 ± 25 µs was measured between pH 7 and 11. The shorter lifetime could be assigned to the third Cm(III)–LPS species due to the results of the LPS concentration dependent measurements at a fixed pH of 10.6 (data not shown). The determination of three different luminescence lifetimes indicates the existence of three Cm(III) binding sites on the LPS molecule.

The SPECFIT calculation procedure is based on the formal complex formation equations (40) and (41) for discrete binding sites. As a result, we got the best fit for i) a complex with protonated phosphoryl coordination and 1:2 stoichiometry, ii) a complex with carboxyl coordination and 1:1 stoichiometry, and iii) a complex with hydroxyl coordination and 1:4 stoichiometry [99]. The averaged stability constants are $\log \beta_{122} = 26.9 \pm 0.6$ ($(R–O–PO_3H)_2–Cm^+$), $\log \beta_{110} = 9.32 \pm 0.20$ ($R–COO–Cm^{2+}$), and $\log \beta_{140} = 26.70 \pm 0.5$ ($(R–O)_4–Cm^-$) (see Tab. 4.3).

Phosphoryl and carboxyl groups can offer, at most, bidentate coordination whereas hydrogen phosphate and hydroxyl groups can offer only monodentate coordination with Cm(III). The average number of water molecules in the first coordination sphere of $(R–O–PO_3H)_2–Cm^+$, $R–COO–Cm^{2+}$ and $(R–O)_4–Cm^-$, calculated with the determined luminescence lifetimes using

the Kimura and Choppin equation [77] are 3.5 (7), 2.2 (7) and 5.6 (5), respectively. The numbers of water molecules estimated from the stoichiometry found with SPECFIT are given in parenthesis. It can be seen that the number of released water molecules is greater (Tab. 4.4). Such findings were also observed in various studies exploring the interaction of Eu(III) and Cm(III) with different microbes [94-98] and with biopolymers [121]. The authors conclude that the coordination of Eu(III) on microbes and biopolymers is through inner-spherical and multidentate processes involving more than one functional group. The occurrence of such processes can be also assumed for the biopolymer LPS. The larger number of released water molecules can be explained by complexation reactions with inner sphere sites ($R–O–PO_3H^-$, $R–COO^-$, $R–O^-$) and additional interactions of Cm(III) with functional groups without the formation of a chemical bond.

Tab. 4.3 Calculated log β_{xyz} values of curium(III)–LPS complexes in comparison with some literature data.

Species	Complex	xyz[a]	Log β_{xyz}	Reference
LPS (*P. aeruginosa*)	$R–COO–Cm^{2+}$	110	9.32[b]	[99]
	$(R–O–PO_3H)_2–Cm^+$	122	26.90[b]	
	$(R–O)_4–Cm^-$	140	26.70[b]	
Phosphoryl / carboxyl groups containing ligands				
Cm-PAA-species 1		112	16.11 ± 0.43[b*]	[116]
Cm-PAA-species 2		111	13.68 ± 0.80[b]**	
Adenosine 5'-Triphosphate	CmH_2ATP^+	112	16.86 ± 0.09[b]	[117]
	CmHATP	111	13.23 ± 0.10[b]	
	$CmATP^-$	110	8.19 ± 0.16[b]	
Phosphoryl / carboxyl / amino groups containing ligands				
O-phospho-L-threonine	CmH_2PThr^{2+}	112	18.03 ± 0.13[b]	[118]
	$CmHPThr^+$	111	14.17 ± 0.09[b]	
Carboxyl / hydroxyl /amino groups containing ligands				
L-threonine	$CmThr^{2+}$	110	6.72 ± 0.07[b]	[118]
	$CmThr_2^+$	120	10.22 ± 0.09[b]	
L2-Aminobutyric acid	CmL^{2+}	110	5.17 ± 0.07[b]	[119]
	CmL_2^+	120	9.00 ± 0.07[b]	
	CmL_3	130	11.30 ± 0.09[b]	
Humic acid	CmHA		6.24 ± 0.28[b]	[120]
Bacillus subtilis	$R–COO–Eu^{2+}$	110	7.13 ± 0.40[b, c]	[94]
	$R–O–PO_3–Eu^+$	110	8.14 ± 0.50[b, c]	
LPS (*P. aeruginosa*)	$R–COO–UO_2^+$	110	5.93 ± 0.17[c]	[37]
	$R–O–PO_3–UO_2$	110	7.53 ± 0.25[b]	
	$R–O–PO_3H–UO_2^+$	111	12.01 ± 0.10[b]	
	$(R–O–PO_3)_2–UO_2^{2-}$	120	13.80 ± 0.37[b]	

a: xyz = metal / ligand / H^+; b: from TRLFS, c: from potentiometric titrations
PAA: phosphonoacetic acid, * involvement of phosphoryl group, ** involvement of carboxyl group.
ATP: adenosine 5'-triphosphate, PTh: phosphothreonine, Thr: threonine, L^-: L2-aminobutyrate anion.

Tab. 4.4 Spectroscopic properties of the identified curium(III) species in aqueous solutions containing 50 mg/L LPS at an ionic strength of 0.1 M $NaClO_4$.

	Cm^{3+} (aq)	**$(R–O–PO_3H)_2–Cm^+$**	**$R–COO–Cm^{2+}$**	**$(R–O)_4–Cm^-$**
pH	2.93	2.80	7.10	11.00
Excitation (nm)	374.4 (3.6) [a]	373.1 [b] 376.8 (1.4)	376.1 (4.8)	377.6 (5.5)
	379.9 (2.9)	381.1 (5.3)	381.8 (5.5)	383.5 (4.3)
	396.0 (2.2)	397.3 (3.4)	398.5 (2.8)	399.2 (2.8)
Emission (nm)	**593.6 (8.3)** [a]	593.8 [b] **599.9** (6.5)	595.2 [b] **602.3** (8.2)	600.3 [b] **606.9** (10.1)
Lifetime (µs)	68 ± 1 [c]	149 ± 8	100 ± 9 (21%) 214 ± 25 (79%)	100 ± 9 (66%) 214 ± 25 (34%)
Number of coordinated waters[1]	9.0	3.5	5.6 2.2	5.6 2.2

[a] Values in parentheses are full width at half- maximum. [b] Shoulder. [c] Excitation wavelength 395 nm. [1] according to the Kimura & Choppin equation [77].

Speciation calculations using the formation constants showed predominant Cm(III) coordination to (a) phosphoryl groups within pH 1 and 4, (b) carboxyl groups within pH 4 and 9, and (c) hydroxyl groups at pH values above 9. A computer simulation study of the Ca^{2+} ion distribution within LPS supports our conclusions concerning different dominant coordination sites of the LPS molecule as a function of pH [122]. With SPECFIT the single component spectra of the individual species in the Cm^{3+}–LPS system were calculated and are shown in Fig. 4.3. The spectroscopic properties of the curium(III) species are summarized in Tab. 4.4. The emission peak maximum is shifted from 593.6 nm for the Cm^{3+} aquo ion to 599.9, 602.3, and 606.9 nm when curium(III) occurs in the three identified LPS complexes (see also Fig. 4.2, Fig. 4.3). The excitation spectra of the determined curium(III)–LPS complexes are presented in Fig. 4.4. The phosphoryl-, carboxyl-, and hydroxyl-bound curium(III) is characterized by sharp and well-resolved absorption bands like those observed for the Cm^{3+} aquo ion. This points to intense transitions to the H-, G-, and F-states of curium(III). The absorption bands of the LPS-bound curium(III) are red-shifted compared to those of the Cm^{3+} aquo ion. Moreover slight differences in the absorption bands within the three curium(III)–LPS complexes are further indications for those species.

A literature review concerning the reported emission bands of curium(III) bound to especially phosphoryl and carboxyl groups of organic and/or biomacromolecules gives further evidence for the postulated Cm(III)–LPS species. The emission maxima of complexes where Cm(III) is predominantly coordinated to organic phosphate groups span a relatively narrow wavelength range between 598.6 and 601 nm [116-118].

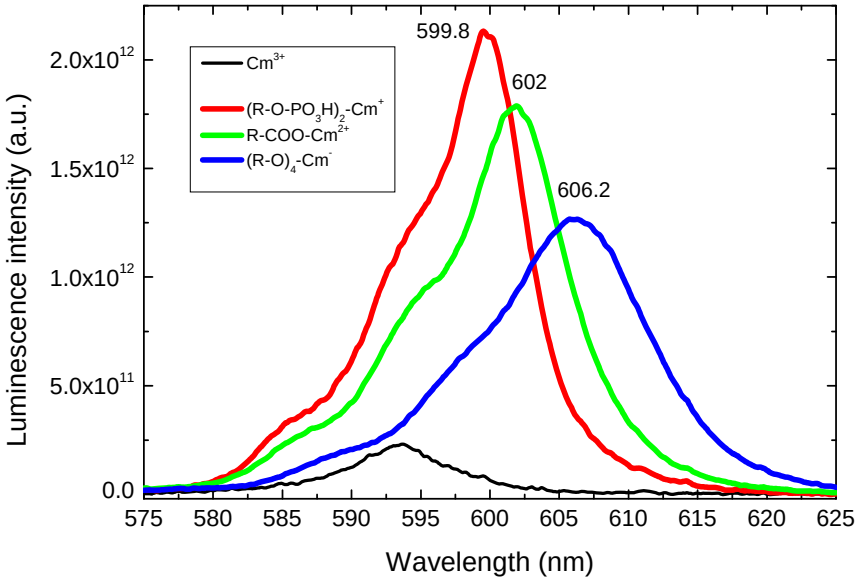

Fig. 4.3 Luminescence spectra of the single components in the Cm^{3+}–LPS system, as derived by peak deconvolution using SPECFIT.

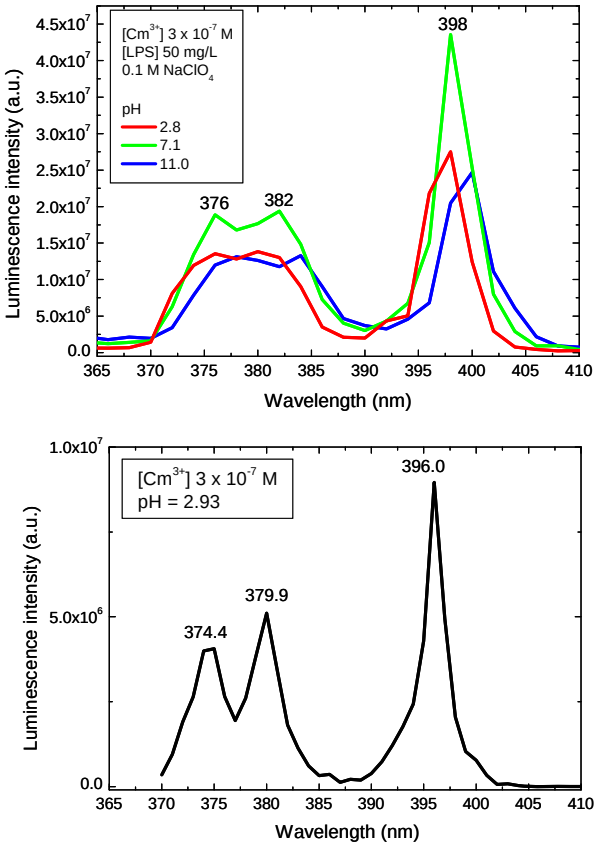

Fig. 4.4 Excitation spectra of curium(III) measured in the LPS system.

The emission maximum of the phosphoryl Cm(III)–LPS complex fits with 599.8 nm in this wavelength range. The emission maxima of carboxylate coordinated Cm(III) are spread over a

broader range between 599 and 611 nm [118-120, 123, 124]. The more red-shifted emission bands here result from multidentate species involving more than one carboxylate group (e.g., EDTA [124]) and/or additional functional sites like hydroxyl groups as in glycolic acid [123]. Up to now no spectroscopic data could be found describing the interaction of biomolecular hydroxyl groups with curium(III).

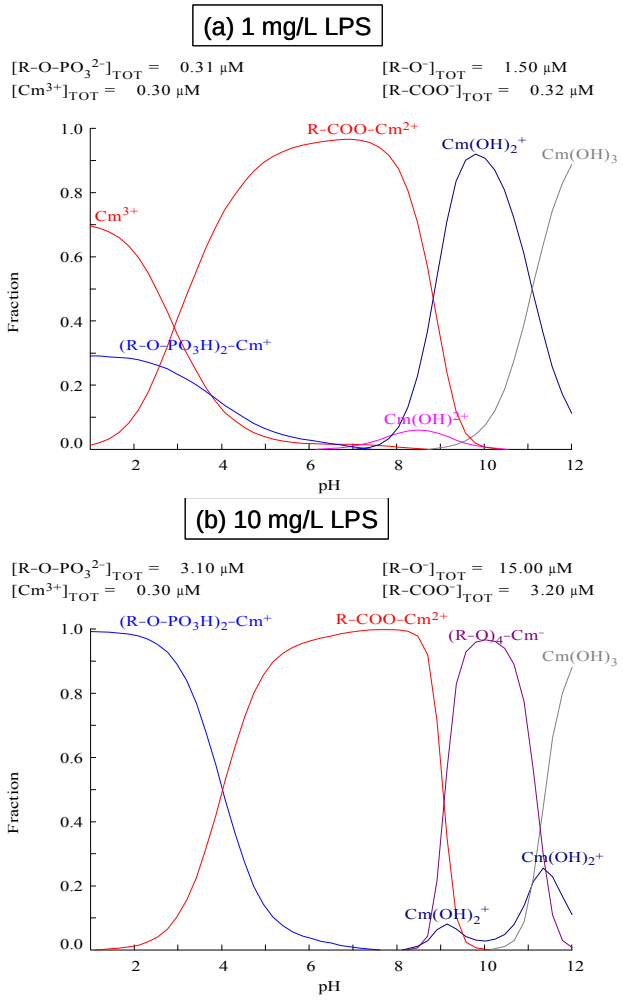

Fig. 4.5 Speciation of curium(III), 3×10^{-7} M, in aqueous solutions as a function of the LPS concentration: (a) Nearly equimolar (1 mg/L LPS equal to 3.2×10^{-7} M carboxyl, 3.1×10^{-7} M phosphoryl and 1.5×10^{-6} M hydroxyl); (b) Excess of LPS (10 mg/L LPS equal to 3.2×10^{-6} M carboxyl, 3.1×10^{-6} M phosphoryl and 1.5×10^{-5} M hydroxyl).

Our data interpretation confirms the general assumption that Eu(III)/Cm(III) association on cell surfaces of microorganisms and biopolymers occurs mostly through binding to carboxyl and phosphoryl groups as described in [92, 93]. In addition this study could show the involvement of hydroxyl groups in the alkaline pH range. In general (see Tab. 4.3), complexation constants of Cm(III) with ligands containing phosphoryl groups (log β values

between 8.2 and 18) are greater than those of ligands containing carboxyl groups (log β values between 5.2 and 14). This is also true for the Cm(III)–LPS complex formation constants. On the other hand, log β values of ligands with dominating deprotonated carboxyl coordination vary between 5.2 and 6.7. The constant determined for the R–COO–Cm^{2+} complex, $\log \beta_{110} \sim 9.0$, is greater than those of the selected carboxylate models. The interaction of Eu(III) with *Bacillus subtilis* cells was interpreted by the formation of Eu(III) complexes with carboxyl (R–COO–Eu^{2+}) and phosphoryl (R–O–PO_3–Eu^{+}) groups of the bacterial cell surface within pH 3 and 7 [94]. Our study showed that Cm^{3+} forms a stronger carboxylate LPS complex. A comparison of the luminescence parameter of the Cm(III)–*Desulfovibrio aespoeensis* surface complex, 600.1 nm and 162 μs [125], with those observed for the Cm(III) LPS complexes (Tab. 4.4) suggests an interaction of Cm(III) with phosphoryl sites of the LPS structures located in the outer cell envelope of this Gram-negative bacterium.

Fig. 4.5 shows the speciation of curium(III) in an aqueous solution with (a) nearly equimolar amounts of Cm(III) and LPS and (b) with an excess of LPS. The speciation was done with the program MEDUSA [19]. The curium(III)-LPS species dominate over a wide pH range. Their influence is already visible under equimolar conditions. Hence, strong Cm^{3+}-LPS species are formed, indicating the great potential of this outer bacterial envelope component of Gram-negative bacteria to bind curium(III) in the biologically relevant pH range. Three functional groups, carboxyl, phosphoryl, and hydroxyl, participate in the coordination to curium(III). Probably due to the "hard" character of the Cm^{3+} ion interactions preferentially with complexation sites containing "hard" donor atoms like oxygen were detected in contrast to the "softer" nitrogen containing sites like amino groups [126].

4.2.1.3 Np(V) and LPS

The results of the spectrophotometric titrations of the NpO_2^+ test solutions in the LPS system are shown in Fig. 4.6A. To the best of our knowledge spectrophotometric titrations of NpO_2^+ with LPS were not reported before. The NIR absorption spectra of the corresponding single components are summarized in Fig. 4.6B. The complexation of neptunium(V) with LPS molecules had started even at a low pH of 2.7 and a LPS concentration of 0.8 g/L (Fig. 4.6A). This LPS amount corresponds to a concentration of phosphoryl groups of 2.48×10^{-4} M which are most likely involved in neptunium bonding at this pH. With a NpO_2^+ concentration of

1.8×10^{-4} M, we have a nearly equimolar concentration ratio between neptunium(V) and available phosphoryl groups.

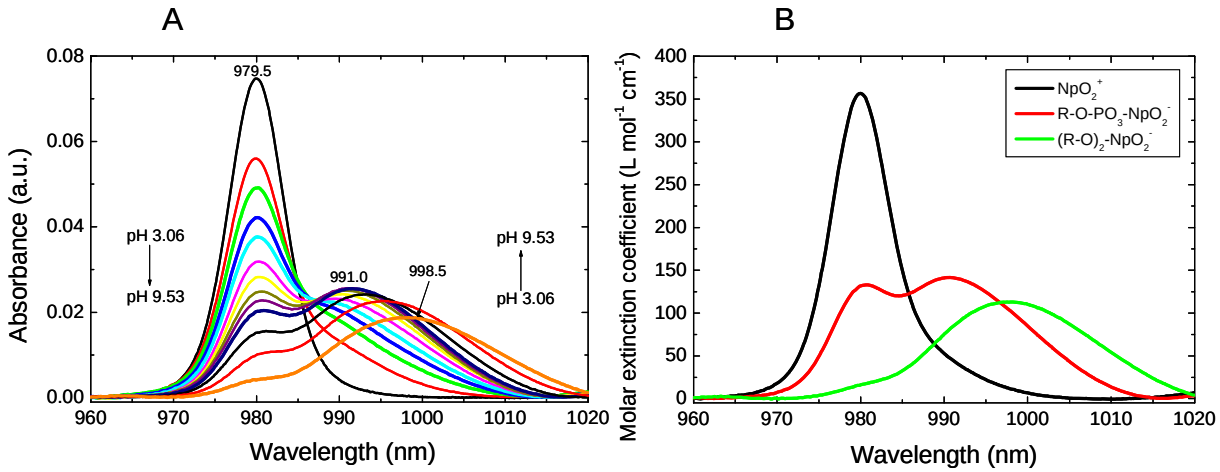

Fig. 4.6 A) Spectrophotometric titrations of 1.8×10^{-4} M NpO_2^+ in solutions containing 0.8 g/L LPS at an ionic strength of 0.1 M $NaClO_4$. B) NIR absorption spectra of the single components in the NpO_2^+–LPS system, as derived by peak deconvolution using SPECFIT.

In all other NpO_2^+ systems investigated in this study the influence of neptunyl ligand species was never observed at pH values less than 5. The changes detected in the NIR spectra between pH 2.7 and 7.8 at fixed LPS concentration of 0.8 g/L exhibit the formation of a first Np(V)–LPS complex. This is evidenced by the formation of the new absorption band at 991 nm compared to 979.5 nm observed for the free NpO_2^+ ion. Then the again red shifted absorption maximum up to 998.5 nm between pH 8.5 and 9.5 indicates the increased influence of a second Np(V)–LPS complex. The SPECFIT calculation procedure is based on the formal complex formation equations (40) and (41) for discrete binding sites. As a result of the SPECFIT calculations, the first Np(V)–LPS species can be described with a phosphoryl bond neptunium(V) complex with an averaged stability constant of $\log \beta_{110} = 6.34 \pm 0.11$ ($R–O–PO_3–NpO_2^-$). We checked also the possibility of a neptunyl(V) complex with carboxyl groups of the LPS molecule. However all attempts to fit a neptunyl(V)–carboxyl and a neptunyl(V)–phosphoryl complexation side by side failed. This might indicate a low affinity of NpO_2^+ towards the carboxyl groups of LPS ($pK_a = 5.56$). The observed changes in the NIR spectra already at pH 2.7 also point to a predominant phosphoryl coordination of NpO_2^+. In order to describe the second Np(V)–LPS species, two site complexation models were tested. In the first one phosphoryl, and amino groups were introduced. However, all attempts to fit the data failed. As a result, the pK_a value of the third complexation site should be larger than

8.9. Therefore, the third complexation site was described with hydroxyl groups as also found for the Cm(III)–LPS system. As a result, the second Np(V)–LPS complex could be allocated to a species with two deprotonated hydroxyl groups. The averaged stability constant was calculated to be log $\beta_{120} = 11.64 \pm 0.90$ ($(R–O)_2–NpO_2^-$). The isolated absorption spectrum of the $R–O–PO_3–NpO_2^-$ complex shows a complex structure with two maxima at 980 and 991 nm (see Fig. 4.6B). Interestingly similar observations were made for the 1:1:2 species between NpO_2^+ and DFO (see Fig. 3.4B). SPECFIT has difficulties in the correct separation of the spectral contributions of both the NpO_2^+ ion and the $R–O–PO_3–NpO_2^-$ complex. Fits introducing a Np(V) complex with a protonated phosphoryl group and also with, for instance, two deprotonated phosphoryl groups failed. The spectrum of the hydroxyl bond Np(V), $(R–O)_2–NpO_2^-$, is characterized by a broad absorption maximum at 998 nm.

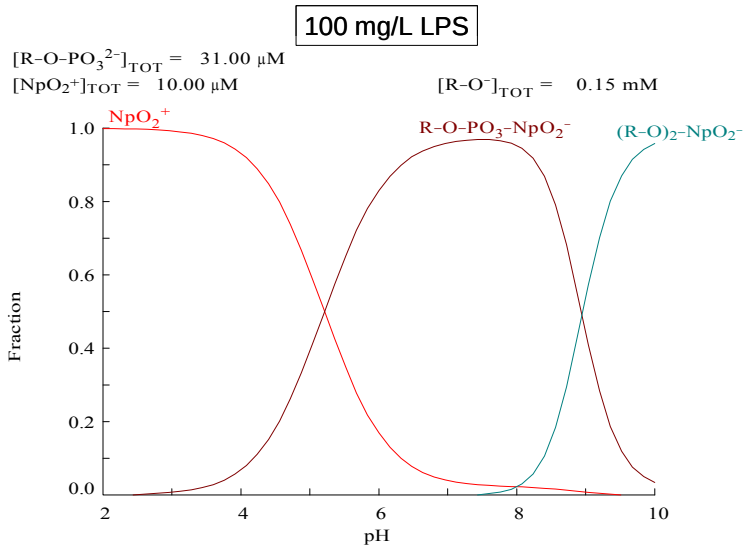

Fig. 4.7 Speciation of neptunium(V), 1×10^{-5} M, in aqueous solutions as a function of pH with 100 mg/L LPS (3.1×10^{-5} M phosphoryl and 1.5×10^{-4} M hydroxyl).

Fig. 4.7 shows the Np(V) speciation, 1×10^{-5} M, in aqueous solutions with a slight excess of LPS functional groups responsible for neptunyl(V) binding. It can be seen that at pH values greater than 6.5 more than 95% of NpO_2^+ is bond on phosphoryl and hydroxyl groups of LPS. Hence relatively strong NpO_2^+ complexes are formed. This is remarkable because it is assumed that NpO_2^+ is very mobile, nonsorptive and forms weak complexes in the environment. However, the comparison of the Cm(III)–LPS results with those of Np(V) shows that Cm(III) forms stronger species with LPS. Between pH 2 and 11 three functional groups, phosphoryl, carboxyl and hydroxyl, participate in the coordination to curium(III). Based on our spectrophotometric titrations, NpO_2^+ showed a much lower affinity to interact

with carboxyl groups of the LPS molecule. Here the predominant binding places are phosphoryl and hydroxyl groups. In contrast to U(VI) and even to Cm(III) the knowledge in the literature about (a) microbial interactions of Np(V), (b) interactions of Np(V) with isolated cell wall compartments, and (c) Np(V) complexation with for instance organic phosphates is very scarce. There is only one study describing the biosorption of NpO_2^+ by *Pseudomonas fluorescens* [127]. At initial neptunyl concentrations of 4.75 µM and biomass concentrations of 930 mg/L at pH 7, as much as 85% of the neptunium was sorbed. *P. fluorescens* is a Gram-negative bacterium and due to the cell wall structure LPS plays a great role in metal complexation on the cell envelope. In the case of isolated LPS molecules we could show that already at pH 6 more than 85% of all Np(V) present is complexed by functional groups of LPS (see Fig. 4.7). The evaluation of the Np(V) biosorption data in [127] with the Freundlich isotherm might indicate the involvement of more than one functional group in Np(V) binding by *P. fluorescens*. On the basis of our Np(V)–LPS speciation study there is evidence that the LPS located in the cell envelope of *P. fluorescens* plays a major role in neptunyl(V) binding.

4.2.2 Actinide interactions with peptidoglycan (PG)

4.2.2.1 U(VI) and PG

Potentiometric titration

The titration curves of the uranyl PG complex solutions were analyzed based on the formal complex formation equation (40) for discrete binding sites and the appropriate mass action law, equation (41), which represents the complex stability constant log K. As initial data, we used the pK_a values and site densities from potentiometric titration of PG (see Tab. 2.7).

If we analyzed the titration data only up to pH 6.0, we could identify two different uranyl carboxyl complexes with glutamic and diaminopimelic acid. The 1:1 uranyl complex $R–COO–UO_2^+$ with the carboxyl group of glutamic acid with a stability constant of $\log \beta_{110} = 4.02 \pm 0.03$ has only a very small formation ratio. The one with the carboxyl group from the diaminopimelic acid with the stability constant of $\log \beta_{110} = 7.28 \pm 0.03$ is formed in higher amounts. If we increase the analyzing pH range up to about 9.3, the best fit is reached with an additional mixed uranyl complex with a carboxyl group from diaminopimelic acid and an amino or hydroxyl group in the coordination sphere. This 1:1:1 complex $R–COO–UO_2^{(+)}–A_i–R$ (with $A_i = NH_2$ or O^-) has a stability constant of $\log \beta_{1110} = 14.95 \pm 0.02$. All determined constants are summarized in Tab. 4.5.

Up to now, only one comparable stability constant of a bacterial uranyl carboxyl complex has been determined, the surface complex R–COO–UO_2^+ with $\log K = 5.4 \pm 0.2$ for uranyl adsorption onto *B. subtilis* [113]. This value lies between ours, indicating that it is an averaged value from different binding carboxyl groups.

TRLFS measurements

Fig. 4.8 depicts one measurement series of the uranyl PG system. The luminescence was measured at fixed uranyl (10^{-5} M) and PG concentrations (0.1 g/L, according to 1.44×10^{-4} M carboxyl groups and 3.05×10^{-4} M amino and/or hydroxyl groups) between pH 2.0 and 9.0. At very low pH no change of the luminescence of the free uranyl ion was observed, which implicates that the complexation is insignificant. Between pH 2.0 and 3.0 a slight decrease of the luminescence intensity, connected with a strong red shift of the peak maxima of about 8 nm at pH 3.0 can be observed (Fig. 4.8, left). Above pH 3.0 up to pH 5.6 the luminescence intensity increases again with the same constant red shift of the peak maxima. From pH about 5.6, the luminescence intensity decreases once more (Fig. 4.8, right). For comparison, the luminescence spectrum of uranyl at pH 2.0 (UO_2^{2+}(aq)) (left) is included. The changes in the peak maxima and luminescence intensities of the uranyl PG system implicate that three complexes are formed, one, which occurs at low pH with a lower luminescence intensity than the free uranyl ion, a second one with a higher luminescence intensity, which dominates until pH 5.6 and a third one, which appears from pH 5.6 and shows no luminescence properties.

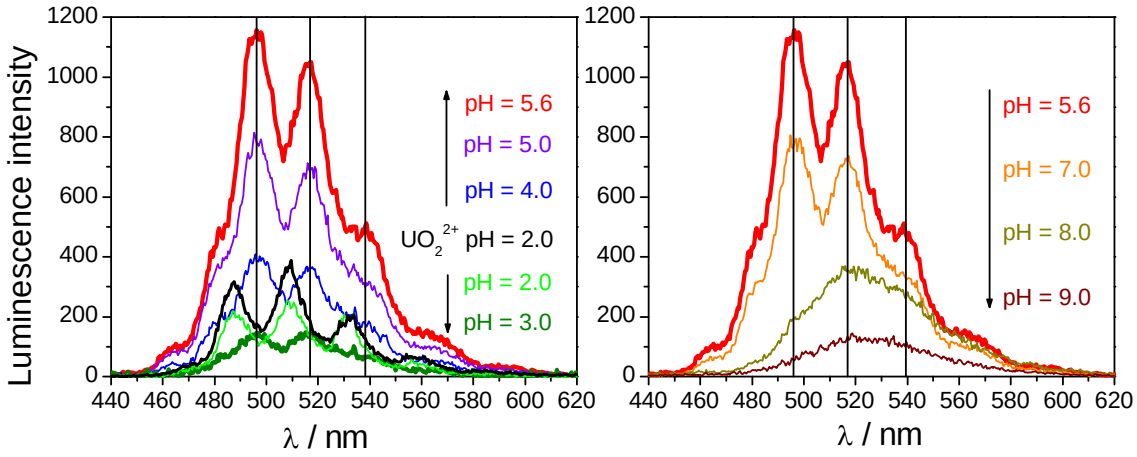

Fig. 4.8 Summary of the measured luminescence spectra of 10^{-5} M U(VI) with 0.1 g/L PG in dependence on pH.

Two measurement series (not shown here) at fixed pH and with varying PG concentration (0.01 – 0.2 g/L) confirm these observations. In the series at pH 2.5, changes in the

luminescence could be observed only at PG concentrations greater than 0.1 g/L. An appropriate series at pH 4.0 showed an increase of the luminescence intensity, connected with a red shift of the peak maxima of about 8 nm, starting even at 0.025 g/L PG.

The time-resolved measurements give information about the lifetimes of the exciting state of the luminescent species in the mixture. Thus, it provides further information on the number of the luminescent species. To evaluate the number of the luminescent species and their lifetimes, the integrated luminescence signal is fitted to a sum of exponential decay functions according to equation (42). The spectra until pH 3 show mono-exponential decay with lifetimes between 1.2 and 1.8 µs, which can be clearly identified as the free uranyl ion (1.7 ± 0.5 µs [128]). From pH 3, we observe mostly bi-exponential decay. At pH 3 a longer lifetime (averaged: 7.3 ± 1.4 µs) appears first and can be observed until pH about 6.2. Its intensity is highest at pH 3, followed by a strong decrease. A second shorter lifetime (averaged 0.7 ± 0.1 µs) was detected from pH about 3.5 with a strong increasing intensity. It can be observed until pH about 6.8. Afterwards only lifetimes of uranyl hydroxides are detectable: A shorter one of about 3.0 to 3.5 µs can be dedicated to $(UO_2)_4(OH)_7^+$ (literature: 4.2 ± 0.4 µs [114]), and a longer lifetime between 15 and 19 µs can be assigned to $(UO_2)_3(OH)_5^+$ (literature 19.8 µs [114]), the two main uranyl hydroxide species in near neutral to slightly basic pH. The progression of the lifetimes (depicted in Fig. 4.9) give the same information like the developing of the peak maxima and luminescence intensities: one uranyl PG complex with characteristic luminescence properties begins to form at pH 3, but will be overlapped soon by a second uranyl PG complex with stronger luminescence intensity. A third complex, which appears at pH about 6, shows no luminescence properties.

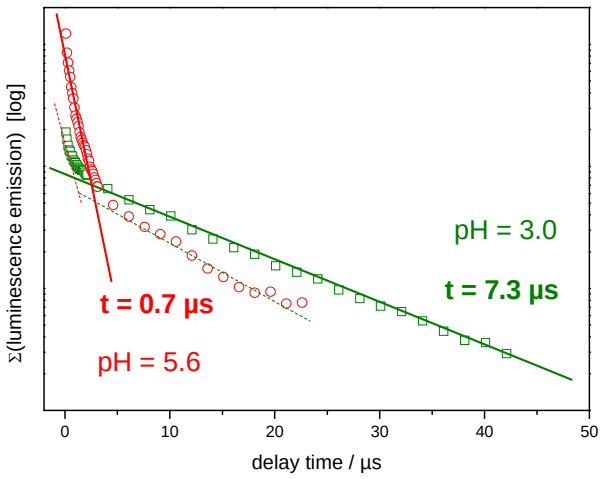

Fig. 4.9 Bi-exponential luminescence decay in the UO_2^{2+} / PG system at two different pH. At lower pH (3.0) dominates the longer lifetime, at higher pH (5.6) the shorter one.

The quantitative investigation of the luminescence spectra with the computer program SPECFIT to calculate complex stability constants is based on the formal complex formation reaction (40) with the appropriate mass action law (41) for discrete binding sites in the biomacromolecule. As initial data we used again the pK_a values and site densities of PG, calculated from the potentiometric titrations (see Tab. 2.7), and the pK_a values for the uranyl hydroxide species [100]. The best fit for the measurement series at pH 4.0 was reached with the 1:1 uranyl carboxyl complex ($R–COO–UO_2^+$) and the 1:2 uranyl carboxyl complex $(R–COO)_2–UO_2$, both with carboxyl groups from diaminopimelic acid. Because of the small formation of the uranyl carboxyl species from glutamic acid (below 5 %) and the accuracy of TRLFS, which is restricted to 5 % at best, it was not possible to detect this complex. The formation ratio of this complex is below the detection limit at these conditions. For the series with varying pH between 2.0 and 9.0 the best fit was reached with the two uranyl carboxyl species $R–COO–UO_2^+$ and $(R–COO)_2–UO_2$ from diaminopimelic acid plus the mixed complex ($R–COO–UO_2^{(+)}–A_i–R$ with $A_i = NH_2$ or O^-), which was found by potentiometry, too. The average stability constants were calculated to be $\log \beta_{110} = 6.9 \pm 0.2$ and $\log \beta_{120} = 12.1 \pm 0.2$ for the two uranyl carboxyl complexes, and $\log \beta_{1110} = 14.5 \pm 0.1$ for the mixed complex (see Tab. 4.5). The values of the 1:1 complex and the mixed species are in good accordance with those determined by potentiometry. Because of the stoichiometry used for potentiometry (a slight deficit of the complexation sites), the probability of the formation of a 1:2 species is low; therefore, we could not detect this species with potentiometry which we found with TRLFS.

Tab. 4.5 Calculated complex species and stability constants of the uranyl PG system.

Species	**log β**	**Method**
$R–COO–UO_2^+$ (glutamic acid)	4.02 ± 0.03	Potentiometry
$R–COO–UO_2^+$ (diaminopimelic acid)	7.08 ± 0.03	Potentiometry
	6.9 ± 0.2	TRLFS
$(R–COO)_2–UO_2$ (diaminopimelic acid)	12.1 ± 0.2	TRLFS
$R–COO–UO_2^{(+)}–A_i–R$ ($A_i = NH_2$ or O^-)	14.95 ± 0.02	Potentiometry
(COO^- from diaminopimelic acid)	14.5 ± 0.1	TRLFS

Resultant, we can assign the luminescence properties to the uranyl PG complex species. The 1:2 uranyl carboxyl PG complex $(R–COO)_2–UO_2$ dominates between pH 4 and 6. It has strong luminescence intensity, causes a red shift of the peak maxima of about 8 nm and has a luminescence lifetime of about 0.7 µs. The 1:1 complex has a lower luminescence intensity then UO_2^{2+}(aq) and a longer lifetime of about 7.3 µs. Because of its significantly lower

luminescence intensity and the quite strong covering by the 1:2 complex, the measured sum spectra could not be deconvoluted successfully to get the single spectrum of the 1:1 complex. These two uranyl carboxyl coordinated PG complexes are only specifiable by the different lifetimes. The uranyl PG complex with the mixed coordination $R–COO–UO_2^{(+)}–A_i–R$ ($A_i = NH_2$ or O^-) shows no luminescence behavior at room temperature. The spectroscopic data of the uranyl PG complex species are summarized in Tab. 4.6.

Tab. 4.6 Summary of measured luminescence data.

Species	**Peak maxima [nm]**							**Lifetime [µs]**
Uranyl (aq) species								
UO_2^{2+} pH 2.0		470.8	488.8	510.0	533.0	559.0	586.3	1.4 ± 0.1
Uranyl PG complexes								
$R–COO–UO_2^+$								7.3 ± 1.4
$(R–COO)_2–UO_2$	466.0	481.6	498.1	518.0	539	566	595	0.7 ± 0.1
$R–COO–UO_2^{(+)}–A_i–R$ ($A_i = NH_2$ or O^-)	No luminescence at room temperature							

4.2.2.2 Cm(III) and PG

Fig. 4.10 depicts a summary of the measured spectra of the Cm(III)–PG system. The complexation of the curium ion starts at about pH 4 (see Fig. 4.10, left), and at nearly neutral pH at very low PG concentration (0.1 mg/L, see Fig. 4.10 right).

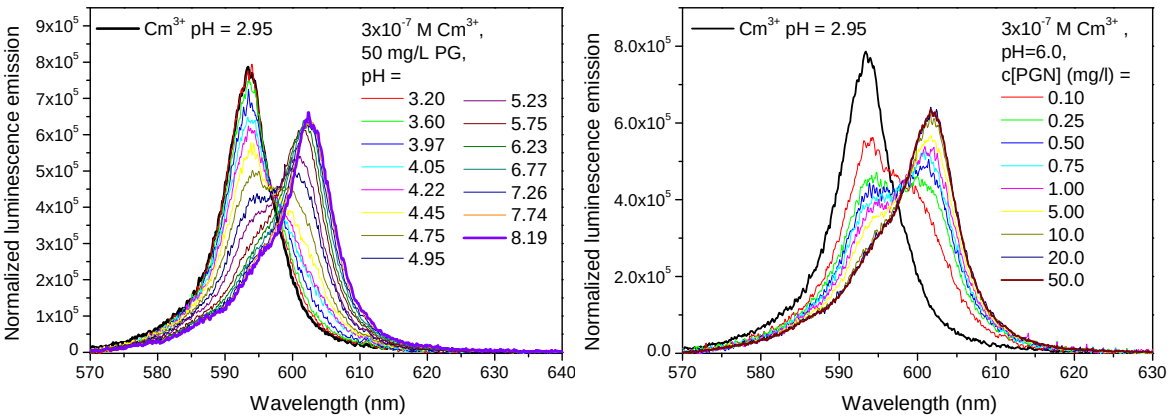

Fig. 4.10 Summary of the measured luminescence spectra of 3×10^{-7} M Cm(III) and PG. Left: in dependence on pH at fixed PG concentration (50 mg/L); right: in dependence on PG concentration at fixed pH (6.0).

In both experiment series the luminescence emission maximum of the Cm^{3+}(aq) ion of 593 nm is red shifted to 602 nm, indicating the formation of only one Cm(III)–PG complex type. The spectra were analyzed quantitatively with the computer program SPECFIT. The

calculation of the complex stability constant is based on the formal complex formation reaction (40) and the corresponding mass action law (41). As initial data we used again the pK_a values and site densities of the biomacromolecule determined by potentiometric titration (see chapter 2.3, Tab. 2.7). As a result, we got the best fit for a complex with carboxyl coordination and 1:2 stoichiometry. The complex stability constant was determined to be $\log \beta_{120} = 10.43 \pm 0.19$.

The analysis of the time resolved measurements give additional information about the number of different species in the solution. At 50 mg/L PG we observed up to pH about 5 a bi-exponential decay, as well as at pH 6 up to 1.0 mg/L PG. The shorter lifetime of about 71 µs can be dedicated to the free Cm^{3+}(aq). The longer lifetime of about 230 µs (average) is assigned to the complex species. At 50 mg/L PG over pH 5 and at pH 6 over 1.0 mg/L PG we observed mono-exponential decay with only the longer lifetime due to a complete complexation of the curium ion by the biomacromolecule.

With the linear correlation between the decay rate and the number of H_2O molecules in the first coordination sphere of curium(III), discovered by Kimura and Choppin [77], we can get an approximate insight into the structure of the formed Cm–PG species. Our finding of 71 µs measured for the Cm^{3+} aquo ion corresponds to nine water molecules in the first coordination sphere of curium(III). The lifetime of 230 µs corresponds to two remaining water molecules. If the two coordinating carboxyl groups coordinate in a bidentate manner, only 4 water molecules would be replaced. We can conclude, that other functionalities of the biomacromolecule coordinate the Cm(III) ion without a chemical bond. A similar structure was proposed from Texier et al. [93] for Eu(III) coordinating by *Pseudomonas aeruginosa* cell wall.

4.2.2.3 Np(V) and PG

Fig. 4.11A shows one example of the spectrophotometric titrations observed in the NpO_2^+–PG system. For comparison, Fig. 4.11B also depicts the results obtained in the NpO_2^+–LPS system. To the best of our knowledge spectrophotometric titrations of NpO_2^+ with peptidoglycan (PG) were not reported before. As the pH of the NpO_2^+–PG test solutions was increased by adding NaOH (at pH values greater than 6.5), the intensity of the absorption peak at 980 nm (free NpO_2^+ ion) decreased (see Fig. 4.11A). This could be the result of the formation of hydrolyzed Np(V) species. It follows that we could not detect any interactions of NpO_2^+ with PG within PG concentrations of 0.05 g/L and 0.3 g/L and a wide pH range using

NIR spectroscopy. The inset of greater PG concentrations is limited due to its low solubility in aqueous solution.

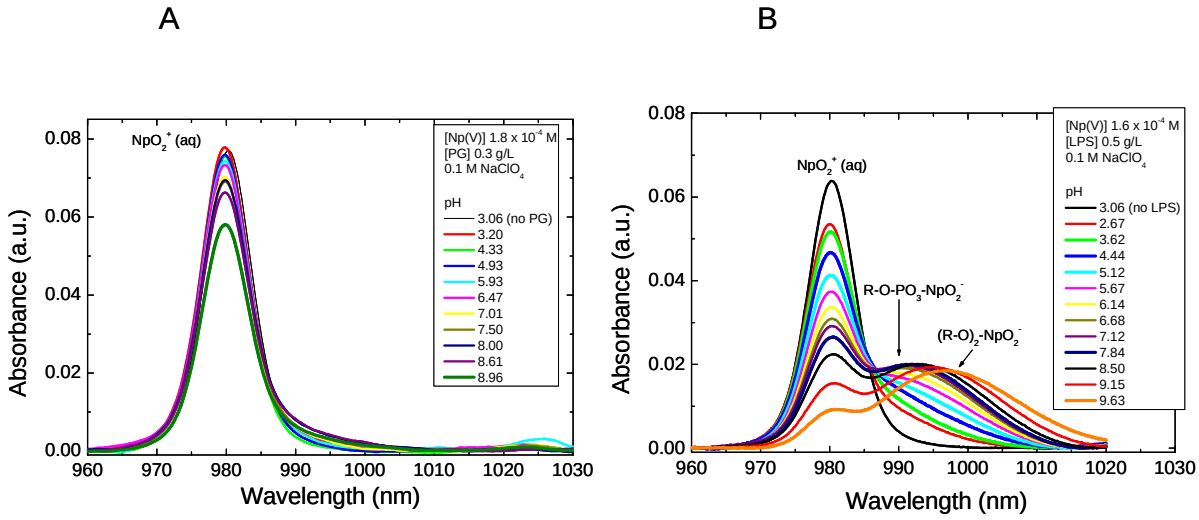

Fig. 4.11 Spectrophotometric titrations of approximately 1.8×10^{-4} M NpO_2^+ as a function of pH in solutions containing (A) 0.3 g/L PG and (B) 0.5 g/L LPS at an ionic strength of 0.1 M $NaClO_4$.

If we compare our Np(V) interaction results detected with the two cell wall components (PG and LPS) large differences are visible (see Fig. 4.11). Whereas Np(V) interacts with functional groups of the LPS macromolecule no interaction with functional groups of the PG macromolecule could be detected. In both examples shown in Fig. 4.11 we have a similar total concentration of functional groups (approximately 1.37×10^{-3} M) available for Np(V) complexation. The difference is that PG provides mainly carboxyl sites between pH 3 and 9.5 and no phosphoryl sites as LPS does. The observed results in the NpO_2^+–PG test solutions underline the conclusions drawn from the corresponding LPS investigations that there is evidence for a low affinity of the neptunyl(V) cation towards carboxyl sites of biomacromolecules. Since PG and LPS are major components of the cell walls of Gram-positive and Gram-negative bacteria, respectively, NpO_2^+ should interact more intensively with Gram-negative bacteria. More experiments on the basis of this project are needed to clarify this issue.

5 Studies on the interaction of pyoverdins secreted by *P. fluorescens* with actinides (U(VI), Cm(III), Np(V))

The leaching of metals from mine waste is a serious problem in many areas of the world and various methods have been developed and applied at large scales to mitigate such leaching processes [129]. Abandoned uranium mines contribute to the dispersal of uranium in the environment [130]. For example, crushed tailings from the Ranstad uranium mine in Falköping, Sweden, still leach metals, including uranium, into the surroundings despite full–scale operations to restore the mine waste area and immobilize the metals in the waste. It was assumed that the continued leaching could be caused by microorganisms. The siderophore–producing bacterium *P. fluorescens* was grown in batch cultures with naturally weathered (unprocessed) uranium ore, kolm, and acid-leached ore in chemically defined media [131, 132]. Significant leaching of uranium was observed in the presence of this bacterium. We concluded that the leaching caused by *P. fluorescens* [12] was due to the observed production of pyoverdins, which then can form complexes with uranium. The complexes resulted in the mobilization of uranium from the studied ore. The role of the exudates from this strain was further explored in solid–aqueous phase partitioning experiments using pico- to submicromolar amounts of ^{59}Fe, ^{147}Pm, ^{234}Th, and ^{241}Am in the presence of quartz sand [133]. Relative to the control, aerobic solutions containing exudates maintained more than 50% of the added ^{59}Fe, ^{234}Th, and ^{241}Am in solution. The highest amount of metal present in the liquid phase of the anaerobic solutions was found in the case of ^{241}Am, with 40% more ^{241}Am being present in samples than in controls. The observed mobilization effects of the studied pyoverdins of this strain on radionuclides motivated detailed investigation of their complexation characteristics, using radionuclides suitable for spectroscopic methods. To the best of our knowledge, the characteristics of the complexation of pyoverdins with trivalent (e.g. curium) and pentavalent actinides (e.g. neptunium) are unknown.

5.1 Experimental

Preparation of actinide pyoverdin solutions

The pyoverdin concentration in the acidic LH_4 stock solutions was determined using the absorbance at the characteristic pyoverdin absorption band at 380 nm and an averaged molar

absorption coefficient of 20000 L mol^{-1} cm^{-1} [8, 15, 134]. The Cm(III) and Np(V) experiments were performed in a glove box under an N_2 atmosphere at 25°C.

For UV-vis measurements three different series of experiments were performed. In two series, in which the pH was set to 3 and 4, respectively, we investigated UO_2^{2+} complex formation by varying the uranyl concentration between 1×10^{-6} and 1×10^{-3} M at a fixed pyoverdin concentration of 5.8×10^{-5} M. In the third series, the uranyl and the pyoverdin concentrations were kept constant at 1×10^{-5} and 5.8×10^{-5} M, respectively, while varying the pH between 3.0 and 8.2. For fs-TRLFS measurements also three different series of experiments were performed to explore the intrinsic luminescence properties of the isolated pyoverdin mixture in the absence and presence of UO_2^{2+}. In two series, one without UO_2^{2+} and one with 1×10^{-6} M UO_2^{2+}, at a total pyoverdin concentration of 8.1×10^{-6} M, the spectral changes were investigated as a function of pH between 2.1 and 8.9. In series 2, at a fixed pyoverdin concentration of 5.7×10^{-5} and a pH of 4.0, the uranyl concentration was changed between 1×10^{-6} and 1×10^{-4} M.

The curium(III) concentration was fixed at 3×10^{-7} M in all TRLFS measurements. Three series of TRLFS experiments were performed. In the first run, we investigated the curium(III) complex formation by varying the pyoverdin concentration between 3×10^{-7} and 1×10^{-5} M at a fixed pH of 4.17; in the second and third runs, the pyoverdin concentrations were kept constant at 3×10^{-6} and 1×10^{-5} M, respectively, while varying the pH between 2.0 and 11.0.

The neptunium(V) concentration was fixed at 1.7×10^{-4} M in all spectrophotometric titrations. In the Np(V)–pyoverdin system low ligand concentrations of 1.62×10^{-5}, 7.2×10^{-5}, 2.0×10^{-4}, and 1.06×10^{-3} M were used. The pH in those test solutions was usually changed between 3 and 9.

Experimental setup of the applied spectroscopic techniques

The complexation of UO_2^{2+} with *P. fluorescens* (CCUG 32456) pyoverdins was investigated using absorption spectroscopy (UV-vis) and fluorescence spectroscopy with ultrafast pulses (fs-TRLFS). The experimental details of both techniques are summarized in chapter 2.1.2.1. The Cm^{3+} complexation with *P. fluorescens* (CCUG 32456) pyoverdins was investigated using time-resolved laser-induced fluorescence spectroscopy (TRLFS) as described in chapter 3.1.

The NpO_2^+ complexation with *P. fluorescens* (CCUG 32456) pyoverdins was investigated using absorption spectroscopy (UV-vis NIR). The experimental details are summarized in chapter 3.1.

The complex formation constants were calculated based in the variations in the measured spectra using the factor analysis program SPECFIT [20]. Three scans were measured for each sample; the results were then averaged and baseline corrected using ORIGIN 6.1G software (OriginLab, Northhampton, MA, USA).

The test solutions prepared for X-ray absorption spectroscopy (XAS) analysis had fixed concentrations of UO_2^{2+} and the ligands. The UO_2^{2+} concentrations varied between 5×10^{-4} and 0.005 M and the ligand concentrations were adjusted between 0.0011 and 0.008 M both depending on the specific properties of the individual ligands. The pH was varied between 2 and 8. The ionic strength was kept constant at 0.1 M $NaClO_4$. Tab. 5.1 gives a summary of the experimental conditions of the XAS test solutions presented in this study.

Tab. 5.1 Summary of sample composition and calculated distribution of the main uranium(VI) species.

Sample	Parameter	Speciation
A	0.05M U(VI), pH 2	100% UO_2^{2+}
B	5×10^{-4} M U(VI), 0.008 M SHA, pH 3.0	82% $UO_2(LH)_2$
C	0.001 M U(VI), 0.008 M BHA, pH 4.0	98% UO_2L_2
D	0.005 M U(VI), 0.008 M DFO, pH 3.2	75% $UO_2H_2DFO^+$
E	0.005 M U(VI), 0.008 M DFO, pH 4.0	98% $UO_2H_2DFO^+$
F	0.001 M U(VI), 0.0015 M NAP, pH 3.5	67% UO_2LH^+
G	0.001 M U(VI), 0.0015 M NAP, pH 8.3	50% $UO_2L_2H^-$
H	0.001 M U(VI), 0.0011 M PYO, pH 6.0	98% UO_2LH^-

EXAFS measurements were carried out on the Rossendorf Beamline BM20 at the European Synchrotron Radiation Facility [135]. The samples were measured at room temperature using a water-cooled Si(111) double-crystal monochromator in channel cut mode (5-35 keV). The

spectra were collected either in fluorescence mode using a 13-element Ge solid-state detector or in transmission mode using Ar filled ionization chambers. For energy calibration of the sample spectra, the K-edge spectrum of an Y metal foil (first inflection point at 17038 eV) was recorded simultaneously. The ionization energy, E_0, of the uranium L_{III} edge was defined as the root of the second derivative of the averaged spectra.

The spectra were treated by using the data analysis programs Sixpack/SamView (Version 0.59) and WinXAS (version 3.11) [136]. Theoretical backscattering phase and amplitude functions were calculated with the FEFF 8 code [137] using a 25 atom cluster having the atomic positions from $UO_2(CH_3COO)_2 \times 2\ H_2O$ [138] and using the 42 atom cluster having the atomic positions from $[UO_2NO_3(\text{salicylic acid}) \times (\text{dimethylaminopyridine})]_2$ [139]. The multiple scattering path U-O_{axial} (4-legged path) was included in the model calculations. The amplitude reduction factor, S_0^2, was held constant at 1.0 for all fits.

5.2 Results and discussion

5.2.1 U(VI) pyoverdin interactions

Fig. 5.1 depicts the absorption spectra of the *P. fluorescens* (CCUG 32456) pyoverdins in the UO_2^{2+} system as they depend on the varied physico–chemical parameter. Processes of interaction between UO_2^{2+} and the pyoverdins can be identified directly in Fig. 5.1 A and B. The absorption maxima at 365 and 379 nm decrease with increasing UO_2^{2+} concentration at pH 3 and 4. The formation of pyoverdin–UO_2^{2+} species is indicated by the increased absorption band at 409 nm as shown in Fig. 5.1 A and B. The formation of complexes of UO_2^{2+} with pyoverdins was dependent on UO_2^{2+} concentration and pH at a constant pyoverdin concentration of 5.8×10^{-5} M. At pH 3, significant changes in the UV-vis spectra were detectable at UO_2^{2+} concentrations greater than 5.0×10^{-5} M, whereas at pH 4 effects were already visible one order of magnitude earlier. Fig. 5.1 C shows the pH dependence of the UO_2^{2+}–pyoverdin complex formation equilibria at fixed concentrations of UO_2^{2+} and LH_4 (1.0×10^{-5} and 5.8×10^{-5} M, respectively). UV-vis measurements at uranyl concentrations above 5×10^{-3} M demonstrated the increased influence of the absorption bands of the uncomplexed UO_2^{2+} ion. This indicates the decreased potential of the pyoverdins to bind UO_2^{2+} in the postulated complexes at UO_2^{2+} : LH_4 ratios greater than 86.

Input parameters for the SPECFIT data fitting were the known total concentrations of UO_2^{2+} and LH_4, the pH of each sample, and the protonation constants of the pyoverdins as determined in this study and reported in [8], i.e., $\log ß_{011} = 12.2$. Furthermore, the known

absorption spectra of UO_2^{2+} and of the pyoverdin species, LH_4, LH_3^-, LH_2^{2-}, and LH^{3-} (Fig. 2.3B) were used in the SPECFIT calculations.

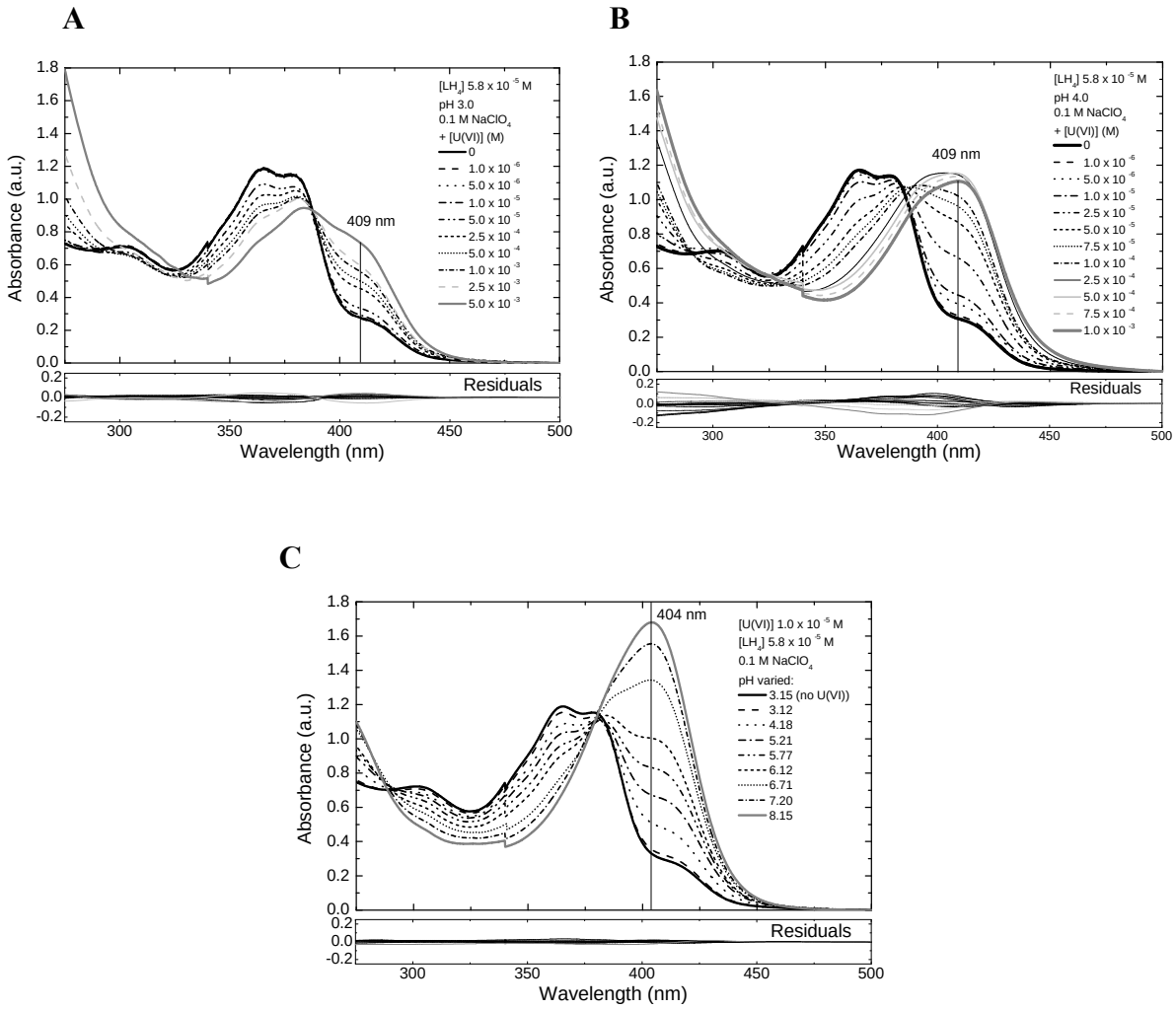

Fig. 5.1 Absorption spectra of the *P. fluorescens* (CCUG 32456) pyoverdins measured in the UO_2^{2+} system at an ionic strength of 0.1 M ($NaClO_4$): A) and B) at [LH_4] 5.8×10^{-5} M and at pH 3 and 4, respectively, as a function of uranyl concentration; and C) at [UO_2^{2+}] 1.0×10^{-5} M and [LH_4] 5.8×10^{-5} M as a function of pH. The residual absorption spectra after SPECFIT analysis are included.

In light of relevant complexation studies of pyoverdin-type bioligands with metals [7, 8, 28, 140, 141], and taking into consideration the deprotonation of the pyoverdin molecule, possible UO_2^{2+}–pyoverdin species of the $M_pL_qH_r$ type were introduced into the data analysis procedure. As a result, we were able to develop a chemical model describing the observed processes in the UO_2^{2+}–*P. fluorescens* (CCUG 32456) pyoverdin system:

$$UO_2^{2+} + L^{4-} + 2H^+ \rightleftharpoons UO_2LH_2 \quad (43)$$

$$UO_2^{2+} + L^{4-} + H^+ \rightleftharpoons UO_2LH^- \quad (44)$$

Formation constants for reactions (43) and (44) were calculated to be $\log \beta_{112} = 30.50 \pm 0.40$ and $\log \beta_{111} = 26.60 \pm 0.40$, respectively [16]. The absorption spectra calculated in the SPECFIT evaluation procedure agree fairly well with the measured ones, as indicated by the residuals in Fig. 5.1 . The single-component spectra derived from SPECFIT can be attributed to the formed species and are shown in Fig. 5.2.

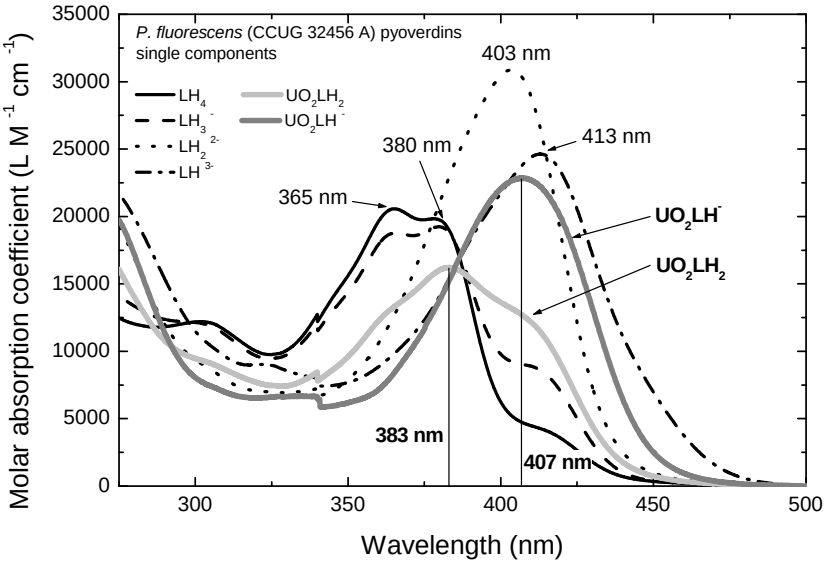

Fig. 5.2 Absorption spectra of the individual components of the aqueous *P. fluorescens* (CCUG 32456) pyoverdin system with and without UO_2^{2+}, as derived by peak deconvolution using SPECFIT.

The UO_2^{2+}–*P. fluorescens* (CCUG 32456) pyoverdin species, UO_2LH_2 and UO_2LH^-, exhibit main absorption bands at 383 and 407 nm with molar absorption coefficients of 16264 and 22823 L mol^{-1} cm^{-1}, respectively. These major absorption peaks are shifted compared to those of the aqueous pyoverdin species. At 6.6 L mol^{-1} cm^{-1}, the molar absorption coefficient of the UO_2^{2+}–ion at 414 nm is much smaller than those of the UO_2^{2+} species formed with *P. fluorescens* (CCUG 32456) pyoverdins (see Fig. 5.2). This could indicate the great potential of the pyoverdin siderophores to bind uranium in the hexavalent oxidation state.

In Fig. 5.3 the luminescence spectra of the *P. fluorescens* (CCUG 32456) pyoverdins are presented as a function of the uranyl concentration at pH 4. In all samples containing UO_2^{2+} a strong quenching of the intrinsic pyoverdin luminescence intensity was observed (Fig. 5.3). It follows that the UO_2^{2+}–pyoverdin species emit no luminescence light. The luminescence lifetimes were not influenced within the investigated [UO_2^{2+}] concentration range. This indicates that a static luminescence quench process occurs due to the complex formation reactions. In addition, we detected a slight red shift of the luminescence emission maximum from 466 to 470 nm at [UO_2^{2+}] > 2×10^{-5} M at pH 4 (Fig. 5.3). The SPECFIT factor analysis

program was then used for further evaluating the measured fs-TRLFS spectra, to determine UO_2^{2+}–pyoverdin complexation constants. As a result, we could confirm the conclusions drawn from the UV-vis measurements. Two 1:1 UO_2^{2+}–pyoverdin species with the following formation constants were identified: log β_{112} = 29.60 ± 0.43 and log β_{111} = 25.40 ± 0.76 [16].

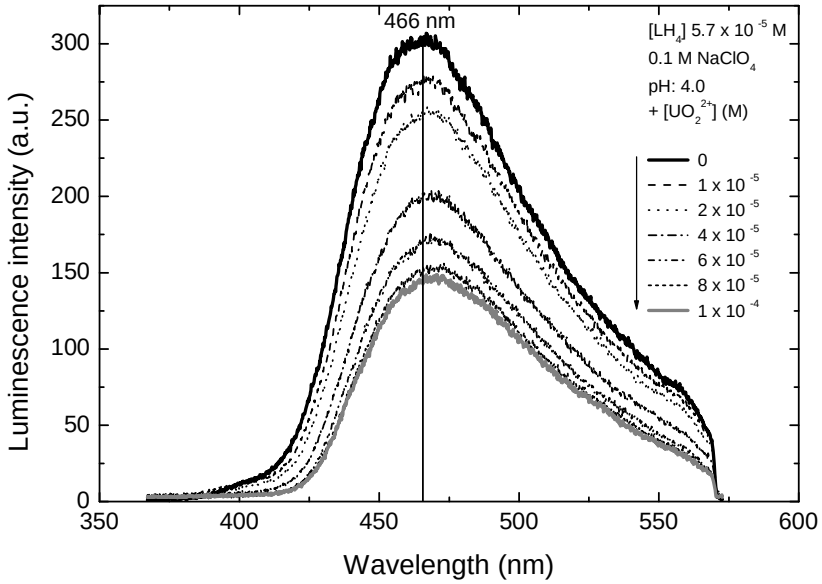

Fig. 5.3 fs-TRLFS spectra of *P. fluorescens* (CCUG 32456) pyoverdins at an ionic strength of 0.1 M ($NaClO_4$) at [LH_4] 5.7×10^{-5} M as a function of [UO_2^{2+}] at pH 4.0.

As shown in Tab. 5.2, the stoichiometry of the identified UO_2^{2+}–pyoverdin species is consistent with what is found in the literature regarding metal complexation with pyoverdins isolated from different Pseudomonads. The relatively large magnitudes of the actinide pyoverdin formation constants reflect the potential of pyoverdin-type bioligands to bind and transport actinides in the environment. Fluorescent Pseudomonads produce pyoverdins that differ in the structure of the peptide moiety (e.g., amino acid pattern) and the acyl chain, depending on the producing strain and growth medium. These structural differences are not reflected in the complexation behavior with UO_2^{2+}, as presented in Tab. 5.2. It follows that pyoverdins produced by *P. fluorescens* and *P. aeruginosa* should display a similar potential to bind UO_2^{2+}. In contrast to the results reported by Bouby et al. [28, 140], a second UO_2^{2+}–pyoverdin species with the stoichiometry 1:1:1 could be identified in the present study. The tetravalent actinides Th^{4+} and U^{4+} form slightly stronger complexes with pyoverdins (Tab. 5.2). Due to the effective charge of the uranyl ion of +3.2 [142] and its effective ionic radius of 0.73 Å [143], one would expect UO_2^{2+} to form the strongest species after Fe^{3+}, with a charge–to–radius ratio of 5.4. However, the results summarized in Tab. 5.2 indicate that the selected tetravalent actinides form species of greater stability. One reason for

this observation could be that the coordination of the pyoverdin molecule is restricted to the equatorial plane of the linear O=U=O unit, hampering interactions of UO_2^{2+} with the pyoverdin molecule.

Tab. 5.2 Molar absorption coefficients at the main absorption bands of the identified species and corresponding formation constants determined in this study, compared to relevant values from the literature.

Species / $M_pL_qH_r$	Producing organism	Absorption band (nm)	ε ($L\ mol^{-1}\ cm^{-1}$)	log β	Reference
LH^{3-} / 011	*P. fluorescens* (CCUG 32456 A)	413	24619		[16]
LH_2^{2-} / 012		403	30906	22.67 ± 0.15	
LH_3^{-} / 013		379	19236	29.15 ± 0.05	
LH_4 / 014		365	20560	33.55 ± 0.05	
UO_2LH_2 / 112		383	16264	30.50 ± 0.40 29.60 ± 0.43**	[16]
UO_2LH^{-} / 111		407	22823	26.60 ± 0.40 25.40 ± 0.76**	
UO_2^{2+} / 100		414	6.6		[16]
UO_2LH_2 / 112	*P. aeruginosa* (ATCC 15692)	n/a	n/a	30.46*	[140]
ULH_2^{2+} / 112		n/a	n/a	31.21*	[28]
$ThLH_2^{2+}$ / 112		n/a	n/a	32.73*	[141]
$FeLH_2^{+}$ / 112		403	19500	47.80 ± 0.20	[8]
FeLH / 111		n/a	n/a	43.00 ± 0.30	
FeL^{-} / 110		n/a	n/a	30.80 ± 0.30	

* recalculated in this study. ** determined using fs-TRLFS.

The fs-TRLFS measurements of UO_2^{2+}–containing solutions of *P. fluorescens* (CCUG 32456) pyoverdin species demonstrated a strong quenching of the pyoverdin luminescence intensity (Fig. 5.3). The observation that the complexation reactions of fluorescent siderophors with metal ions (i.e., Eu^{3+}, Tb^{3+}, Fe^{3+}, Al^{3+}, Ga^{3+}, In^{3+}) change the luminescence properties of the siderophors had already been reported in [29] and [31]. Whereas Eu^{3+}, Tb^{3+}, and Fe^{3+} interact via a static luminescence quench mechanism, as does UO_2^{2+}, the process is the opposite for Al^{3+}, Ga^{3+}, and In^{3+}; here the siderophore complexes emit luminescence light and the luminescence decay kinetics also change. These luminescence characteristics make pyoverdins attractive for use as luminescence probes for investigating siderophore actions and siderophore-mediated transport processes [31].

5.2.2 Cm(III) pyoverdin interactions

An overview of the emission spectra of 3×10^{-7} M curium(III) in 0.1 M $NaClO_4$ measured in the *P. fluorescens* (CCUG 32456) pyoverdin system is presented in Fig. 5.4. The

complexation of curium(III) with these bioligands had started even at pH 4.2 and low pyoverdin concentrations of 3×10^{-7} M. This is depicted in Fig. 5.4A by the decreased emission band of the Cm^{3+} aquo ion at 593.8 nm and the formation of a shoulder at 602 nm. A pyoverdin concentration of 3×10^{-7} M lies in the range of hydroxamate siderophores identified in a variety of different soils [11]. Fig. 5.4B presents the changes observed in the emission spectra at fixed concentrations of curium(III) and pyoverdin of 3×10^{-7} M and 1×10^{-5} M, respectively, as a function of pH. Three different complex species can be differentiated on the basis of their individual emission bands at 601, 606, and 611 nm.

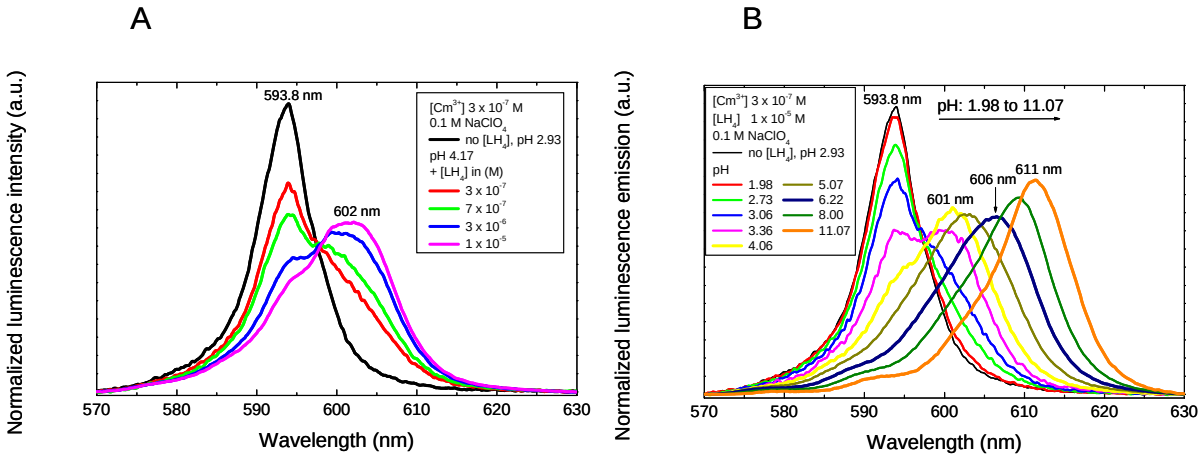

Fig. 5.4 Luminescence emission spectra of 3×10^{-7} M curium(III) measured: A) as a function of the pyoverdin concentration, LH_4, at pH 4.17 in 0.1 M $NaClO_4$; and B) at a fixed pyoverdin concentration of $[LH_4]$ 1×10^{-5} M as a function of pH. The spectra are scaled to the same peak area.

In light of relevant complexation studies of pyoverdin-type bioligands with metals [7, 8, 28, 140, 141], and taking into consideration the deprotonation of the pyoverdin molecule, possible curium(III)–pyoverdin species of the $M_pL_qH_r$ type were introduced into the SPECFIT data analysis procedure. The variations observed in the emission data (see Fig. 5.4) could be described by the following equilibria:

$$Cm^{3+} + 2H^{+} + L^{4-} \rightleftharpoons CmH_2L^{+} \qquad \log \beta_{112} \qquad (45)$$

$$Cm^{3+} + H^{+} + L^{4-} \rightleftharpoons CmHL \qquad \log \beta_{111} \qquad (46)$$

$$Cm^{3+} + L^{4-} \rightleftharpoons CmL^{-} \qquad \log \beta_{110} \qquad (47)$$

Formation constants for reactions (45)–(47) were calculated to be $\log \beta_{112} = 32.50 \pm 0.06$, $\log \beta_{111} = 27.40 \pm 0.11$, and $\log \beta_{110} = 19.30 \pm 0.17$, respectively (see Tab. 5.3) [17]. The corresponding single-component spectra of the individual species are summarized in Fig. 5.5. These results indicate that *P. fluorescens* (CCUG 32456) pyoverdins form strong 1:1

complexes with curium(III). No published data exist for curium(III) to provide a basis for comparison.

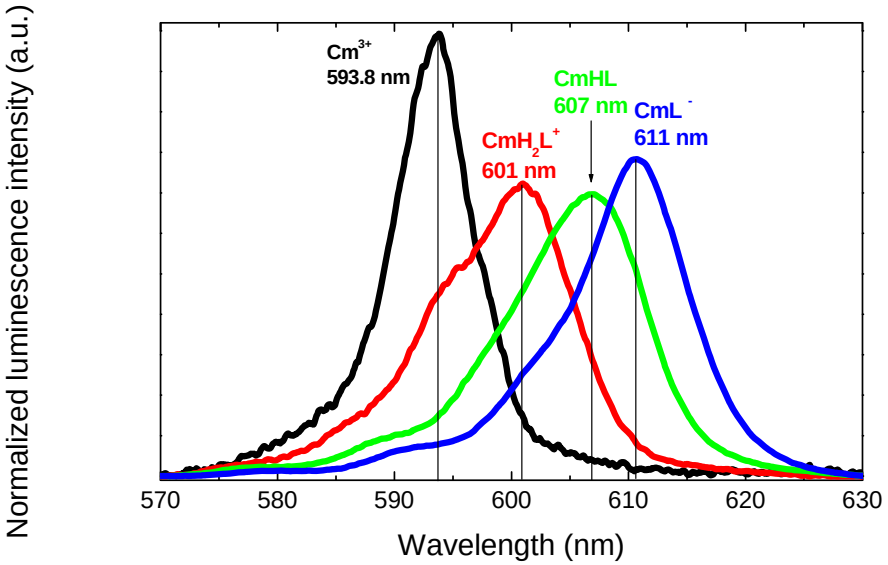

Fig. 5.5 Luminescence emission spectra of the single components in the Cm^{3+}–*P. fluorescens* (CCUG 32456) pyoverdin system, as derived by peak deconvolution using SPECFIT. The spectra are scaled to the same peak area.

Tab. 5.3 Summary of the relevant stability constants of metal bioligand species in comparison to the Cm^{3+}–*P. fluorescens* (CCUG 32456) pyoverdin constants determined in this study at an ionic strength of 0.1 M ($NaClO_4$).

Species / $M_pL_qH_r$	Bacteria / Chelating agent	Methods	log ß	Reference
$Cm(III)H_2L^+$ / 112 $Cm(III)HL$ / 111 $Cm(III)L^-$ / 110	*P. fluorescens* (CCUG 32456 A) / Pyoverdin mixture	Fluorescence spectroscopy	32.50 ± 0.06 27.40 ± 0.11 19.30 ± 0.17	[17]
$Fe(III)H_2L^+$ / 112 $Fe(III)HL$ / 111 $Fe(III)L^-$ / 110	*P. aeruginosa* (ATCC 15692) / Pyoverdin PaA	Spectroscopy & Cyclic voltammetry	47.80 ± 0.20 43.00 ± 0.30 30.80 ± 0.30	[8]
$Eu(III)HDFO^+$ / 111	Desferrioxamine B (DFO)	Potentiometry	26.18 [a]	[50]
$Cm(III)H_2DFO^{2+}$ / 112 $Cm(III)HDFO^+$ / 111 Cm(III)DFO / 110	Desferrioxamine B (DFO)	Fluorescence spectroscopy	31.62 ± 0.23 25.73 ± 0.17 16.80 ± 0.40	[81]

[a] Recalculated in this study.

As shown in Tab. 5.3 pyoverdins are also able to complex elements other than Fe(III) at a considerably high efficiency. Due to the lack of data describing the complexation of trivalent actinides with pyoverdin-type siderophores, the presented results are compared to those

obtained for curium(III) and europium(III) with desferrioxamine B (DFO); this is a commercially available microbially produced trihydroxamate siderophore with good actinide-binding properties [80, 81, 144, 145]. The Cm^{3+}–pyoverdin complexation constant, log β_{111}, is comparable to those of the europium(III) 1:1 complex with desferrioxamine B [50], which emphasizes the good actinide-binding properties of the investigated pyoverdins. A direct comparison of the Cm(III) stability constants determined with the two types of natural bioligands (pyoverdins and DFO) shows slightly stronger species between Cm(III) and the pyoverdins secreted by *P. fluorescens* (CCUG 32456). This can be explained by the additional participation of the catechol groups of the pyoverdin chromophore in the complex formation. Whereas, the unique binding properties provided by the pyoverdin molecule, e.g., structure, might be a further explanation. The complexation of curium(III) with *P. fluorescens* (CCUG 32456) pyoverdins is stronger than the complexation with EDTA (log β_{110} = 18.41) [146], hydroxide (log β_{110} = 6.8 ± 0.5) [51], or carbonate (log β_{110} = 8.1 ± 0.3) [51].

The spectroscopic properties of the identified curium(III) complexes are summarized in Tab. 5.4.

Tab. 5.4 Spectroscopic properties of the identified curium(III) pyoverdin species.

	Cm^{3+} (aq)	**CmH_2L^{+} [a]**	**CmHL [b]**	**CmL^{-} [c]**
Excitation (nm)	374.4 (3.6)[d] 379.9 (2.9) 396.0 (2.2)	372.6 (5.4) 377.8 (4.6) 386.0 (7.6) 395.4 (8.4)	373 [e] 385 [f] 389 [f] 395 [f] 400 [f]	366 (25) 377 [e] 386 (4.8) 394 [f]
Emission (nm)	**593.8 (8.2)** [d]	593.7 [e] **602.2** (11.6)	602.5 [e] **608.4** (7.9)	605.3 [e] **610.8** (6.9) 614.6 [e]
Lifetime (µs)	68 ± 1	86 ± 2 (80%) 198 ± 10 (20%)	83 ± 2 (64%) 229 ± 5 (36%)	100 ± 5 (71%) 330 ± 10 (29%)
$I_{rel}(395)$	1	3.36	19.63	8.10
$I_{rel}(360)$	1	197.2	1112.7	575.3

[a] In 1×10^{-5} M LH_4 at pH 4.17 (88% CmH_2L^{+} and 12% CmHL). [b] In 3×10^{-6} M LH_4 at pH 7.00 (98% CmHL and 2% CmH_2L^{+}). [c] In 1×10^{-5} M LH_4 at pH 11.07 (98% CmL^{-} and 2% CmHL). [d] Values in parentheses are full width at half- maximum. [e] Shoulder. [f] Broad, poorly resolved bands.

The emission peak maximum is shifted from 593.8 nm for the Cm^{3+} aquo ion to 601, 606, and 611 nm when curium(III) occurs in the three identified 1:1 pyoverdin complexes (see also Fig. 5.4). Simultaneously, the emission intensity is increased by factors of 3.36, 19.63, and 8.10 for the three pyoverdin complexes, respectively. In agreement with previous findings regarding the absorption spectrum of the Cm^{3+} aquo ion [147], we found that the emission intensity of this species decreased by a factor of 65 when the excitation wavelength was

changed from 395 to 360 nm. Under the same conditions, the intensities of the CmH_2L^+ and the CmHL complexes decreased by factors of only 1.12 and 1.16, respectively, whereas the intensity of the CmL^- complex increased by a factor of 1.08. At an excitation wavelength of 360 nm, the intensities of these complexes relative to that of the Cm^{3+} aquo ion are 197, 1113, and 575, respectively. This indicates that luminescence emission of the Cm^{3+}–pyoverdin species can be generated either by direct excitation of the metal ion or by indirect excitation of the ligand followed by energy transfer from the ligand molecule to the metal ion.

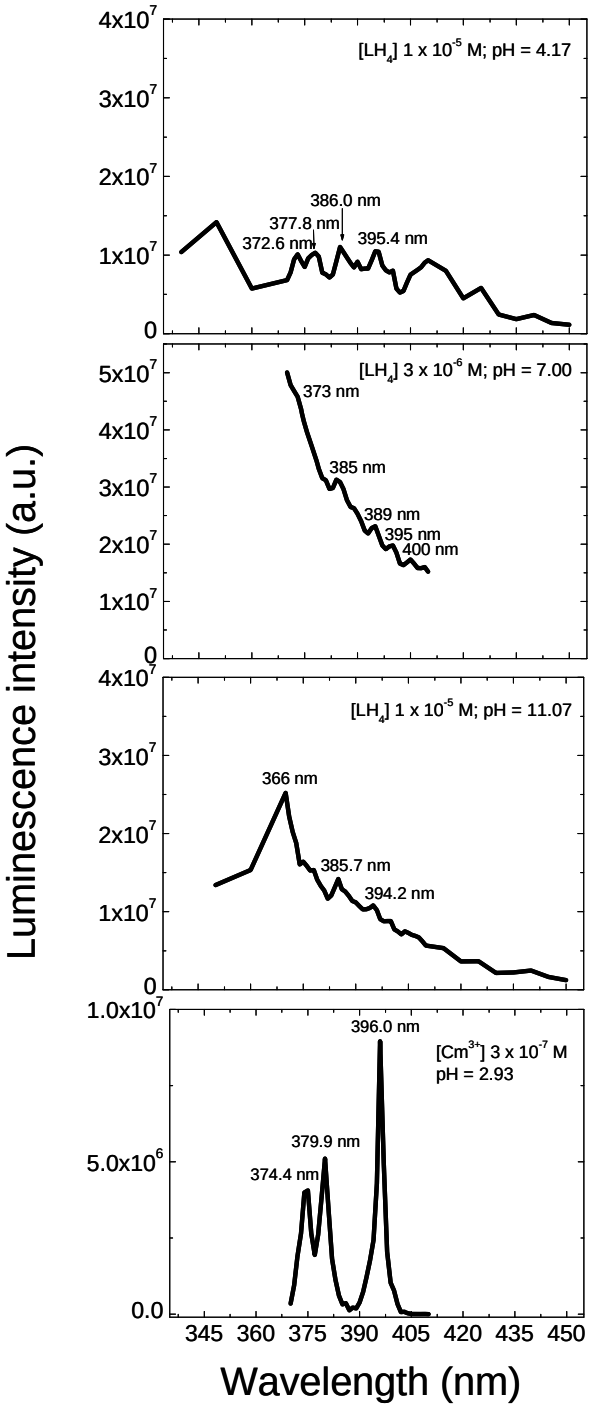

Fig. 5.6 Excitation spectra of curium(III) measured in the *P. fluorescens* (CCUG 32456) pyoverdin system.

The excitation spectra of the identified curium(III) complexes are summarized in Fig. 5.6. The above effects are reflected in the corresponding excitation spectra. Instead of sharp, well-resolved absorption bands like those observed for the Cm^{3+} aquo ion and intense transitions to the H-, G-, and F -states, only broad and poorly resolved absorption bands were measured for the Cm^{3+}–pyoverdin species. This behavior indicates the coordination of curium(III) to organic molecules containing aromatic entities [75], which could be characterized in the pyoverdins, i.e. pyoverdin-chromophore, as shown in Fig. 2.2B. Flat and structurally poor excitation spectra have previously been reported, for example for Cm^{3+} humate/fulvate complexes [75] and Cm^{3+} humates sorbed onto γ-Al_2O_3 [74]. We tested the idea of selectively exciting the Cm^{3+} aquo ion and the Cm^{3+}–pyoverdin species using direct and indirect excitation modes. In the pH 2–4 range, the Cm^{3+} aquo ion coexists with the first 1:1 pyoverdin complex, CmH_2L^+. Irradiation of the test solution with an excitation wavelength of 360 nm induces only a very weak measurable luminescence of the Cm^{3+} aquo ion. When complexation with the pyoverdins starts, energy transfer from excited electronic or vibronic states of the pyoverdin molecule to curium(III) is enabled and luminescence spectra are obtained. Unlike the results reported for the Cm^{3+}–humic acid–γ-Al_2O_3 system [74], we observed emission spectra that are almost congruent and independent of the excitation mode over the whole pH range investigated. It follows that the unique luminescence properties of the pyoverdin polyelectrolyte likely inhibit the spectroscopic differentiation of non-pyoverdin-bound and pyoverdin-bound curium(III).

In all samples in which the Cm^{3+} aquo ion and the first pyoverdin complex, CmH_2L^+, are present, a mono-exponential decay was measured with an average lifetime of 83 μs (see Tab. 5.4); this lifetime could correspond to the CmH_2L^+ species. In all samples with pH values above 3.4 and $[LH_4]$ of 3×10^{-6} and 1×10^{-5} M, bi-exponential decay was always detected with average lifetimes of 83 and 210 μs. The latter might correspond to the second pyoverdin species, CmHL. At pH values above 10, the second lifetime increased to 340 μs, indicating the formation of a third complex, CmL^-. This suggests a low ligand exchange rate for the pyoverdin complexes, compared to the luminescence decay rate of the excited Cm^{3+} aquo ion. The increasing lifetimes of the curium(III) species reflect the exclusion of water molecules from the first coordination sphere of curium(III) due to the identified complex formation reactions. The luminescence lifetimes as measured by direct and indirect excitation match closely.

In conclusion, use of TRLFS in combination with the SPECFIT factor analysis software provides a applicable method for investigating the speciation of curium(III) in the aqueous *P.*

fluorescens (CCUG 32456) pyoverdin system. Strong Cm^{3+}-pyoverdin species are formed, indicating the great potential of these unique siderophores to mobilize curium(III) in the biologically relevant pH range.

5.2.3 Np(V) pyoverdin interactions

The results of the spectrophotometric titrations of the NpO_2^+ test solutions in the aqueous *P. fluorescens* (CCUG 32456) pyoverdin system are shown in Fig. 5.7A.

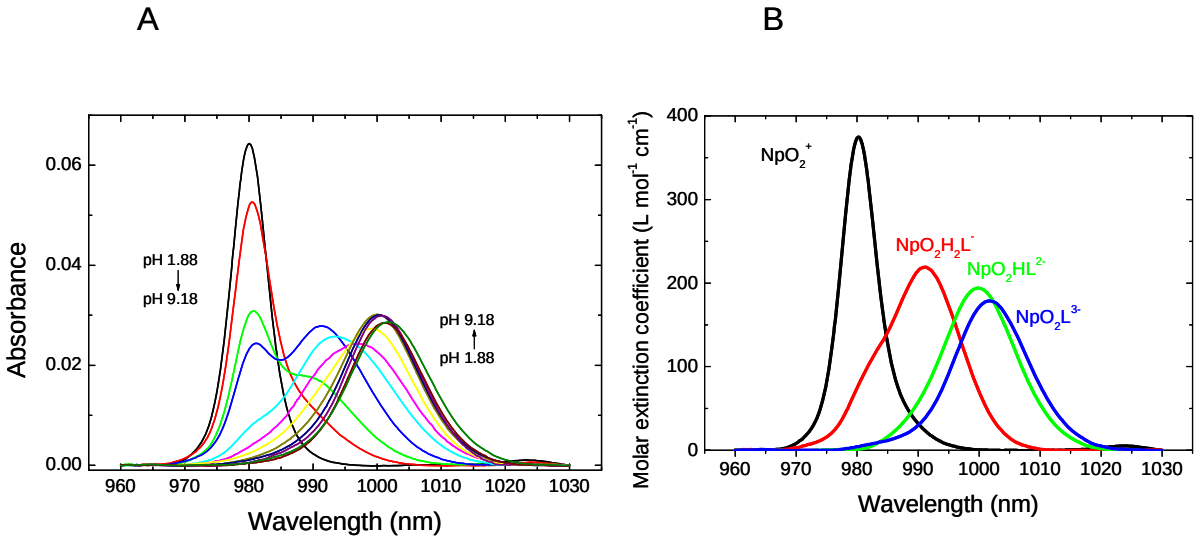

Fig. 5.7 A) Spectrophotometric titrations of 1.6×10^{-4} M NpO_2^+ in solutions containing 1.06×10^{-3} M LH_4 at an ionic strength of 0.1 M $NaClO_4$. B) NIR absorption spectra of the single components in the NpO_2^+–pyoverdin (LH_4) system, as derived by peak deconvolution using SPECFIT.

The strong changes of the Np(V) absorption band centered at 980 nm observed in aqueous pyoverdin solutions are not connected with defined isosbestic points. This might indicate the occurrence of more than two Np(V)–PYO species at the same time. In contrast to the pyoverdin models (see chapter 3.2), the neptunyl(V) complexation in the Np(V)–pyoverdin (LH_4) system started even at metal-to-ligand ratios below 1:1 (data not shown). The program SPECFIT was used to extract the neptunyl(V)–pyoverdin stability constants, single component spectra (see Fig. 5.7B) and the molar absorptivities of the formed neptunyl(V) species. As a result, the variations observed in the absorption data (see Fig. 5.7A) could be described by the following equilibria:

$$NpO_2^+ + 2H^+ + L^{4-} \rightleftharpoons NpO_2H_2L^- \qquad \log \beta_{121} \qquad (48)$$

$$NpO_2^+ + H^+ + L^{4-} \rightleftharpoons NpO_2HL^{2-} \qquad \log \beta_{111} \qquad (49)$$

$$NpO_2^+ + L^{4-} \rightleftharpoons NpO_2L^{3-} \qquad \log \beta_{101} \qquad (50)$$

Formation constants for reactions (48) to (50) were calculated to be $\log \beta_{121} = 26.90 \pm 0.69$, $\log \beta_{111} = 20.90 \pm 0.60$, and $\log \beta_{101} = 13.40 \pm 0.17$, respectively.

By comparing these results with those obtained with the pyoverdin model ligands (see chapter 3.2) it follows that Np(V) forms the strongest complexes with the natural pyoverdins. Three NpO_2^+–*P. fluorescens* (CCUG 32456) pyoverdin species, $NpO_2H_2L^-$, NpO_2HL^{2-} and NpO_2L^{3-}, could be identified by their individual absorption spectra (Fig. 5.7B) having absorption maxima at 991.0, 1000.0, and 1002.0 nm, respectively.

To the best of our knowledge, spectrophotometric titrations of NpO_2^+ with pyoverdins were not reported before. NpO_2^+ forms strong complexes with the pyoverdins providing hydroxamate and catechol functionalities for Np(V) binding. In general the absorption maxima of 1:1 complexes of NpO_2^+ with the bioligands investigated (see chapter 3.2) span a wavelength range between 988.6 to 1002 nm, whereas the identified 1:2 species are redder shifted with 996.5 to 1006 nm. These absorption bands exhibit an increased bathochromic shift compared to literature values of NpO_2^+ species with (a) hydroxycarboxylates: 983.4 to 988.6 nm [60], (b) dicarboxylates: 987.4 to 990.4 nm [62], and (c) humates: 994.3 nm [53]. This can serve as an indicator for a strong affinity of NpO_2^+ to complexing agents containing hydroxamate and catechol functionalities. The main absorption band and the magnitude of the stability constant of the identified Np(V) species could be used for an estimate which functional groups participate most likely in Np(V) bonding. A direct comparison of the absorption maxima of the 1:0:1 Np(V) species showed an increased red shift in the following order: α–hydroxycarboxylates 985 nm [60], hydroxamates 991 nm, catecholate 996 nm, and pyoverdins 1002 nm. The magnitude of the 1:0:1 stability constants display the same trend: PYO > NAP > SHA > BHA > α–hydroxy acids. This might suggest a stronger affinity of NpO_2^+ to the catechol groups of the pyoverdin molecule and a lower affinity to interact with the two other functionalities. As a result, pyoverdin molecules are besides UO_2^{2+} [16, 28, 140] and Cm^{3+} [17] also efficient in complexing and mobilizing NpO_2^+ [18].

A literature survey of Np(V) formation constants of 1:1 species with relevant organic molecules like benzoate ($\log \beta = 0.82$) [60], acetate ($\log \beta = 1.70$) [58], glycolate ($\log \beta = 1.43$) [60], EDTA ($\log \beta = 7.33$) [59], malonate ($\log \beta = 2.03$) [62], and humate ($\log \beta = 2.44$-3.60) [54, 53, 56] underline the good Np(V) binding properties of hydroxamate- and catecholate-model compounds as well as pyoverdin-type siderophores. The complexation of neptunium(V) with *P. fluorescens* (CCUG 32456) pyoverdins is clearly stronger than complexation with hydroxide ($\log \beta_{1:1} = 2.50$) [67], carbonate ($\log \beta_{1:1} = 4.6$) [148], phosphate

(log $\beta_{1:1}$ = 6.33) [149], or sulfate (log $\beta_{1:1}$ = 0.5) [150]. It is known that ethylenediaminetetraacetic acid (EDTA) may form the strongest actinide complexes among the various organic components of nuclear wastes [151]. The stability constants of 1:1 species formed between Cm^{3+} and UO_2^{2+} and *P. fluorescens* (CCUG 32456) pyoverdins [16, 17] are by a factor of 1.05 and 1.3, respectively, larger compared to the corresponding EDTA stability constants [151, 145]. Remarkable is that the Np(V)–PYO stability constant is by a factor of 1.83 greater than the EDTA stability constant. To the best of our knowledge, the identified NpO_2^+–PYO species belong to the strongest NpO_2^+ species with organic material reported so far.

5.2.4 Summary of actinide speciation studies with pyoverdins

Tab. 5.5 gives a summary of the stability constants determined for the different actinide *P. fluorescens* (CCUG 32456) pyoverdin species.

Tab. 5.5 Summary of the Ac–*P. fluorescens* (CCUG 32456) pyoverdin (LH_4) stability constants determined in this study at an ionic strength of 0.1 M ($NaClO_4$).

Reaction	Method	log β_{xyz}	Reference
$Fe^{3+} + L^{4-} + 2H^+ \rightleftharpoons FeLH_2^+$ $Fe^{3+} + L^{4-} + H^+ \rightleftharpoons FeLH$ $Fe^{3+} + L^{4-} \rightleftharpoons FeL^-$	Spectroscopy & Cyclic voltammetry	47.80 ± 0.20 43.00 ± 0.30 30.80 ± 0.30	[8]
$UO_2^{2+} + L^{4-} + 2H^+ \rightleftharpoons UO_2LH_2$ $UO_2^{2+} + L^{4-} + H^+ \rightleftharpoons UO_2LH^-$	UV-vis & fs-TRLFS	30.00 ± 0.64 26.00 ± 0.85	[16]
$Cm^{3+} + L^{4-} + 2H^+ \rightleftharpoons CmLH_2^+$ $Cm^{3+} + L^{4-} + H^+ \rightleftharpoons CmLH$ $Cm^{3+} + L^{4-} \rightleftharpoons CmL^-$	TRLFS	32.50 ± 0.06 27.40 ± 0.11 19.30 ± 0.17	[17]
$NpO_2^+ + L^{4-} + 2H^+ \rightleftharpoons NpO_2LH_2^-$ $NpO_2^+ + L^{4-} + H^+ \rightleftharpoons NpO_2LH^{2-}$ $NpO_2^+ + L^{4-} \rightleftharpoons NpO_2L^{3-}$	NIR absorption spectroscopy	26.90 ± 0.69 20.90 ± 0.60 13.40 ± 0.17	[18]

As shown in Tab. 5.5 pyoverdins have their largest formation constants with Fe^{3+}. This is not surprising because pyoverdins are chelating agents synthesized by fluorescent *Pseudomonas* spp. to provide the cells with the essential Fe^{3+}. However, it can be also seen that pyoverdins are also able to complex elements other than Fe(III) at a considerably high efficiency. Fig. 5.8 shows the speciation of uranium(VI), curium(III) and neptunium(V) in aqueous solution with equimolar amounts of actinides and pyoverdins. The speciation was done with the program MEDUSA [19]. Our complexation studies showed that the pyoverdins are very effective in

binding the trivalent actinide element curium (see Fig. 5.8) over a wide pH range. Less stable are the species formed with uranium(VI). The weakest complexes are formed with the pentavalent actinide neptunium. However, also these constants are surprisingly strong for organic neptunyl(V) complexes (please see discussion in chapter 3.2). That the complexation strength of the Np(V) species is lower compared to the U(VI) and Cm(III) species can be explained with the lower effective charge density of NpO_2^+ of +2.2 compared to +3.3 for UO_2^{2+} [126].

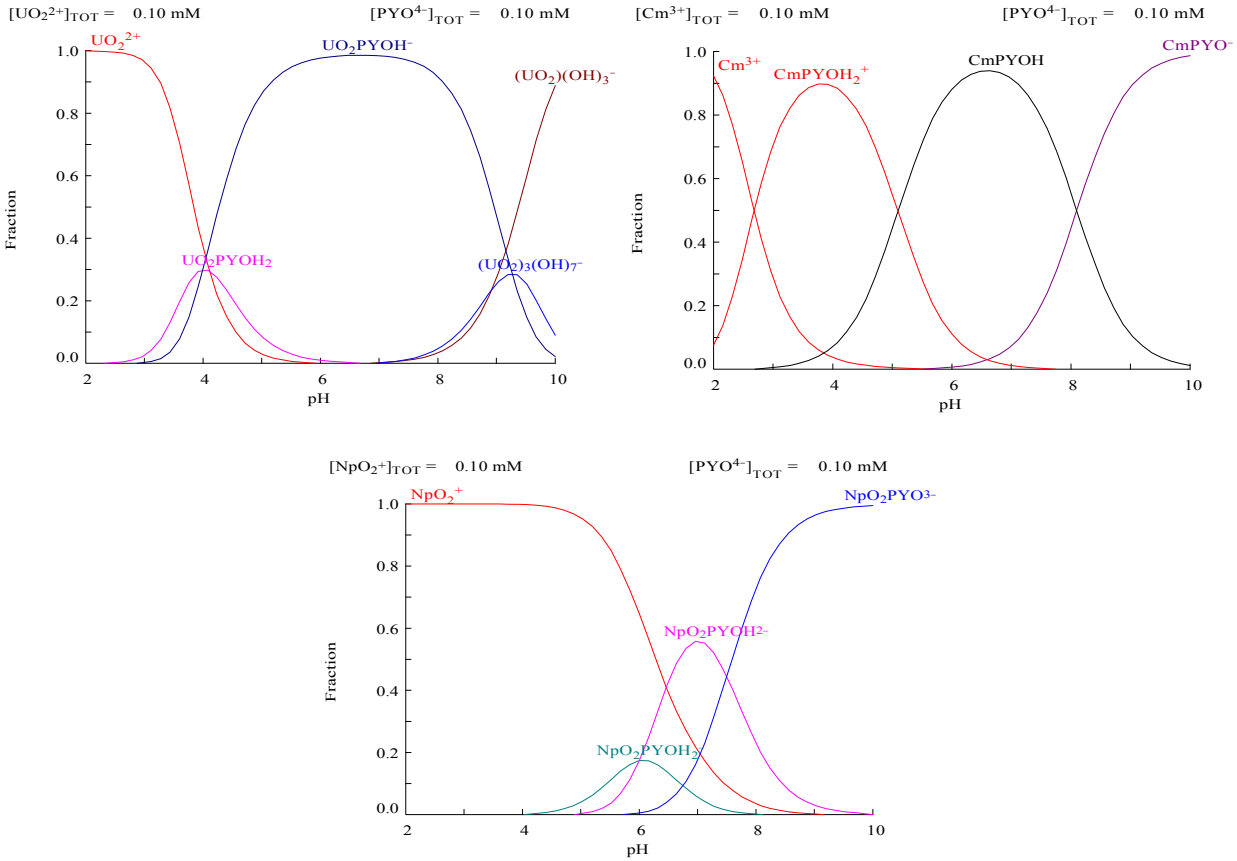

Fig. 5.8 Speciation of uranium(VI), curium(III), and neptunium(V), 1×10^{-4} M, in aqueous solutions of pyoverdins (PYO), 1×10^{-4} M, as a function of the pH.

The broadest stability range in terms of pH units could be observed for Cm(III) pyoverdin species between pH 3 and 10, whereas the U(VI) pyoverdin complexes dominate between pH 4.5 and 8. The range of existence of the Np(V) pyoverdin species starts from pH 5.5 up to pH values greater than 10. To conclude, strong actinide pyoverdin species are formed, indicating the great potential of these unique siderophores to mobilize all three actinides (U(VI), Cm(III), Np(V)) in the biologically relevant pH range.

5.2.5 Structural aspects of the uranium(VI) complexation with pyoverdins and related model compounds by EXAFS and ATR-FTIR

Fig. 5.9 shows the raw uranium L_{III}-edge k^3-weighted EXAFS spectra and their corresponding Fourier transforms including the fits of the experimental data. The results of the fits to the experimental data are listed in Tab. 5.6. The coordination number (N) of the axial oxygen of the linear uranyl(VI) unit was held constant at two during the fitting procedure. The mean U-O_{ax} distance is 1.78 ± 0.01 Å and the average Debye-Waller factor is 0.002(2) $Å^2$. Within the experimental uncertainties, these values are the same for all samples. However, there is a small tendency of a lengthening of the U-O_{ax} bond with increasing pH values as observed in the NAP-, DFO-system, and also in the UO_2^{2+}–PYO sample.

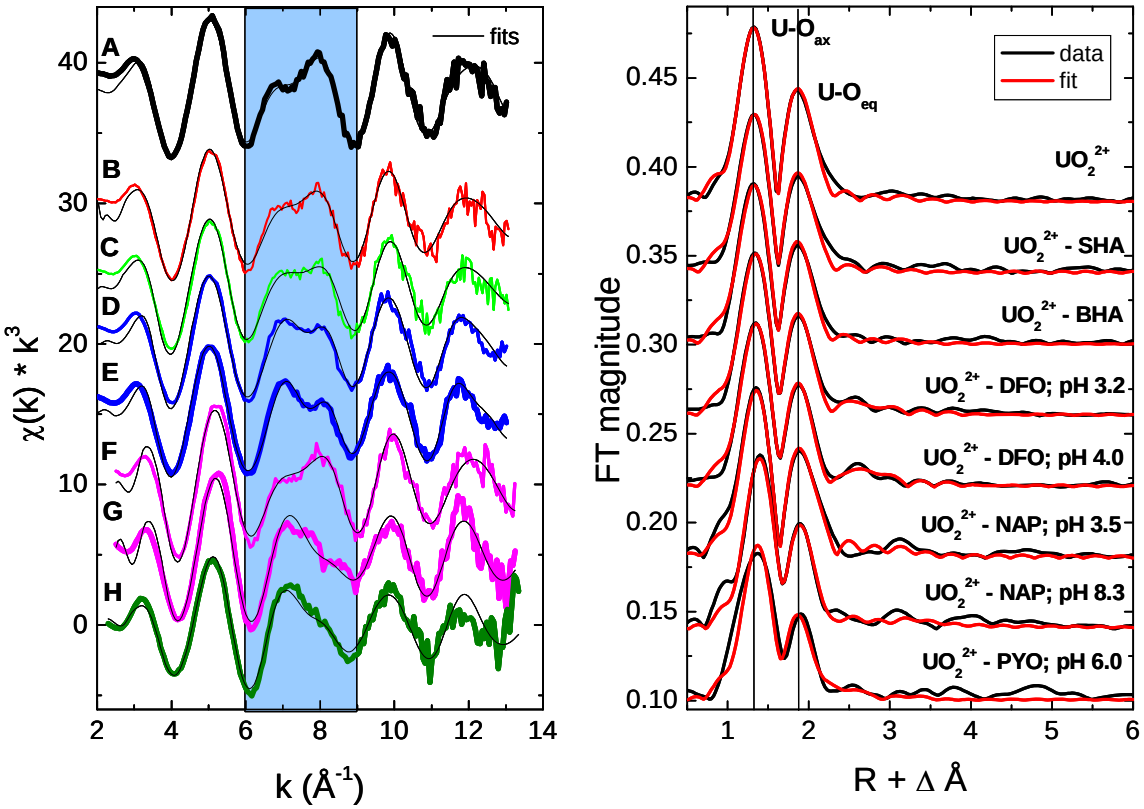

Fig. 5.9 Raw U L_{III}-edge k^3-weighted EXAFS spectra of uranium(VI) complexes with the selected bioligands at different pH values (left) and corresponding Fourier transforms (right).

Significant differences are observed in the equatorial coordination shell of the uranyl(VI) cation. Hence the EXAFS oscillations exhibit variations in the 6 to 9 $Å^{-1}$ k-range which is highlighted in Fig. 5.9. In samples B and C approximately five equatorial oxygen atoms with an average U-O_{eq} distance of 2.41 and 2.40 Å, respectively, were determined (see Tab. 5.6). In the two simple hydroxamate systems, we observed mean U-O_{eq} bond length being by

0.01 Å shorter than in the free UO_2^{2+}. This decrease points to a bidentate coordination via the hydroxamate oxygen atoms [79].

Tab. 5.6 EXAFS structural parameters for the aqueous UO_2^{2+} and UO_2^{2+}–L (SHA, BHA, DFO, NAP, PYO) systems[a].

Sample	Shell	N	R (Å)	σ^2 (Å^2)	ΔE_0 (eV)
A	U-O_{axial}	2[b]	1.76_6	0.0016	10.5
	U-$O_{equatorial}$	5.0	2.41_8	0.0068	
B (SHA)	U-O_{axial}	2[b]	1.77_5	0.0026	13.4
	U-$O_{equatorial}$	4.7	2.41_5	0.0063	
C (BHA)	U-O_{axial}	2[b]	1.77_3	0.0027	12.3
	U-$O_{equatorial}$	4.8	2.40_2	0.0064	
D (DFO)	U-O_{axial}	2[b]	1.78_1	0.0023	10.3
pH 3.2	U-$O_{equatorial}$	4.9	2.40_0	0.0070	
	U-C/N	2[b]	3.22	0.0040	
E (DFO)	U-O_{axial}	2[b]	1.78_5	0.0024	9.7
pH 4.0	U-$O_{equatorial}$	4.8	2.38_7	0.0069	
	U-C/N	2[b]	3.22	0.0015	
F (NAP)	U-O_{axial}	2[b]	1.76_8	0.0017	18.6
pH 3.5	U-$O_{equatorial}$	5.6	2.40_5	0.0078	
G (NAP)	U-O_{axial}	2[b]	1.79_7	0.0018	18.3
pH 8.3	U-$O_{equatorial}$	6.3	2.36_9	0.0095	
H (PYO)	U-O_{axial}	2[b]	1.78_8	0.0023	12.8
pH 6.0	U-$O_{equatorial}$	6[b]	2.35_3	0.0107	
	U-C/N	2[b]	2.89	0.0047	
U(VI)-PCA[152]	U-O_{axial}	2[b]	1.81	0.0013	-14
pH 10.0	U-$O_{equatorial}$	5.8	2.37_4	0.0071	

[a] Given are the coordination number N (error (15%)), the bond length R (in Å; error (0.01 Å)), the Debye–Waller factor σ^2 (in Å^2), and the energy threshold ΔE_0 (in eV). [b] Parameter has been fixed during the fit.

Structural parameters of aqueous uranyl(VI) species within the DFO, NAP and PYO systems were not reported before. Desferrioxamine B (DFO) is a microbial produced trihydroxamate siderophore which is commercially available and could occur naturally in soils. Recently, Essen et al. [153] could show the production of desferrioxamine siderophors by *Pseudomonas stutzeri* (CCUG 36651). This strain was also isolated at the Äspö HRL. In samples D and E approximately five equatorial oxygen atoms with an average U-O_{eq} distance of 2.40 and 2.38 Å, respectively, were determined (see Tab. 5.6). Hence, when the amount of DFO–complexed uranyl(VI) increased a decrease in the distance of the equatorial oxygen atoms was observed. Indications were found for nitrogen and carbon atoms of the chelating hydroxamate groups belonging to the DFO molecule in the near order surrounding of the linear uranyl(VI) unit. The fit could be significantly improved by including a U-C/N shell at

3.22 Å. Structural data of uranyl(VI) hydroxamate compounds in solution and solid state are very scarce to provide a basis for comparison.

NAP serves as a simple model describing the catechol functionality of the pyoverdin molecule (see Fig. 2.2). To the best of our knowledge, structural information of aqueous uranyl(VI)–NAP species is unknown. The pH dependent formation of uranyl(VI) species with NAP are expressed in the EXAFS oscillation especially of sample G within the k-range 6 to 9 $Å^{-1}$ in comparison of the one measured for the free uranyl(VI) ion (see sample A in Fig. 5.9). In samples F and G approximately six equatorial oxygen atoms with an average U-O_{eq} distance of 2.40 and 2.36 Å, respectively, were determined (see Tab. 5.6). The shortening of the equatorial oxygen distance as a function of pH can be explained by an increased amount of deprotonated phenolic OH groups participating in bonding to uranyl(VI). Our observations are in agreement with the results of Rossberg et al. [152]. If uranyl(VI) is coordinated to the deprotonated neighboring phenolic OH groups of catechol at pH 10 this results in an average U-O_{eq} distance of 2.37 Å and a coordination number of 5.9.

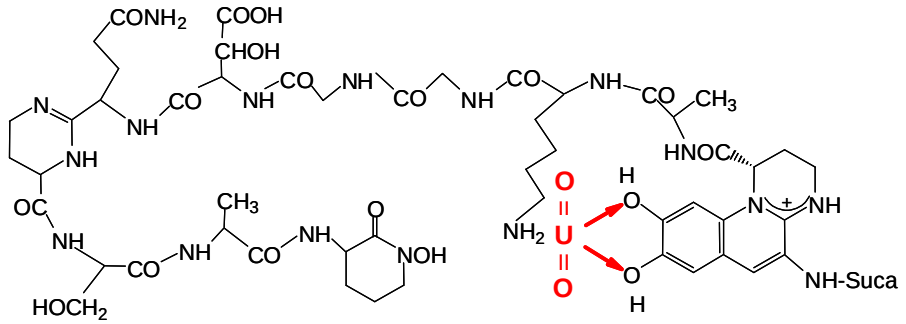

Fig. 5.10 Simplified scheme of the favored uranyl(VI) coordination within the pyoverdin molecule.

The EXAFS analysis of sample H yielded approximately 6 equatorial oxygen atoms at 2.35 Å. There are indications for an additional U-C/N shell at 2.89 Å. The EXAFS oscillation and resulting structural parameters of the U(VI)–pyoverdin sample showed strong similarities with those of 1:1 complexes of U(VI) with protocatechuic acid and catechol reported in [152] (see Tab. 5.6). One can conclude from these findings a strong affinity of U(VI) to the catechol functionality of the pyoverdin molecule (see Fig. 5.10). However, the coordination of U(VI) to hydroxamate groups results also in a shortening of the distance of the equatorial oxygen atoms.

Within selected systems, we performed attenuated total reflectance Fourier-transform infrared spectroscopy (ATR-FTIR) measurements to ensure our XAS data interpretation. Fig. 5.11 shows the corresponding results. The absorption band at 1269 cm^{-1} obtained in the uranyl(VI)

free NAP sample is connected with vibrations of the two phenolic OH groups (Fig. 5.11A). This absorption band is shifted to 1259 cm^{-1} in the UO_2^{2+} containing sample. The asymmetric stretching vibration of the uranyl ion UO_2^{2+} measured at 930 cm^{-1} indicates a bidentate coordination mode of U(VI). The characteristic absorption band of U(VI) in acidic aqueous solution occur in the IR spectra at 961 cm^{-1}. We can conclude from these observations an interaction of UO_2^{2+} with the phenolic OH groups of the NAP molecule.

The interpretation of the IR spectra measured in the pyoverdin system is more complex. The absorption bands at 1287 and 1249 cm^{-1} might indicate vibrations of the phenolic OH groups of the pyoverdin chromophore. In the uranyl(VI) test solution these bands are shifted to 1286 cm^{-1}. The broad band at 910 cm^{-1} (υ_{as} UO_2^{2+}) could indicate that U(VI) is bound to more than one functional group of the pyoverdin molecule. This is in agreement with the interpretation of the absorption bands at 1461 and 1533 cm^{-1} in the uranyl(VI) containing pyoverdin sample. Here one can conclude uranyl(VI) interactions with carboxyl sites of the pyoverdin molecule.

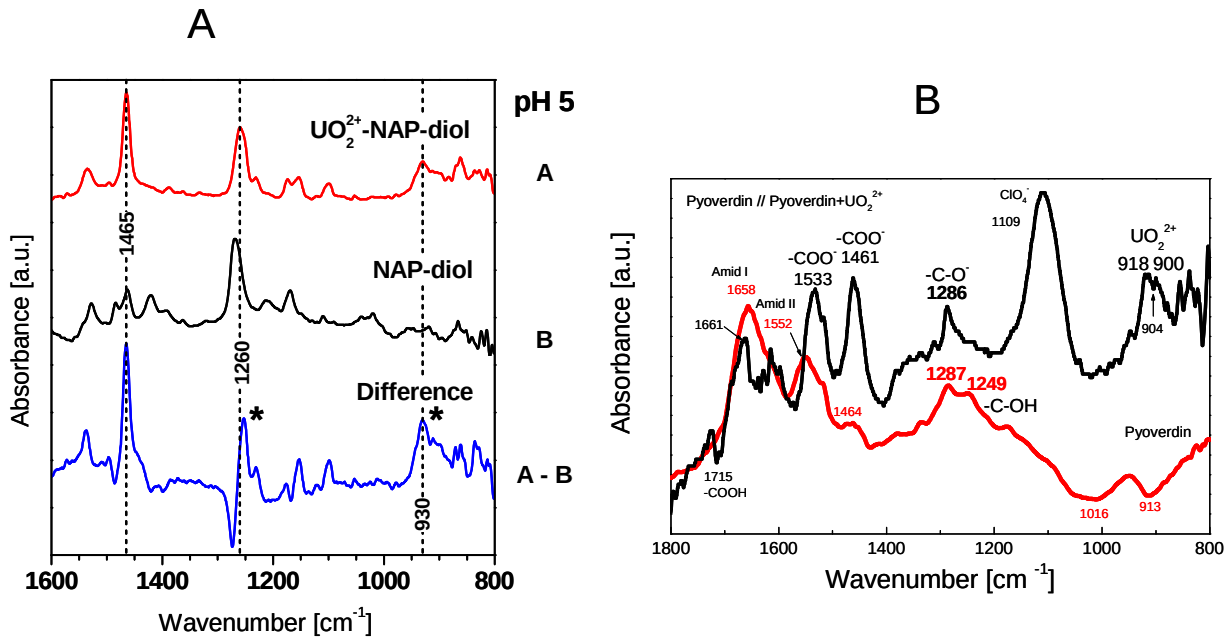

Fig. 5.11 ATR-FTIR spectra of UO_2^{2+}–bioligand solutions. (A) 8×10^{-4} M UO_2^{2+} and 0.0012 M NAP; (B) 1×10^{-4} M UO_2^{2+} and 1.5×10^{-4} M PYO at pH 6.

To summarize the preliminary IR results, we found indications in both systems (NAP and PYO) for uranyl(VI) interactions with phenolic OH groups. This underlines the structural findings from the XAS investigations.

6 Summary and outlook

The aim of this project was to study the interaction reactions of bioligands secreted by the groundwater bacterium *Pseudomonas fluorescens* (CCUG 32456) with the actinides uranium, curium, and neptunium. This includes also complexation studies with model systems simulating the main functionalities of both the identified bioligands and the surface of microbes.

The groundwater bacterium *Pseudomonas fluorescens* (CCUG 32456) identified at a depth of 70 m in the Äspö Hard Rock Laboratory, Sweden, secretes pyoverdin-type siderophores. The isolation of the different bioligand fractions was performed by our Swedish colleagues at the Department of Cell and Molecular Biology, Microbiology, Göteborg. Mass spectrometry indicated that the cells produce a pyoverdin–mixture with four main components: pyoverdin with a succinamide side chain, pyoverdin with a succinic acid side chain, ferribactin with a succinamide side chain, and ferribactin with a glutamic acid side chain. However, the results of an absorption spectroscopy study of the aqueous bioligand mixture demonstrated the dominant influence of the pyoverdins. Three pK values could be determined from the pH–dependent changes in the absorption spectra of the pyoverdin mixture: $\log \beta_{012} = 22.67 \pm 0.15$ ($pK_1 = 4.40$), $\log \beta_{013} = 29.15 \pm 0.05$ ($pK_2 = 6.48$), and $\log \beta_{014} = 33.55 \pm 0.05$ ($pK_3 = 10.47$). The fluorescence properties of the pyoverdin mixture were pH–dependent. The emission maximum changed from 448 nm at pH = 2.1 to 466 nm in the pH 3.8–8.9 range. A drastic change in the intrinsic fluorescence properties, e.g., static fluorescence quenching, occurred due to the complex formation with UO_2^{2+}.

The functional groups of the pyoverdins that participate in the metal binding are the catechol group of the chromophore and one or two ligand sites in the peptide chain, i.e. the hydroxamate groups and the α-hydroxy acid moieties. Model ligands were chosen to simulate these functionalities. For the simulation of the hydroxamate functionality the monohydroxamates salicylhydroxamic acid (SHA) and benzohydroxamic acid (BHA) and the natural trihydroxamate desferrioxamine B (DFO) and for the simulation of the catechol groups 6-hydroxyquinoline (6-HQ) and 2,3-dihydroxynaphthalene (NAP) were used. The surface of the microbes was simulated by two isolated bacterial cell wall components. Lipopolysaccharide (LPS) is an important compartment of the cell envelope of Gram-negative

bacteria and contains a high amount of phosporyl groups. The other biomacromolecule simulating the bacterial cell wall was the peptidoglycan (PG). This molecule is the main part of the cell envelope of Gram-positive bacteria. The functionalities for metal binding of PG are carboxyl and amino groups from the peptide chains and hydroxyl groups from the polysaccharide chains.

The comparison of the stability constants of actinide species (U(VI), Cm(III), and Np(V)) with model ligands simulating the functional groups of the pyoverdins results in the following order of complex strength: DFO > NAP > 6-HQ > SHA, BHA.
Both monohydroxamates, SHA and BHA, form 1:1 and 1:2 complexes with similar stability. The natural occurring siderophore DFO has the highest stability constants with the three actinides and forms the strongest complexes. The reason therefore is the structure and high number of functional groups, three hydroxamate groups, of this molecule. The model ligands for the chromophore functionality NAP and 6-HQ form stronger complexes than SHA and BHA, but weaker complexes than DFO. From this it can be reasoned that the chromophore functionality probably plays an important role for the coordination of the actinides to the pyoverdins. The actinides form strong complexes with the selected bioligands providing hydroxamate and catechol functionalities for metal binding. The comparison of the stability constants of the complexes with the three studied actinides U(VI), Cm(III) and Np(V) with each other shows that the strength of the complex formation decreases from U(VI) via Cm(III) to Np(V).

The dissociation constants and corresponding site densities of functional groups provided by the biopolymers LPS and PG were determined with potentiometry. The best fit of the titration data of LPS was obtained with a four-site model. The pK_a of 5.56 ± 0.28 can be assigned to carboxyl groups, the pK_a of 6.96 ± 0.24 to the second dissociation step of phosphoryl groups, and the pK_a of 8.90 ± 0.56 to amino or hydroxyl groups. With some test solutions titrated up to pH 11 an additional pK_a over 10 could be detected, due to the dissociation of amino or hydroxyl groups. The best fit for all titration curves of PG was obtained with a three site model. The pK_a values of 4.55 and 6.31 can be dedicated both to carboxyl groups. The PG molecule offers two different free carboxyl groups, from the glutamic acid and the diaminopimelic acid. The third pK_a of 9.56 can be dedicated to both, amino and hydroxyl groups.

The results of this project showed that different functionalities of LPS and PG are involved in actinide coordination depending on the pH of the test solutions. In general strong species are formed with all three actinides. With one exception, no Np(V) species could be detected with PG using NIR spectroscopy. Probably due to the low affinity of Np(V) to interact with carboxyl sites of biopolymers as shown for LPS. At an excess of LPS, the uranyl(VI) ion is mainly complexed through monodentate coordinated phosphoryl groups (log β 7.5-13.8). At equimolar ratios of uranyl(VI) and functional groups of LPS additional carboxyl coordination (log β 5.9) in a bidentate manner becomes important. In the Cm(III)–LPS system three complexes were identified with high stability constants. Speciation calculations using the formation constants showed predominant Cm(III) coordination to (a) phosphoryl groups within pH 1 and 4 (log β 26.9; 1:2 stoichiometry), (b) carboxyl groups within pH 4 and 9 (log β 9.3; 1:1 stoichiometry), and (c) hydroxyl groups at pH values above 9 (log β 26.7; 1:4 stoichiometry). Two relatively strong NpO_2^+ complexes were formed with coordination to the phosporyl (log β 6.3; 1:1 stoichiometry) and deprotonated hydroxyl (log β 11.6; 1:2 stoichiometry) groups of LPS.

In the U(VI)–PG system four complex species were identified, three with the carboxyl group as functionality (log β 4.0 and 7.0; 1:1 stoichiometry and log β 12.1; 1:2 stoichiometry) and one with an additional involvement of an amino or hydroxyl group (log β 14.9). One Cm(III)–PG complex species was detected with the carboxyl site as the binding group (log β 10.4; 1:2 stoichiometry). Possible Np(V) interactions with the dominant carboxyl groups of the PG molecule were to weak for a detection using the NIR spectroscopy.

The interaction of *P. fluorescens* (CCUG 32456) pyoverdins with the actinides U(VI), Cm(III) and Np(V) was studied using absorption spectroscopy (UV-vis-NIR) and time-resolved laser-fluorescence spectroscopy (TRLFS, fs-TRLFS). Two 1:1 UO_2^{2+}–pyoverdin species with formation constants of $\log \beta_{121} = 30.50 \pm 0.4$ (UO_2H_2PYO) and $\log \beta_{111} = 26.60 \pm 0.40$ (UO_2HPYO^-) were identified. Strong Cm^{3+}–pyoverdin species with 1:1 stoichiometry are formed. The three Cm^{3+}–pyoverdin complexes, CmH_2PYO^+, CmHPYO, and $CmPYO^-$, could be identified by their individual emission spectra. The stability constants of the three complexes were calculated to be $\log \beta_{121} = 32.50 \pm 0.06$, $\log \beta_{111} = 27.40 \pm 0.11$ and $\log \beta_{101} = 19.30 \pm 0.17$. Also three NpO_2^+–pyoverdin complex species, $NpO_2H_2PYO^-$, NpO_2HPYO^{2-}, and NpO_2PYO^{3-}, are formed with stability constants of $\log \beta_{121} = 26.90 \pm 0.69$, $\log \beta_{111} = 20.90 \pm 0.60$ and $\log \beta_{101} = 13.40 \pm 0.17$, respectively.

The different Np(V)–pyoverdin species could be identified by their individual absorption spectra.

It is not surprising that pyoverdins have their largest formation constants with Fe^{3+}. Because pyoverdins are chelating agents synthesized by fluorescent *Pseudomonas* spp. to provide the cells with the essential Fe^{3+}. However, this project shows that pyoverdins are also able to complex elements other than Fe(III) at a considerably high efficiency. The comparison of the stability constants of the complexes with the three studied actinides U(VI), Cm(III) and Np(V) with each other shows that the strength of the complex formation decreases from Cm(III) via U(VI) to Np(V). It is known that ethylenediaminetetraacetic acid (EDTA) may form the strongest actinide complexes among the various organic components of for instance nuclear wastes. The stability constants of 1:1 species formed between Cm^{3+} and UO_2^{2+} and *P. fluorescens* (CCUG 32456) pyoverdins are by a factor of 1.05 and 1.3, respectively, larger compared to the corresponding EDTA stability constants. Remarkable is that the Np(V)–PYO stability constant is by a factor of 1.83 greater than the EDTA stability constant. To the best of our knowledge, the identified NpO_2^+–PYO species belong to the strongest NpO_2^+ species with organic material reported so far. The results of this project contribute to an improved understanding of the chemistry of uranium(VI), curium(III), and neptunium(V) coordination with bioligands containing hydroxamate and catecholate functionalities in aqueous solution. The determined stability constants can be used directly in safety calculations to quantify the actinide-mobilizing effect of pyoverdin-type bioligands released, for example, in the vicinity of a nuclear waste disposal site.

With the simplified assumption that the metal binding properties of microbes are mainly determined by the functional groups of the cell wall (LPS: Gram-negative bacteria and PG: Gram-positive bacteria), raw estimates are possible, on the basis of the determined stability constants, if actinides prefer to interact with the cell wall compartments of the microbes (LPS, PG) or with the secreted pyoverdin bioligands (PYO). The calculations were performed using nearly equimolar conditions of actinides and functional groups of the biosystems (LPS, PG, and PYO). All identified species influence the uranyl(VI) speciation within the biologically relevant pH range. For U(VI) strong interactions were measured in all three biosystems. By taking pH 5 as an example, uranyl(VI)–pyoverdin interactions (~90% bound) are slightly stronger than those observed with LPS (~70% bound) and PG (~65% bound). For Cm(III) we found a much stronger affinity to aqueous pyoverdin species (~100% bound at pH 5) than to

functional groups of the cell wall compartments (~35% bound at pH 5 to LPS). A similar behavior was observed for Np(V). More than 85% of all Np(V) is bound to pyoverdin species at pH 8 compared to ~37% bound to LPS and less than 1% bound to PG. This shows the importance of indirect interaction processes between actinides and bioligands secreted by resident microbes.

Further studies should focus on interaction processes of actinides with other bioligands than pyoverdins. Due to the large microbial diversity found in nature more microbes are secreting bioligands than *P. fluorescens* investigated in this project. The database about complexation reactions between actinides and released bioligands has to be expanded. These investigations include the determination of the microbial diversity of potential host rock formations (clay, salt) for a nuclear waste repository. Such studies are planned for Opalinus clay. Further investigations will be performed for a better insight of the structure of actinide complexes formed with functional groups of bacterial cell wall compartments.

7 References

[1] Moll, H., Merroun, M., Stumpf, Th., Roßberg, A., Geipel, G., Selenska-Pobell, S., Bernhard, G. (2005). Interactions of actinides with the predominant indigenous bacteria in Äspö aquifer – Interactions of selected actinides U(VI), Cm(III), Np(V) and Pu(VI) with *Desulfovibrio aespoeensis*. Wissenschaftlich-Technische Berichte, FZR-422, Forschungszentrum Rossendorf, Dresden and references therein.

[2] Pedersen, K., Arlinger, J., Ekendahl, S., Hallbeck, L. (1996). 16S rRNA gene diversity of attached and unattached bacteria in boreholes along the access tunnel to the Äspö hard rock laboratory, Sweden. FEMS Microbiol. Ecol. **19**, 249.

[3] Kotelnikova, S., Pedersen, K. (1998). Distribution and activity of methanogens and homoacetogens in deep granitic aquifers at Äspö Hard Rock Laboratory, Sweden. FEMS Microbiol. Ecol. **26**, 121.

[4] Pedersen, K. (1999). Subterranean microorganisms and radioactive waste disposal in Sweden. Engineer. Geol. **52**, 163.

[5] Panak, P., Selenska-Pobell, S., Kutschke, S., Geipel, G., Bernhard, G. and Nitsche, H. (1999). Complexation of U(VI) with cells of *Thiobacillus ferrooxidans* and *Thiomonas cuprina* of different geological origin. Radiochim. Acta **84**, 183.

[6] Shroll, M.R., Straatsma, T.P. (2002). Molecular structure of the outer bacterial membrane of *Pseudomonas aeruginosa* via classical simulation. Biopolymers **65**, 395.

[7] Albrecht-Gary, A.M., Blanc, S., Rochel, N., Abdallah, M. (1991). Pyoverdin and related Siderophores: A physico-chemical Study of the Iron Coordination Mechanism. Inorg. Biochem. **43**, 143.

[8] Albrecht-Gary, A.M., Blanc, S., Rochel, N., Ocakatan, A.Z., Abdallah, M.A. (1994). Bacterial Iron Transport: Coordination Properties of Pyoverdine PaA, a Peptidic Siderophore of *Pseudomonas aeruginosa*. Inorg. Chem. **33**, 6391.

[9] Meyer, J.M. (2000). Pyoverdines: pigments, siderophores and potential taxonomic markers of fluorescent Pseudomonas species. Arch. Microbiol. **174**, 135.

[10] Budzikiewicz, H. (2004). Siderophores of the Pseudomonadaceae *sensu stricto* (Fluorescent and Non-Fluorescent *Pseudomonas* spp.). Fortschr. Chem. Org. Naturst. **87**, 83.

[11] Powell, P.E., Cline, G.R., Reid, C.P.P., Szaniszlo, P.J. (1980). Occurrence of hydroxamate siderophore iron chelators in soils. Nature **287**, 833.

[12] Pedersen, K. (1997). Microbial life in deep granitic rock. FEMS Microbiol. Rev. **20**, 399.

[13] Schäfer, H., Taraz, K., Budzikiewicz, H. (1991). Zur Genese der amidisch an den Chromophor von Pyoverdinen gebundenen Dicarbonsäuren. Z. Naturforsch. [C] **46**, 398.

[14] Teintze, M., Hossain, M.B., Barnes, C.L., Leong, J., van der Helm, D. (1981). Structure of Ferric Pseudobactin, a Siderophore from a Plant Growth Promoting *Pseudomonas*. Biochemistry **20**, 6446.

[15] Meyer, J.M., Abdallah, M.A. (1978). The Fluorescent Pigment of *Pseudomonas fluorescens*: Biosynthesis, Purification and Physicochemical Properties. J. Gen. Microbiol. **107**, 319.

[16] Moll, H., Glorius, M., Bernhard, G., Johnsson, A., Pedersen, K., Schäfer, M., Budzikiewicz, H. (2008). Characterization of Pyoverdins Secreted by a Subsurface Strain of *Pseudomonas fluorescens* and their Interactions with Uranium(VI). Geomicrobiol. J. **25**, 157.

[17] Moll, H., Johnsson, A., Schäfer, M., Pedersen, K., Budzikiewicz, H., Bernhard, G. (2008). Curium(III) complexation with pyoverdins secreted by a groundwater strain of *Pseudomonas fluorescens*. BioMetals **21**, 219.

[18] Moll, H., Glorius, M., Johnsson, A., Schäfer, M., Pedersen, K., Bernhard, G. (2009). Neptunium(V) complexation with natural pyoverdins and related model compounds. Manuscript in preparation.

[19] Puigdomenech, I. (2002). *Input, Sed and Predom: Computer Programs Drawing Equilibrium Diagrams.* Trita-OOK-3010, RIT, Stockholm (1983), Version 29.

[20] Binstead, R.A., Zuberbühler, A.D., Jung, B. (2004). SPECFIT Global Analysis System Version 3.0.35.

[21] Geipel, G., Acker, M., Vulpius, D., Bernhard, G., Nitsche, H., Fanghänel, Th. (2004). An ultrafast time-resolved fluorescence spectroscopy system for metal ion complexation studies with organic ligands. Spectrochim. Acta. A Mol. Biomol. Spectrosc. **60**, 417.

[22] Baysse, C., Budzikiewicz, H., Uría Fernández, D., Cornelis, P. (2002). Impaired maturation of the siderophore pyoverdine chromophore in *Pseudomonas fluorescens* ATCC 17400 deficient for the cytochrome c biogenesis protein CcmC. FEBS Lett. **523**, 23.

[23] Demange, P., Bateman, A., MacLeod, J.K., Dell, A., Abdallah, M.A. (1990). Bacterial Siderophores: Unusual 3,4,5,6-Tetrahydropyrimidine-based Amino Acids in Pyoverdins from *Pseudomonas fluorescens*. Tetrahedron Lett. **31**, 7611.

[24] Budzikiewicz, H., Schäfer, M., Uría Fernández, D., Matthijs, S., Cornelis, P. (2007). Characterization of the chromophores of pyoverdins and related siderophores by electrospray tandem mass spectrometry. BioMetals **20**, 135.

[25] Boukhalfa, H., Reilly, S.D., Michalczyk, R., Iyer, A., Neu, M.P. (2006). Iron(III) Coordination Properties of a Pyoverdin Siderophore Produced by *Pseudomonas putida* ATCC 33015. Inorg. Chem. **45**, 5607.

[26] Gipp, S., Hahn, J., Taraz, K., Budzikiewicz, H. (1991). Two Pyoverdins from *Pseudomonas aeruginosa R*. Z. Naturforsch. [C] **46**, 534.

[27] Budzikiewicz, H., Schäfer, M., Uría Fernández, D., Meyer, J.-M. (2006). Structure proposal for a new pyoverdin from *Pseudomonas* sp. PS 6-10. Z. Naturforsch. [C] **61**, 815.

[28] Bouby, M., Billard, I., MacCordick, J. (1999). Selective behavior of the siderophore pyoverdine A towards UO_2^{2+}, Th^{4+}, U^{4+} and other cations. Czechoslovak. J. Phys. **49**, 147.

[29] MacDonald, J.C., Bishop, G.G. (1984). Spectral Properties of a Mixture of Fluorescent Pigments Produced by *Pseudomonas aeruginosa*. Biochim. Biophys. Acta **800**, 11.

[30] Philson, S.B., Llinas, M. (1982). Siderochromes from *Pseudomonas fluorescens*. I. Isolation and Characterization. J. Biol. Chem. **257**, 8081.

[31] Kumke, M.U., Dorsche, C., Flehr, R., Trowitzsch-Kienast, W., Löhmannsröben, H.-G. (2006). Spectroscopic Characterization of the Artificial Siderophore Pyridinochelin. Z. Naturforsch. [C] **61**, 741.

[32] Khairy, E.M., Shoukry, M.M., Khalil, M.M., Mohamed, M.M.A. (1996). Metal complexes of salicylhydroxamic acid: Equilibrium studies and synthesis. Transition Met. Chem. **21**(2), 176.

[33] Garcia, B., Ibeas, S., Leal, J.M., Secco, F., Venturini, M., Senent, M.L., Nino, A., Munoz, C. (2005). Conformations, protonation sites, and metal complexation of benzohydroxamic acid. A theoretical and experimental study. Inorg. Chem. **44**(8), 2908.

[34] Farkas, E., Enyedy, E.A., Csoka, H. (1999). A comparison between the chelating properties of some dihydroxamic acids, desferrioxamine B and acetohydroxamic acid. Polyhedron **18**(18), 2391.

[35] Mason, S.F., Philp, J., Smith, B.E. (1968). Prototropic Equilibria of Electronically Excited Molecules. 2. 3-, 6-, and 7-Hydroxyquinoline. J. Chem. Soc. A -Inorganic Physical Theoretical Chemistry **12**, 3051.

[36] Bartusek, M. (1967). Komplexe des Uranyls mit phenolischen Liganden. 8. Potentiometrische Untersuchung der Uranylkomplexe mit p-Nitrophenol, 4-Nitrobrenzcatechin, 2,3-Dihydroxynaphthalin, Alizarin S, Pyrogallolcarbonsäure, Pyrogallolsulfonsäure und mit dem Gemisch von Tiron und Sulfosalicylsäure. Coll. Czech. Chem. Commun. **32**(2), 757.

[37] Barkleit, A., Moll, H., Bernhard, G. (2008). Interaction of uranium(VI) with lipopolysaccharide. Dalton Trans., 2879.

[38] Barkleit, A., Moll, H., Bernhard, G. (2009). Complexation of uranium(VI) with peptidoglycan. Dalton Trans., 5379.

[39] Turner, B.F., Fein, J.B. (2006). Protofit: a program for determining surface protonation constants from titration data. Comput. Geosci. **32**, 1344.

[40] Gans, P., Sabatini, A., Vacca, A. (1996). Investigation of equilibria in solution. Determination of equilibrium constants with the HYPERQUAD suite of programs. Talanta **43**, 1739.

[41] Knirel, Y.A. (1990). Polysaccharide Antigens of *Pseudomonas Aeruginosa*. Crit. Rev. Microbiol. **17**, 273.

[42] Knirel, Y.A., Bystrova, O.V., Kocharova, N.A., Zahringer, U., Pier, G.B. (2006). Conserved and variable structural features in the lipopolysaccharide of *Pseudomonas aeruginosa*. J. Endotoxin. Res. **12**, 324.

[43] Warth, A.D., Strominger, J.I. (1971). Structure of peptidoglycan from vegetative cell walls of *bacillus subtilis*. Biochemistry **10**, 4349.

[44] Johnson, K.J., Cygan, R.T., Fein, J.B. (2006). Molecular simulations of metal adsorption to bacterial surfaces. Geochim. Cosmochim. Acta **70**, 5075.

[45] Martell, A.E., Smith, R.M. (1998). NIST- Critical stability constants.

[46] Haas, J.R., Dichristina, T.J., Wade, R. (2001). Thermodynamics of U(VI) sorption onto *Shewanella putrefaciens*. Chem. Geol. **180**, 33.

[47] Fein, J.B., Daughney, J.C., Yee, N., Davis, T.A. (1997). A chemical equilibrium model for metal adsorption onto bacterial surfaces. Geochim. Cosmochim. Acta **61**, 3319.

[48] Baroncelli, F., Grossi, G. (1965). Complexing power of hydroxamic acids and its effect on behavior of organic extractants in reprocessing of irradiated fuels - I.

Complexes between benzohydroxamic acid and zirconium, iron (III) and uranium (VI). Inorg. Nucl. Chem. **27**, 1085.

[49] Mullen, L., Gong, C., Czerwinski, K. (2007). Complexation of uranium(VI) with the siderophore desferrioxamine B. J. Radioanal. Nucl. Chem. **273**, 683.

[50] Brainard, J.R., Strietelmeier, B.A., Smith, P.H., Langston-Unkefer, P.J., Barr, M.E., Ryan, R.R. (1992). Actinide binding and solubilization by microbial siderophores. Radiochim. Acta **58/59**, 357.

[51] Edelstein, N.M.; Klenze, R.; Fanghänel, Th.; Hubert, S. (2006). Optical properties of Cm(III) in crystals and solutions and their application to Cm(III) speciation. Coord. Chem. Rev. **250**, 948.

[52] Rizkalla, E.N., Nectoux, F., Dabos-Seignon, S., Pages, M. (1990). Complexation of neptunium(V) by polyaminocarboxylate ligands. Radiochim. Acta **51**, 151.

[53] Kim, J.I., Sekine, T. (1991). Complexation of Neptunium(V) with Humic Acid. Radiochim. Acta **55**, 187.

[54] Rao, L., Choppin, G.R. (1995). Thermodynamic Study of the Complexation of Neptunium(V) with Humic Acids. Radiochim. Acta **69**, 87.

[55] Seibert, A., Mansel, A., Marquardt, C.M., Keller, H., Kratz, J.V., Trautmann, N. (2001). Complexation behavior of neptunium with humic acid. Radiochim. Acta **89**, 505.

[56] Sachs, S., Bernhard, G. (2005). NIR spectroscopic study of the complexation of neptunium(V) with humic acids: influence of phenolic OH groups on the complex formation. Radiochim. Acta **93**, 141.

[57] Shcherbina, N.S., Perminova, I.V., Kalmykov, S.N., Kovalenko, A.N., Haire, R.G., Novikov, A.P. (2007). Redox and Complexation of Neptunium(V) with Quinonoid-Enriched Humic Derivatives. Environ. Sci. Technol. **41**, 7010.

[58] Borkowski, M., Lis, S., Choppin, G.R. (1996). Complexation Study of NpO_2^+ and UO_2^{2+} Ions with Several Organic Ligands in Aqueous Solutions of High Ionic Strength. Radiochim. Acta **74**, 117.

[59] Eberle, S.H., Wede, U. (1970). Chelatgleichgewichte fünfwertiger Transurane mit Aminopolykarbonsäuren. J. Inorg. Nucl. Chem. **32**, 109.

[60] Rizkalla, E.N., Nectoux, F., Dabos-Seignon, S., Pages, M. (1990). Complexation of neptunium(V) by halo- and hydroxycarboxylate ligands. Radiochim. Acta **51**, 113.

[61] Budantseva, N.A., Andreev, G.B., Fedoseev, A.M., Antipin, M.Y., Krupa, J.C. (2006). Interaction of neptunium(V) with picolinic, nicotinic and isonicotinic acids. Radiochim. Acta **94**, 69.

[62] Jensen, M.P., Nash, K.L. (2001). Thermodynamics of dioxoneptunium(V) complexation by dicarboxylic acids. Radiochim. Acta **89**, 557.

[63] Zhang, Z., Clark, S.B., Tian, G., Zanonato, P.L., Rao, L. (2006). Protonation of D-gluconate and its complexation with Np(V) in acidic to neutral solutions. Radiochim. Acta **94**, 531.

[64] Bonin, L., Den Auwer, C., Ansoborlo, E., Cote, G., Moisy, Ph. (2007). Study of Np speciation in citrate medium. Radiochim. Acta **95**, 371.

[65] Racine, R., Moisy, Ph., Paquet, F., Metivier. H., Madic, C. (2003). *In vitro* study of the interaction between neptunium ions and aposerumtransferrin by absorption spectrophotometry und ultrafiltration: the case of Np(V). Radiochim. Acta **91**, 115.

[66] Runde, W., Neu, M.P., Clark, D.L. (1996). Neptunium(V) hydrolysis and carbonate complexation: Experimental and predicted neptunyl solubility in concentrated NaCl using Pitzer approach. Geochim. Cosmochim. Acta **60**, 2065.

[67] Neck, V., Kim, J.K., Kanellakopulos, B. (1992). Solubility and Hydrolysis Behavior of Neptunium(V). Radiochim. Acta **56**, 25.

[68] Keller, C. (1971). The Chemistry of the Transuranium Elements (K.H. Lieser, ed.). Verlag Chemie GmbH, Weinheim, p. 294.

[69] O'Brien, E.C., Farkas, E., Gil, M.J., Fitzgerald, D., Castineras, A., Nolan, K.B. (2000). Metal complexes of salicylhydroxamic acid (H_2Sha), anthranilic hydroxamic acid and benzohydroxamic acid. Crystal and molecular structure of $[Cu(phen)_2(Cl)]Cl \times H_2Sha$, a model for a peroxidase-inhibitor complex. J. Inorg. Biochem. **79**(1-4), 47.

[70] Schwarzenbach, G., Schwarzenbach, K. (1963). Hydroxamatkomplexe 1. Die Stabilität der Eisen(III)-Komplexe einfacher Hydroxamsäuren und des Ferrioxamins B. Helvetica Chim. Acta **46**(4), 1390.

[71] Farkas, E., Enyedy, E.A., Csoka, H. (2000). Some factors affecting metal ion-monohydroxamate interactions in aqueous solution. J. Inorg. Biochem. **79**(1-4), 205.

[72] Lam, A.W.H., Wong, W.T., Gao, S., Wen, G., Zhang, X.X. (2003). Synthesis, crystal structure, and photophysical and magnetic properties of dimeric and polymeric lanthanide complexes with benzoic acid and its derivatives. Eur. J. Inorg. Chem. **1**, 149.

[73] Kim, M.A., Panak, P.J., Breban, D.C., Priemyshev, A., Yun, J.I., Mansel, A., Kim, J.I. (2007). Interaction of actinides(III) with aluminosilicate colloids. Part IV. Influence of humic acid. Colloid Surf. A-Physicochem. Eng. Asp. **296**(1-3), 206.

[74] Wang, X.K., Rabung, Th., Geckeis, H., Panak, P.J., Klenze, R., Fanghänel, Th. (2004). Effect of humic acid on the sorption of Cm(III) onto gamma-Al_2O_3 studied by the time-resolved laser fluorescence spectroscopy. Radiochim. Acta **92**, 691.

[75] Panak, P., Klenze, R., Kim, J.I., Wimmer, H. (1995). A study of intramolecular energy transfer in Cm(III) complexes with aromatic ligands by time-resolved laser fluorescence spectroscopy. J. Alloys Compd. **225**, 261.

[76] Glorius, M., Moll, H., Bernhard, G. (2008). Complexation of Curium(III) with hydroxamic acids investigated by time-resolved laser-induced fluorescence spectroscopy. Polyhedron **27**, 2113.

[77] Kimura, T., Choppin, G.R. (1994). Luminescence study on determination of the hydration number of Cm(III). J. Alloys Compd. **213-214**, 313.

[78] Lindqvist-Reis, P., Klenze, R., Schubert, G., Fanghänel, Th. (2005). Hydration of Cm^{3+} in aqueous solution from 20 to 200 ºC. A time-resolved laser fluorescence spectroscopy study. J. Phys. Chem. B **109**, 3077.

[79] Wiebke, J., Moritz, A., Glorius, M., Moll, H., Bernhard, G., Dolg, M. (2008). Complexation of uranium(VI) with aromatic acids in aqueous solution – A combined computational and experimental study. Inorg. Chem. **47**, 3150.

[80] Whisenhunt, D.W., Neu, M.P., Hou, Z., Xu, J., Hoffman, D.C., Raymond, K.N. (1996). Specific sequestering agents for the actinides. 29. Stability of the thorium(IV) complexes of desferrioxamine B (DFO) and three octadentate catecholatee or hydroxypyridinonate DFO derivates: DFOMTA, DFOCAMC, and DFO-1,2-HOPO. Comparative stability of the plutonium(IV) DFOMTA Complex. Inorg. Chem. **35**, 4128.

[81] Moll, H., Glorius, M., Bernhard, G. (2008). Curium(III) complexation with desferrioxamine B (DFO) investigated using fluorescence spectroscopy. Bull. Chem. Soc. Jpn. **81**, 857.

[82] Hosny, W.M. (1998). Dioxouranium(VI) mixed ligand complexes containing 8-Hydroxyquinoline and some amino acids. Synth. React. Inorg. Met.-Org. Chem. **28**, 1029.

[83] Beveridge, T.J., Doyle, R.J. (1989). Metal ion and bacteria. John Wilex & Sons, Inc., New York.

[84] Beveridge, T.J. (1988). The bacterial surface – general considerations towards design and function. Can. J. Microbiol. **34**, 363.

[85] Panak, P., Raff, J., Selenska-Pobell, S., Geipel, G., Bernhard, G., Nitsche, H. (2000). Complex formation of U(VI) with *Bacillus*-isolates from a uranium mining waste pile. Radiochim. Acta **88**, 71.

[86] Merroun, M.L., Geipel, G., Nicolai, R., Heise, K.H., Selenska-Pobell, S. (2003). Complexation of uranium (VI) by three eco-types of *Acidithiobacillus ferrooxidans* studied using time-resolved laser-induced fluorescence spectroscopy and infrared spectroscopy. BioMetals **16**, 331.

[87] Merroun, M.L., Raff, J., Rossberg, A., Hennig, C., Reich, T., Selenska-Pobell, S. (2005). Complexation of uranium by cells and S-layer sheets of *Bacillus sphaericus* JG-A12. Appl. Environ. Microbiol. **71**, 5532.

[88] Merroun, M.L., Nedelkova, M., Rossberg, A., Hennig, C., Selenska-Pobell, S. (2006). Interaction mechanisms of bacterial strains isolated from extreme habitats with uranium. Radiochim. Acta **94**, 723.

[89] Macaskie, L.E., Bonthrone, K.M., Yong, P., Goddard, D.T. (2000). Enzymically mediated bioprecipitation of uranium by a *Citrobacter sp*.: a concerted role for exocellular lipopolysaccharide and associated phosphatase in biomineral formation. Microbiology-(UK) **146**, 1855.

[90] Francis, A.J., Gillow, B.J., Dodge, J.C., Harris, R., Beveridge, T.J., Papenguth, H.W. (2004). Uranium association with halophilic and non-halophilic bacteria and archaea. Radiochim. Acta **92**, 481.

[91] Kelly, S.D., Kemner, K.M., Fein, J.B., Fowle, D.A., Boyanov, M.I., Bunker, B.A., Yee, N. (2002). X-ray absorption fine structure determination of pH-dependent U-bacterial cell wall interactions. Geochim. Cosmochim. Acta **66**, 3855.

[92] Texier, A.C., Andres, Y., Le Cloirec, P. (1999). Selective biosorption of lanthanide (La, Eu, Yb) ions by *Pseudomonas aeruginosa*. Environ. Sci. Technol. **33**, 489.

[93] Texier, A.C., Andres, Y., Illemassene, M., Le Cloirec, P. (2000). Characterization of Lanthanide Ions Binding Sites in the Cell Wall of *Pseudomonas aeruginosa*. Environ. Sci. Technol. **34**, 610.

[94] Markai, S., Andres, Y., Montavon, G., Grambow, B. (2003). Study of the interaction between europium(III) and *Bacillus subtilis*: fixation sites, biosorption modeling and reversibility. J. Colloid. Interf. Sci. **262**, 351.

[95] Ozaki, T., Gillow, J.B., Francis, A.J., Kimura, T., Ohnuki, T., Yoshida, Z. (2002). Association of Eu(III) and Cm(III) with *Bacillus subtilis* and *Halobacterium salinarum*. J. Nucl. Sci. Technol. Suppl. **3**, 950.

[96] Ozaki, T., Gillow, J.B., Kimura, T., Ohnuki, T., Yoshida, Z., Francis, A.J. (2004). Sorption behavior of europium(III) and curium(III) on the cell surfaces of microorganisms. Radiochim. Acta **92**, 741.

[97] Ozaki, T., Kimura, T., Ohnuki, T., Francis, A. J. (2005). Association of Eu(III) with Gram-Negative Bacteria, *Alcaligenes faecalis*, *Shewanella putrefaciens*, and *Paracoccus denitrificans*. J. Nucl. Radiochem. Sci. **6**, 73.

[98] Ozaki, T., Kimura, T., Ohnuki, T., Francis, A.J. (2006). Effects of ionic strength on the coordination of Eu(III) and Cm(III) to a Gram-negative bacterium, *Paracoccus denitrificans*. Radiochim. Acta 94, 715.

[99] Moll, H., Barkleit, A., Bernhard, G. (2009). *Interactions of curium(III) with lipopolysaccharide.* Manuscript in preparation.

[100] Guillaumont, R., Fanghänel, T., Fuger, J., Grenthe, I., Neck, V., Palmer, D.A., Rand, M.H. (2003). Update on the Chemical Thermodynamics of Uranium, Neptunium, Plutonium, Americium and Technetium. Elsevier Amsterdam.

[101] Geipel, G., Brachmann, A., Brendler, V., Bernhard, G., Nitsche, H. (1996). Uranium(VI) sulfate complexation studied by time-resolved laser-induced fluorescence spectroscopy (TRLFS). Radiochim. Acta **75**, 199.

[102] Geipel, G. (2006). Some aspects of actinide speciation by laser-induced spectroscopy. Coord. Chem. Rev. **250**, 844.

[103] Koban, A., Bernhard, G. (2007). Uranium(VI) complexes with phospholipid model compounds - A laser spectroscopic study. J. Inorg. Biochem. **101**, 750.

[104] Bernhard, G., Geipel, G., Reich, T., Brendler, V., Amayri, S., Nitsche, H. (2001). Uranyl(VI) carbonate complex formation: Validation of the $Ca_2UO_2(CO_3)_3$(aq.) species. Radiochim. Acta **89**, 511.

[105] Moll, H., Geipel, G., Reich, T., Bernhard, G., Fanghänel, T., Grenthe, I. (2003). Uranyl(VI) complexes with alpha-substituted carboxylic acids in aqueous solution. Radiochim. Acta **91**, 11.

[106] Brachmann, A., Geipel, G., Bernhard, G., Nitsche, H. (2002). Study of uranyl(VI) malonate complexation by time resolved laser-induced fluorescence spectroscopy (TRLFS). Radiochim. Acta **90**, 147.

[107] Günther, A., Geipel, G., Bernhard, G. (2006). Complex formation of U(VI) with the amino acid L-threonine and the corresponding phosphate ester O-phospho-L-threonine. Radiochim. Acta **94**, 845.

[108] Günther, A., Geipel, G., Bernhard, G. (2007). Complex formation of uranium(VI) with the amino acids L-glycine and L-cysteine: A fluorescence emission and UV-vis absorption study. Polyhedron **26**, 59.

[109] Scapolan, S., Ansoborlo, E., Moulin, C., Madic, C. (1997). Uranium speciation in biological medium by means of capillary electrophoresis and time-resolved laser-induced fluorescence. J. Radioanal. Nucl. Chem. **226**, 145.

[110] Scapolan, S., Ansoborlo, E., Moulin, C., Madic, C. (1998). Uranium(VI)-transferrin system studied by time-resolved laser-induced fluorescence. J. Alloys Compd. **271**, 106.

[111] Bonhoure, I., Meca, S., Marti, V., De Pablo, J., Cortina, J.L. (2007). A new time-resolved laser-induced fluorescence spectrometry (TRLFS) data acquisition procedure applied to the uranyl-phosphate system. Radiochim. Acta **95**, 165.

[112] Geipel, G., Bernhard, G., Rutsch, M., Brendler, V., Nitsche, H. (2000). Spectroscopic properties of uranium(VI) minerals studied by time-resolved laser-induced fluorescence spectroscopy (TRLFS). Radiochim. Acta **88**, 757.

[113] Fowle, D.A., Fein, J.B., Martin, A.M. (2000). Experimental study of uranyl adsorption onto *Bacillus subtilis*. Environ. Sci. Technol. **34**, 3737.

[114] Sachs, S., Brendler, V., Geipel, G. (2007). Uranium(VI) complexation by humic acid under neutral pH conditions studied by laser-induced fluorescence spectroscopy. Radiochim. Acta **95**, 103.

[115] Brendler, V., Geipel, G., Bernhard, G., Nitsche, H. (1996). Complexation in the System $UO_2^{2+}/PO_4^{3-}/OH^-$(aq): potentiometric and spectroscopic investigations at very low ionic strengths. Radiochim. Acta **74**, 75.

[116] Calvert, M., Hui, A., Nitsche, H. (2007). Multi-ligand model systems for Cm(III)/Eu(III) binding on microbial surfaces. Presented at the 11th International Conference MIGRATION`07, München, Germany; Paper B4-5.

[117] Moll, H., Geipel, G., Bernhard, G. (2005). Complexation of Curium(III) by Adenosine 5'-triphosphate (ATP): A Time-resolved Laser-induced Fluorescence Spectroscopy (TRLFS) Study. Inorg. Chim. Acta **358**, 2275.

[118] Moll, H., Bernhard, G. (2007). Complex formation of curium(III) with amino acids of different functionalities: L-threonine and O-phospho-L-threonine, J. Coord. Chem. **60**, 1795.

[119] Moll, H., Bernhard, G. (2007). Complexation of curium(III) with L2-aminobutyric acid investigated by time-resolved laser-induced fluorescence spectroscopy, J. Radioanal. Nucl. Chem. **274**, 603.

[120] Kim, J.I., Rhee, D.S., Wimmer, H., Buckau, G., Klenze, R. (1993). Complexation of trivalent actinide ions (Am^{3+}, Cm^{3+}) with humic acids: A comparison of different experimental methods, Radiochim. Acta **62**, 35.

[121] Ozaki, T., Kimura, T., Ohnuki, T., Kirishima, A., Yoshida, T., Isobe, H., Francis, A. J. (2006). Association of europium(III), americium(III), and curium(III) with cellulose, chitin, and chitosan. Environ. Toxicol. Chem. **25**, 2051.

[122] Lins, R.D., Straatsma, T.P. (2001). Computer Simulation of the Rough Lipopolysaccharide Membrane of *Pseudomonas aeruginosa*. Biophys. J. **81**, 1037.

[123] Stumpf, Th., Fanghänel, Th., Grenthe, I. (2002). Complexation of trivalent actinide and lanthanide ions by glycolic acid: a TRLFS study, J. Chem. Soc., Dalton Trans., 3799.

[124] Wang, Z., Felmy, A.R., Xia, Y.X., Mason, M.J. (2003). A fluorescence spectroscopic study on the speciation of Cm(III) and Eu(III) in the presence of organic chelates in highly basic solutions, Radiochim. Acta **91**, 329.

[125] Moll, H., Stumpf, Th., Merroun, M., Roßberg, A., Selenska-Pobell, S., Bernhard, G. (2004). Time-resolved Laser Fluorescence Spectroscopy Study on the Interaction of Cm(III) with *Desulfovibrio äspöensis* DSM 10631^{T}. Environ. Sci. Technol. **38**, 1455.

[126] Choppin, G.R. (2005). Actinide Science: Fundamental and Environmental Aspects. J. Nucl. Radiochem. Sci. **6**, 1.

[127] Songkasiri, W., Reed, D.T., Rittmann, B.E. (2002). Bio-sorption of neptunium(V) by *Pseudomonas fluorescens*. Radiochim. Acta **90**, 785.

[128] Rutsch, M., Geipel, G., Brendler, V., Bernhard, G., Nitsche, H. (1999). Interaction of uranium(VI) with arsenate(V) in aqueous solution studied by time-resolved laser-induced fluorescence spectroscopy (TRLFS). Radiochim. Acta **86**, 135.

[129] Ledin, M., Pedersen, K. (1996). The environmental impact of mine wastes: roles of microorganisms and their significance in treatment of mine waste. Earth Sci. Rev. **41**, 67.

[130] Landa, E.R. (2004). Uranium mill tailings: nuclear waste and natural laboratory for geochemical and radioecological investigations. J. Environ. Radioact. **77**, 1.

[131] Kalinowski, B.E., Oskarsson, A., Albinsson, Y., Arlinger, J., Ödegaard-Jensen, A., Andlid, T, Pedersen, K. (2004). Microbial leaching of uranium and other trace elements from shale mine tailings at Ranstad. Geoderma **122**, 177.

[132] Kalinowski, B.E., Johnsson, A., Arlinger, J., Pedersen, K., Ödegaard-Jensen, A., Edberg, F. (2006). Microbial Mobilization of Uranium from Shale Mine Waste. Geomicrobiol. J. **23**, 157.

[133] Johnsson, A., Arlinger, J., Pedersen, K., Ödegaard-Jensen, A., Albinsson, Y. (2006). Solid−Aqueous Phase Partitioning of Radionuclides by Complexing Compounds Excreted by Subsurface Bacteria. Geomicrobiol. J. **23**, 621.

[134] Xiao, R., Kisaalita, W.S. (1995). Purification of pyoverdins of *Pseudomonas fluorescens* 2−79 by copper-chelate chromatography. Appl. Environ. Microbiol. **61**, 3769.

[135] Matz, W., Schell, N., Bernhard, G., Prokert, F., Reich, T., Claussner, J., Oehme, W., Schlenk, R., Dienel, S., Funke, H., Eichhorn, F., Betzl, M., Prohl, D., Strauch, U., Hüttig, G., Krug, H., Neumann, W., Brendler, V., Reichel, P., Denecke, M.A., Nitsche, H. (1999). ROBL - a CRG Beamline for Radiochemistry and Materials Research at the ESRF. J. Synchrot. Radiat. **6**, 1076.

[136] Ressler, T. (1998). WinXAS: a program for X-ray absorption spectroscopy data abalysis under MS-Windows. J. Synchrot. Radiat. **5**, 118.

[137] Ankudinov, A.L., Ravel, B., Rehr, J.J., Conradson, S.D. (1998). Real-space multiple-scattering calculation and interpretation of x-ray-absorption near-edge structure Phys. Rev. B **58**, 7565.

[138] Howatson, J., Grev, D.M., Morosin, B. (1975). Crystal and molecular-structure of Uranyl acetate dihydrate. J. Inorg. Nucl. Chem. **37**, 1933.

[139] Nassimbeni, L.R., Rodgers, A.L., Haigh, J.M. (1976). Crystal and molecular-structure of Bis(4-N,N'-Dimethylaminopyridine) solvate of Di-Mu-Salicylicacidato Bis[Nitratodioxouranium(VI)]. Inorg. Chim. Acta **20**, 149.

[140] Bouby, M., Billard, I., MacCordick, J. (1998). Complexation of Uranium VI with the Siderophore Pyoverdine. Radiochim. Acta **80**, 95.

[141] Bouby, M., Billard, I., MacCordick, J. (1998). Complexation of Th(IV) with the siderophore pyoverdine A. J. Alloys Compd. **271-273**, 206.

[142] Choppin, G.R. (1983). Solution Chemistry of the Actinides. Radiochim. Acta **32**, 43.

[143] Shannon, R.D. (1976). Revised Effective Ionic Radii and Systematic Studies of Interatomic Distances in Halides and Chalcogenides. Acta Cryst. A **32**, 751.

[144] Jarvis, N.V., Hancock, R.D. (1991). Some correlations involving the stability of complexes of transuranium metal ions and ligands with negatively charged oxygen donors. Inorg. Chim. Acta **182**, 229.

[145] Neu, M.P., Matonic, J.H., Ruggiero, C.E., Scott, B.L. (2000). Structural characterization of a plutonium(IV) siderophore complex: single-crystal structure of Pu-Desferrioxamine E. Angew. Chem. Int. Ed. **39**, 1442.

[146] Choppin, G.R., Thakur, P., Mathur, J.N. (2006). Complexation thermodynamics and structural aspects of actinide–aminopolycarboxylates. Coord. Chem. Rev. **250**, 936.

[147] Carnall, W.T., Rajnak, K. (1975). Electronic energy level and intensity correlations in the spectra of the trivalent actinide aquo ions. II. Cm(III). J. Chem. Phys. **63**, 3510.

[148] Neck, V., Runde, W., Kim, J.I., Kanellakopulos, B. (1994). Solid-Liquid Equilibrium Reactions of Neptunium(V) in Carbonate Solution at Different Ionic Strength. Radiochim. Acta **65**, 29.

[149] Morgenstern, A., Kim, J.I. (1996). The Phosphate Complexation of Neptunium(V). Radiochim. Acta **72**, 73.

[150] Xia, Y., Friese J.I., Moore D.A., Rao, L. (2006). Stability constants of Np(V) complexes with fluoride and sulfate at variable temperatures. J. Radioanal. Nucl. Chem. **268**, 445.

[151] Pokrovsky, O.S., Bronikowski, M.G., Moore, R.C., Choppin, G.R. (1998). Interaction of Neptunyl(V) and Uranyl(VI) with EDTA in NaCl Media: Experimental Study and Pitzer Modeling. Radiochim. Acta **80**, 23.

[152] Roßberg, A., Baraniak, L., Reich, T., Hennig, C., Bernhard, G., Nitsche, H. (2000). EXAFS structural analysis of aqueous uranium(VI) complexes with lignin degradation products. Radiochim. Acta **88**, 593.

[153] Essen, S.A., Johansson, A., Bylund, D., Pedersen, K., Lundström, U.S. (2007). Siderophore production by *Pseudomonas stutzeri* under aerobic and anaerobic conditions. Appl. Environ. Microbiol. **73**, 5857.

8 Acknowledgement

The authors are indebted for the use of the Cm-248 to the U.S. Department of Energy, Office of Basic Energy Sciences, through the transplutonium element production facilities at Oak Ridge National Laboratory which was made available as part of a collaboration between FZD and the Lawrence Berkeley National Laboratory (LBNL).

The authors would like to thank Prof. K. Pedersen and his group at the Göteborg University, Department of Cell and Molecular Biology (Sweden) and especially Dr. A. Johnsson for the fruitful discussions and helpful comments concerning all questions about *P. fluorescens* (CCUG 32456) pyoverdins.

We thank Dr. H. Foerstendorf and K. Heim for recording of FTIR and ATR FTIR spectra and for their help in the spectra interpretation. For technical support we thank J. Schott and P. Jähnigen (potentiometry) and U. Schaefer (ICP-MS analyses).

We thank Prof. H. Budzikiewicz and Dr. M. Schäfer (Institut für Organische Chemie, Universität zu Köln) for the analysis of the pyoverdin mixtures using mass spectrometry.

Thanks are given to Dr. A. Moritz, Dr. J. Wiebke, and D. Weißmann (Institut für Theoretische Chemie, Universität zu Köln) for their helpful computational calculations on 1:1 and 1:2 complexes of U(VI) with SHA and BHA.

The XAS measurements were performed at BM20 (ROBL) at the European Synchrotron Radiation Facility (ESRF) in Grenoble (France). In particular, thanks are given to Dr. A. Scheinost, Dr. C. Hennig, and Dr. H. Funke for their support during the XAS measurements and their help in evaluating the data.

At this place we would like to take the opportunity to thank all colleagues who contributed to the success of this work.